
Toxicity, uptake and applications of intracellular delivery by cell penetrating peptides

Gisela Tünnemann



München 2009

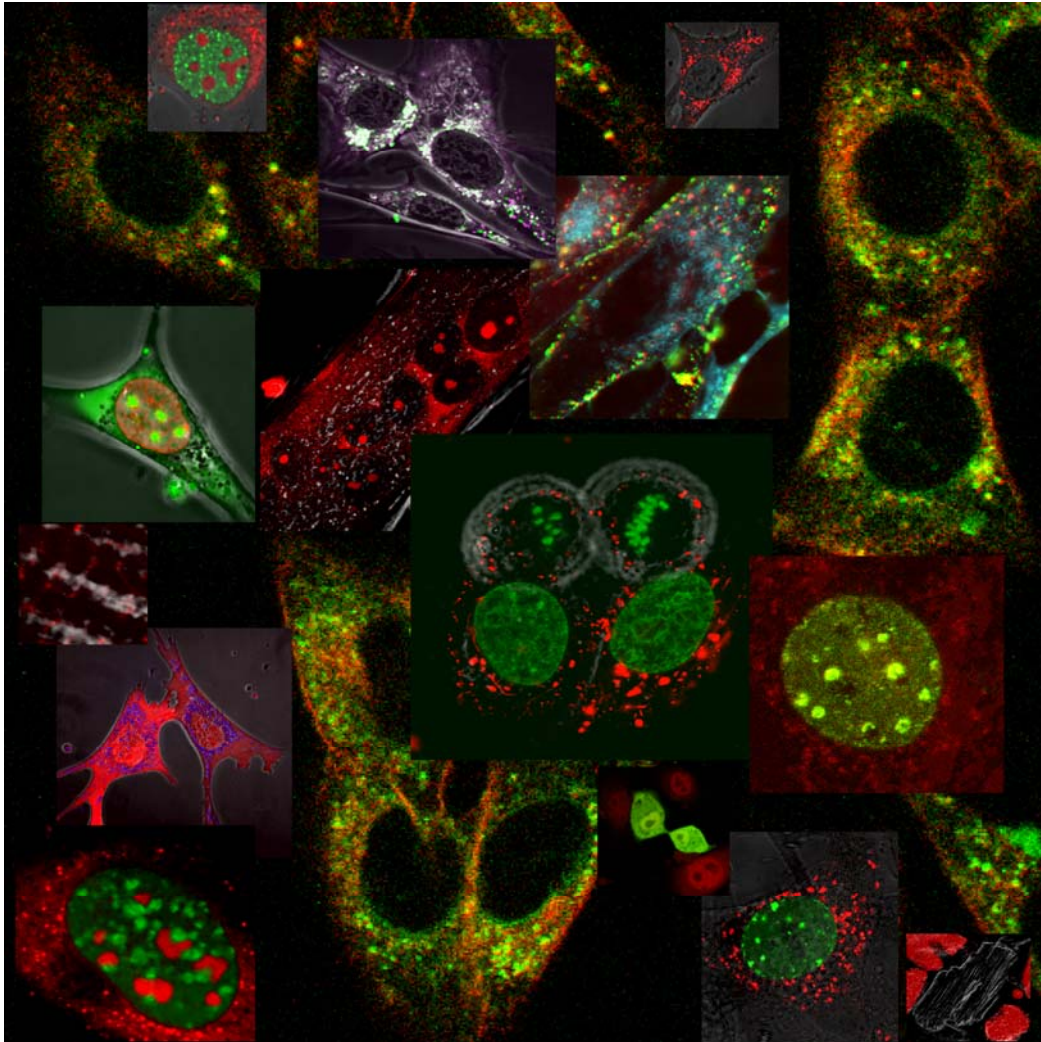
Toxicity, uptake and applications of intracellular delivery by cell penetrating peptides

Gisela Tünnemann

**Dissertation
an der Fakultät für Biologie
der Ludwig-Maximilians-Universität
München**

vorgelegt von
Diplom-Chemikerin Gisela Tünnemann
aus Fröndenberg

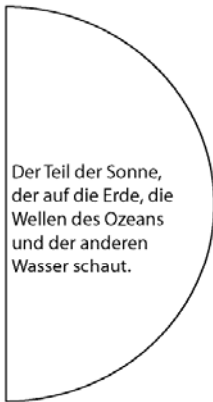
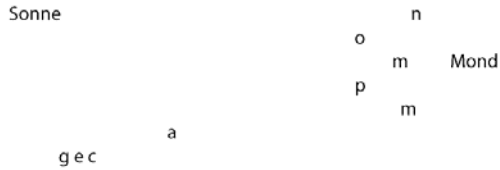
München, den 31. Juli 2008



Erstgutachter:
Zweitgutachter:

Prof. Dr. Heinrich Leonhardt
Prof. Dr. Ruth Brack-Werner

Tag der mündlichen Prüfung: 27.02.2009



Hier wird gezeigt, daß der Mond, der kein eigenes Licht hat, das Licht, das er von der Sonne bekommt, weder empfangen noch zu uns zurückwerfen könnte, wenn er keine dicht, glänzende Oberfläche hätte, wie die Oberflächen von Spiegeln und Flüssigkeiten sind, wenn der Mond aber seiner Natur nach einem dichten, glänzenden Spiegel ähnlich wäre, so gäbe er uns von dem ganzen Licht n o p m nur den Teil o p, als wäre das

Auge, das ihn sieht in dem Punkt a ge-

- a gen, was nur ein sehr kleines
- b Licht erzeugen würde;
- c wenn aber sein
- d Schimmern von
- e einem flüssigen Körper
- f kommt, dann werden die
- g zurückgeworfenen Strahlen

ihrem Wesen nach keinen großen

Glanz..., aber wenn sie sich wellenförmig bewegen, wie wir es hier bei uns an den Wassern des Meeres sehen, dann wird jede Welle für sich glänzen, und alle zusammen werden eine große Menge Glanz..., der aber nicht so stark ist wie der zuerst erwähnte, wegen der schattigen Teile der Welle, die sich...

Hier wird gezeigt, daß der Körper des Mondes, auch wenn er gleich weit vom betrachtenden Auge entfernt bleibt, seine Größe für dieses Auge beachtlich wechseln wird, weil hier das Auge, da der Mond als Vollmond im Osten steht, nur den Teil beleuchtet sieht, der zwischen der Linie b f liegt und von den Wassern bedeckt ist.

Modified from the catalog 'Leonardo da Vinci: Joseph Beuys. Der Codex Leicetster im Spiegel der Gegenwart'. With kind permission of Haus der Kunst, München; Museum der Dinge, Berlin and the authors Marianne Schneider, Nikolaus G. Schneider.

Content:

SUMMARY:	I
1 INTRODUCTION	1
1.1 BITS AND PIECES OF CPP HISTORY.....	1
1.2 INFLUENCE OF CARGOES ON THE MODE OF UPTAKE.....	2
1.2.1 High molecular weight cargoes	2
1.2.2 Low molecular weight cargoes	4
1.2.3 Special role of arginine-rich peptides (RRPs) in cellular uptake	5
1.2.4 Relevant parameters when measuring CPP uptake.....	6
1.3. MODELS FOR THE MECHANISM OF TRANSDUCTION.....	7
1.3.1. Pore formation.....	7
1.3.2. Formation of inverted micelles	8
1.3.3. Adaptive translocation.....	8
1.4. TOXICITY OF CELL PENETRATING PEPTIDES (CPPs)	11
1.4.1. In vitro	11
1.4.2. In vivo	12
1.5 APPLICATIONS OF CPP-MEDIATED INTRACELLULAR DELIVERY IN MOLECULAR MEDICINE	12
1.5.1 Labeling and imaging	13
1.5.2 Modulation of intracellular function	13
2. RESULTS	17
2.1 LIVE CELL ANALYSIS OF CELL PENETRATION ABILITY AND TOXICITY OF OLIGOARGININES	17
2.2 CELL ENTRY OF ARGININE-RICH PEPTIDES IS INDEPENDENT OF ENDOCYTOSIS	26
2.3 CIRCULARIZATION AND CHARGE CLUSTERING PROMOTES CELLULAR UPTAKE OF ARGININE-RICH CELL PENETRATING PEPTIDES.....	41
2.4 NUCLEOLAR MARKER FOR LIVING CELLS.....	53
2.5 MODULATION OF MUSCLE CONTRACTION BY A CELL PERMEABLE PEPTIDE	64
2.6 CARGO-DEPENDENT MODE OF UPTAKE AND BIOAVAILABILITY OF TAT- CONTAINING PROTEINS AND PEPTIDES IN LIVING CELLS.	73
3. DISCUSSION & OUTLOOK	84
4. APPENDIX	90
4.1 ABBREVIATIONS.....	90
4.2 DECLARATION OF CONTRIBUTIONS	94
4.3 ACKNOWLEDGEMENTS	98
4.4 REFERENCES.....	100
4.5 CURRICULUM VITAE	104
4.6 CONFERENCE CONTRIBUTIONS	105
4.7 LIST OF PUBLICATIONS	106
4.8 MOVIES	107

Summary:

The family of cell penetrating peptides (CPPs) consists of small cationic or amphipathic peptides that aid the uptake of attached cargoes into living cells. This bears a tremendous potential for the introduction of yet non-deliverable hydrophilic compounds into living cells *in vitro* and *in vivo*. In the beginnings of CPP-research the bioavailability of cargoes after translocation into the intracellular compartments of cells was often overestimated due to the use of inappropriate protocols and invasive detection methods.

In this study we employed laser scanning confocal microscopy (LSCM) as a non-invasive method to delineate differences between fluorescently labeled distinct CPPs and to understand the mechanism of uptake of arginine-rich CPPs with and without cargoes. We further tracked bioavailability, localization and functional effects of a variety of cargoes after being transduced into different cells.

The subgroup of arginine-rich CPPs (RRPs) includes the well studied CPPs TAT and penetratin. We assessed the short- and long-termed toxic effects of oligo-arginines with different chain length (5-12) relative to their concentration in living cells. Nona-arginine gained access in an instantaneously bioavailable manner at a reasonable concentration and was associated with little short-termed or no long-termed toxicity.

Regarding the mechanism of uptake for RRP themselves two distinct modes have been discussed controversially in the literature since now. (I) The cationic peptides enrich at the plasma membrane and become adsorptively endocytosed. The main portion of the CPP-cargoes remains thus extracellular and release from those vesicles could be detected only by strongly amplifying methods (TAT-Cre-recombinase reporter gene assay). (II) Transduction of RRP occurs in a way that the peptide distributes homogenously inside the cytoplasm and nucleoplasm and accumulates inside nucleoli. We could show that the latter pathway is chosen as an additional option besides endocytosis, if a certain threshold concentration or critical concentration is exceeded. By inhibiting different endocytic pathways and endocytosis per se we unambiguously demonstrated that transduction differs fundamentally from pinocytic or endocytic events. Finally, transduction only takes place if the

attached cargoes are small (fluorophores, peptides below 25 additional amino acids), large components (nanoparticles, globular protein domains) attached to RRP abolish transduction and become adsorptively endocytosed.

To understand the process of transduction of RRP better and because structural information of CPPs could only be modeled until now, the method of analytical ultracentrifugation was utilized to delineate required features which permit a CPP to transduce. We show that RRP exhibit an extended conformation and the only prerequisite for a peptide to transduce is a minimal number of arginines that are accumulated over a small peptide sequence. Furthermore a circular variant of TAT, that presents the arginines on a much smaller diameter, was delivered to a higher amount than its linear counterpart into living cells. Therefore a certain accumulation of arginines is the only determinant which permits the uptake mode of transduction.

CPPs can be used to label subcellular structures inside living cells. Fluorescently labeled deca-arginine enriched inside the nucleolar compartment and stained the granular components and to a lesser extent the fibrillar components of the nucleoli. As another example a TAT fusion attached to a peptide derived from ventricular light chain-1 (VLC-1) showed enhanced presence at the I-bands of isolated cardiomyocytes

In another approach we demonstrated that a transducible versions of a peptide can be utilized to modify protein interactions even in primary cells, which are usually difficult to transfect and have limited life-time. VLC-1 fused to TAT enhanced muscle contraction in primary cultures of adult cardiomyocytes.

In order to generate an antiproliferative peptide we fused peptides derived from the PCNA-interacting domains of p21^{WAF/CIP} and ligase1 to the RRP TAT and investigated its potential to inhibit cell cycle progression. We found that after being incubated with synchronized mouse myoblast for only ten minutes these peptides were able to decelerate cell cycle progression to 50 %.

In summary, we provide an explanatory basis for the conflicting reports in the literature, leaving only RRP or RRP fused to low molecular weight cargoes the option to enter living cells via the mechanism of transduction. For this peptide or peptide chimeras transduction can be observed, if they are applied above a peptide- and cell type-specific concentration threshold in *in vitro*

experiments. Whereas transduced constructs immediately exert effects, larger cargoes fused to RRP and other CPPs become internalized by an endocytic process and only a marginal portion of the constructs escapes from endo- or lysosomes. Therefore peptides fused to RRP are ideal tools to label subcellular structures and to interfere with protein function in living cells.

1 Introduction

1.1 Bits and pieces of CPP history

In 1988, Frankel and Pabo ¹ and Green and Loewenstein ² reported that the viral protein transactivator of transcription (TAT) from HIV-1 was able to cross biological membranes and to subsequently alter gene transcription. This discovery was followed by the mapping of the peptide domain responsible for the cellular uptake ability and termed protein transduction domain (PTD) or cell penetrating peptide (CPP). Subsequently, other PTDs have been identified, e.g., the homeobox of the antennapedia protein of *Drosophila melanogaster* ^{3,4}, the viral tegument protein VP22 of herpes simplex virus-1 ⁵⁻⁷, human calcitonin derived peptides ^{8,9} and the PreS2-domain of hepatitis-B virus surface antigen ¹⁰. The homeobox of antennapedia was the first example of a shuttle that promoted the intracellular delivery of a part of the Rab 3 protein as a cargo into cells in culture ³. For some of the factors mentioned above the minimal transducing domains were mapped and will hereafter be referred to as CPPs. The TAT-CPP was narrowed down to a short peptide motif of nine residues GRKKRRQRRR (amino acids 48-57) ^{11,12}. The well studied CPP penetratin comprises the third helix of the homeobox of antennapedia RQIKIWFQNRRMKWKK (amino acids 43-58) ¹³, but a shorter C-terminal segment (52-58) is sufficient to induce translocation ¹⁴. To the panoply of CPPs derived from naturally occurring proteins artificially designed peptide sequences were soon added, which can be categorized as amphipathic or model amphipathic (MAP) ¹⁵⁻¹⁷, lysine-, arginine- ^{14,18-21}, proline-rich ²²⁻²⁴ and chimeric ²⁵⁻²⁷ peptides or peptoids ^{21,28}. Equipped with this armamentarium, cellular uptake of all sorts of cargoes linked to CPPs, like fluorophores, drugs ²⁹, peptides ³⁰, nucleic acids ³¹, proteins ^{11,32,33}, nanoparticles ³⁴ and liposomes ³⁵ was achieved. Their internalization seemed to follow an energy-independent, unknown pathway. Importantly, the effects of interconnected cargoes measured in mammalian cells and animals raised hopes that biological membranes could be conquered by any hydrophilic compound, if shuttled by CPPs. Unfortunately, these expectations had to be reconsidered, when in 2003 Richard *et al.* published that the CPPs TAT and

penetratin themselves became internalized into mammalian cells by an endocytic mechanism³⁶. Even under mild fixation conditions, fluorescently labeled CPPs escaped from the endosomal compartment and were redistributed into the cytoplasm and the nucleus. The cationic nature of CPPs and their consequent strong affinity to negatively charged cell membrane constituents, was proposed to lead to their artifactual internalization after treatment of cells with membrane disruptive methods³⁶. Thus, the uptake of CPPs was overestimated in many studies using flow cytometric analysis to quantify the amount of presumably internalized CPPs. Consequently, published work on CPP-mediated internalization needs to be critically reassessed.

1.2 Influence of cargoes on the mode of uptake

An analysis of the available data suggests a correlation between size and/or structure of the cargo and the mechanism of cellular uptake. This is also supported by the observation that peptides and proteins fused to CPPs simultaneously incubated with mammalian cells end up in different subcellular compartments^{37,38}. In addition, some biophysical properties of the cargoes might also interfere with the uptake mechanism.

1.2.1 High molecular weight cargoes

Proteins and quantum dots fused to CPPs follow an endocytic route and uptake can be prevented by inhibitors of endocytosis³⁷⁻⁴². For TAT-fusion proteins caveolar-dependent endocytosis³⁹, lipid raft macropinocytosis⁴³ or clathrin-dependent endocytosis⁴⁴ were suggested as possible mechanisms. Brooks et al. promoted the idea that the CPP TAT due to its strong adherence to negatively charged membrane constituents gets internalized by any pinocytic process occurring at cell membranes⁴⁵. Recently, arginine-rich CPPs (RRPs) were reported to simultaneously use at least three endocytic pathways⁴⁶. Hence, the term adsorptive endocytosis, as already used by the discoverers of TAT-mediated transduction⁴⁷, still applies. The main pathways

for pinocytotic and endocytic uptake are depicted in Fig. 1. For the ionic interaction of the positively charged amino acid residues with cellular membranes, a crucial role of heparin sulfate proteoglycans or phospholipids was established^{37,47-50}, but the influence of particular negatively charged membrane constituents on the translocation event may vary for individual CPPs⁴¹. Endocytic uptake is associated with storage of the internalized CPP-species in endosomes or lysosomes for extended periods of time and thus reduced bioavailability and activity. Nevertheless, a sensitive and non-invasive reporter gene assay based on Cre-mediated recombination after delivery of the protein TAT-Cre recombinase^{51,52} indirectly revealed the presence and activity of the recombinase inside the nucleus^{38,43}. In addition,

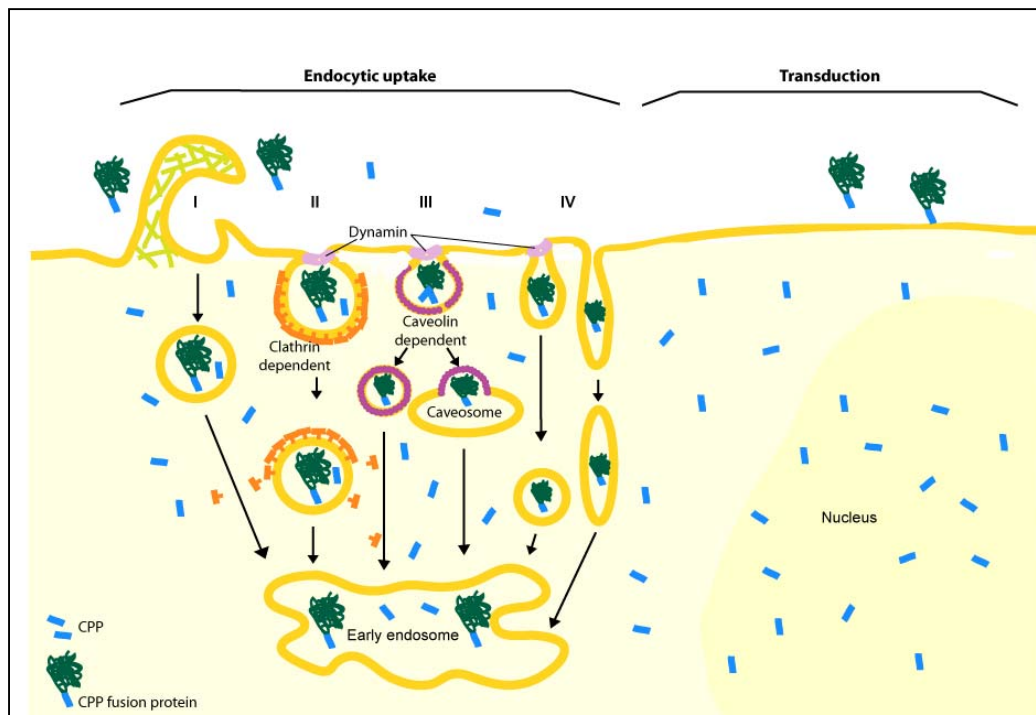


Figure 1: Main pinocytotic uptake pathways and transduction:

Pinocytotic events include (I) Macropinocytosis, (II) clathrin-dependent endocytosis, (III) caveolin-dependent endocytosis and (IV) clathrin- and caveolin-independent types of endocytosis. In contrast to any pinocytotic event that is associated with intermediate storage of CPPs in vesicles, CPPs gain direct access to all intracellular compartments via the yet not fully understood mechanism of transduction.

numerous examples of CPP-mediated delivery of high molecular weight cargoes like protein and DNA / RNA constructs with functional effects after internalization *in vitro* and *in vivo* have been reported and are reviewed in⁵³.

As the release from cytoplasmic vesicles is the bottleneck for a successful delivery of bioavailable cargoes by CPPs, several studies aimed to increase the efficiency of vesicular release. Using the TAT-Cre recombinase functional assay, lysosomotropic agents like chloroquine or endosome-disruptive agents like PEI (polyethylenimine) or high concentrations of sucrose (1-2 M)⁵⁴, as well as the co-application of the transducible and fusogenic TAT-HA2 peptide together with the TAT-fusion protein markedly enhanced Cre recombinase activity^{43,55}. Other methods to destabilize vesicle architecture include Ca²⁺ treatment at millimolar concentrations⁵⁶ or photochemical treatment in the presence of photosensitizers like CPPs themselves⁵⁴ or membrane soluble chemical compounds⁵⁷, e.g. aluminium phthalocyanine enhanced the antisense effect of a peptide nucleic acid conjugate delivered by TAT by two orders of magnitude⁵⁸.

1.2.2 Low molecular weight cargoes

Although an endocytic mode of uptake for high molecular weight cargoes is generally accepted, the entry route of low molecular weight cargoes like peptides (< 50 aa) attached to CPPs is still a controversial issue. Several groups reported that uptake of CPPs like TAT, oligo-arginines or penetratin did not differ from internalization of high molecular weight cargoes fused to CPPs and fell in the category of adsorptive endocytosis (see above)⁵⁹⁻⁶¹. From the initial studies defining the minimal transduction domains a very rapid, energy-independent mechanism of entry was observed concomitantly using non-invasive detection methods, e.g. fluorescence microscopy^{12,37,38,60,62,63}. This kind of mechanism will hereafter be called transduction. Transduction was not affected by inhibitors of endocytosis and was reported to occur^{12,13,21,62} or even to be enhanced at lower temperature⁶⁴. In addition, D-amino acid analogues of CPPs were taken up in the same rapid manner and a receptor-dependent mechanism could therefore be excluded^{21,65-68}. Furthermore, the process of transduction exhibited faster kinetics and lead to immediate overall intracellular bioavailability (Fig. 1). The uptake kinetics of deca-arginine into HeLa cells were recently shown to start directly after application of the fluorescently labeled CPP and reached a plateau after 40

minutes⁶⁸. The membrane potential was proposed as one of the potential driving forces for this mode of uptake of CPPs^{38,69-71}. Interestingly, there exists a CPP- and cell type-specific transduction threshold^{38,46}. For the CPP TAT coupled to a fluorophore transduction into mouse myoblasts occurred at or above 1 μM and, when fused to a 20 amino acid-long peptide, the threshold increased to 7.5 μM . Below these concentration thresholds internalization occurred only via the mechanism of adsorptive endocytosis³⁸. TAT, penetratin and oligoarginine exhibited a critical concentration or transduction threshold in cases where non-degradable D-amino acid variants were analyzed^{38,46,64}. Furthermore, freeze-fracture electron microscopy of DMPC-liposomes treated with TAT at a ratio 1:20 (peptide/lipid) showed TAT assembled in small bundles with a spacing of about 5 nm⁷² and in a recent atomic force microscopy analysis of TAT on DSPC/DOPC planar biomembranes, the peptide associated with increasing concentration on the fluid phase⁷³. For antimicrobial peptides the re-alignment and self-assembly of peptides in membranes was reported to be concentration-dependent also, e.g. a solid-state NMR study with the membrane-disruptive peptide PGLa revealed that with increasing peptide/lipid ratio the peptide changed from a monomeric surface-bound S-state over a dimeric tilted T-state to an oligomeric membrane-inserted I-state⁷⁴. These cooperative effects might explain, why for a given CPP both possible uptake modes are controversially reported in the literature.

1.2.3 Special role of arginine-rich peptides (RRPs) in cellular uptake

The unifying feature among most known CPPs is the presence of several lysines and/or arginines within the individual peptide motifs. The high positive net charge of CPPs leads to an increased local peptide concentration at the cellular membranes driven by electrostatic interactions^{75,76}. CPPs such as transportan, mastoparan and MAPs form a subgroup of amphipathic CPPs, in which hydrophobic and hydrophilic amino acid side chains are spatially separated in the α -helical peptide structure, a property often found in antimicrobial peptides. Their membrane translocation was reported to occur in

an energy-dependent and -independent fashion in living cells ¹⁶. A structure-function study astonishingly revealed that membrane association due to positive net charge was not correlated with uptake efficiency and lysines were even dispensable; rather helical amphipathicity and a length of at least four complete helical turns were essential to allow membrane translocation ¹⁷. Therefore, the mechanism of translocation for this type of CPPs might differ from that of TAT and penetratin analogues, where positive charge is absolutely required for the crossing of biomembranes. But charge alone is insufficient to explain the process of transduction. The uptake of oligomers of histidine, ornithine and lysines, as well as that of branched lysines (oligomers) was demonstrated to be sensitive to temperature, which argues for an endocytic uptake ^{21,77,78}. On the other hand a minimum of six consecutive arginines was enough to cause transduction ^{14,18} and the D-form as well as guanidino peptoids worked equivalently ²¹. These results, the absence of a common secondary structure element in known RRP and the flexibility in the position of arginines within a given peptide sequence without affecting its transduction efficiency ¹⁸ suggests a decisive role for arginine in the mechanism of transduction, which probably resides in its guanidinium function ^{21,28}.

1.2.4 Relevant parameters when measuring CPP uptake

Several parameters influence the transduction efficiency of CPP-peptides. Among them the type of CPP, its D or L amino acid composition and its concentration, the application buffer, the cell type, as well as the administration or application mode can influence the optimal concentrations for transduction. Such methodological details are usually described in the material & methods section. However, only few publications mention, e.g., the final volume in which the CPP was applied on the cells during experiments, although increasing peptide-to-cell ratio has been shown to influence the mode of uptake. Higher peptide-to-cell ratios permit, in addition to endocytosis, direct membrane transduction ⁷⁹. Therefore, besides the particular CPP concentration the parameter liquid m^3 / cells m^2 in combination with cell density and cell type should be included in future work. Another

important determinant is the temperature, as RRP transduce more quickly at lower temperatures. This is especially important to allow any meaningful comparison of results and to draw conclusions on CPP uptake and its efficiency.

1.3. Models for the mechanism of transduction

Although to date the mechanism of transduction (i.e., the non-endocytic mode of CPP uptake with membrane permeation and direct intracellular availability) is still not clarified, several models have been developed to explain this intriguing property of CPPs.

1.3.1. Pore formation

Some CPPs (MAPs¹⁵) exhibit amphipathicity or adopt α -helical conformation in the presence of artificial micelles, e.g. mastoparan and transportan⁸⁰, which is also a known property of pore-forming antimicrobial or lytic peptides. Such peptides lead to leakage of protons, metal ions, proteins etc, finally resulting in cell death due to the collapse of the membrane potential⁸¹. Amphipathic peptides insert into the membrane and multimerize in such a way, that hydrophobic residues are exposed and hydrophilic residues form the cavity of a channel (Fig. 2A, amphipathic peptides). Thereby short-living mastoparan pores permit influx of compounds < 1000 Da into mammalian cells⁸². Moreover they are able to traverse the membrane with a flip-flop mechanism⁸³. However, this mechanism can only apply for the subgroup of amphipathic CPPs. RRP do not form pores in both artificial and mammalian cellular membranes^{13,84} and small miscible compounds applied simultaneously do not gain access to the intracellular milieu of the cells upon transduction⁸⁵. Consequently, MAPs exert rather strong toxic effects^{16,17,86}, whereas penetratin causes only little membrane perturbations⁸⁶ and TAT and oligo-arginines are well tolerated by living cells^{12,85,86}.

1.3.2. Formation of inverted micelles

The interaction of CPPs with artificial membranes has been the subject of several biophysical studies. The observation by ^{31}P -NMR that penetratin induced micelle formation in artificial membranes led to the assumption that CPPs might translocate biomembranes inside the hydrophilic cavity of inverted micelles⁸⁷⁻⁸⁹. In Fig. 2B the mechanism proposed starts by strong electrostatic interactions of the CPP with the phospholipids or glycolipids, which causes membrane perturbation. The cationic peptide enters the lipid bilayer inside of an inverted micelle and is released in the reverse process into the cytoplasm. Further analysis of the interaction of penetratin with artificial zwitterionic and anionic model membranes revealed that penetratin forms a β -sheet hairpin structure and orients in parallel to the membrane^{75,90}. Penetratin enriches at the lipid water interface and is anchored by its tryptophan residues inside the lipid bilayer. It causes a membrane curvature and from a certain threshold concentration on becomes internalized. The driving force for this event is the electrostatic field created by the differential peptide concentration inside and outside the membrane⁹¹. However, the TAT CPP showed weaker binding to anionic membranes than penetratin, presumably due to the fact, that no hydrophobic amino acid residue is available for anchoring inside the bilayer⁷⁶. A biophysical study compared the CPPs TAT, octa-arginine, octa-lysine, and other amphipathic peptides and their influence on artificial membranes. TAT induced a pronounced isotropic ^{31}P -NMR signal, (indicative of micelles, very small vesicles or cubic phases) in zwitterionic, but not in anionic membranes. Octa-arginine and to a lesser extent octa-lysine had the same effect, whereas other amphiphilic CPPs did not influence the line shape of the ^{31}P -NMR signal. Moreover freeze-fracture electron microscopy indicated that the changes detected by ^{31}P -NMR were due to the formation of rod-like structures on the membrane surface⁷².

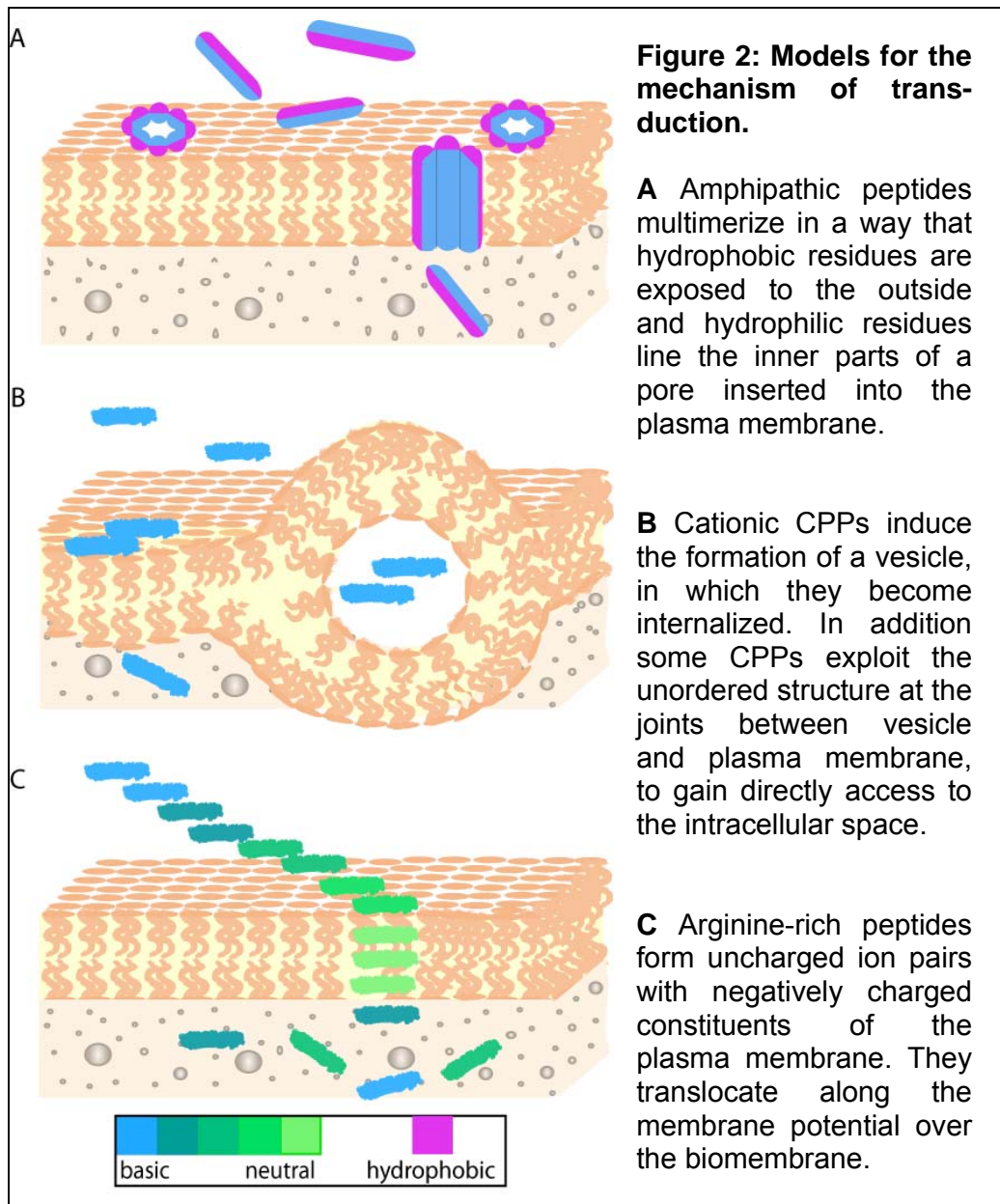
1.3.3. Adaptive translocation

The superior transduction activity of consecutive arginines over the corresponding lysines, histidines and ornithines is mainly dependent on the guanidine function of arginine^{21,78,85}. The efficiency could be enhanced by

using polyarginines prepared from D-amino acids or polyguanidine peptoids with different spacers, comprising at least seven guanidine head groups²¹. Also highly branched guanidinium-rich oligosaccharides or dendrimers were shown to transduce readily^{67,92,93}. In a two-phase partitioning experiment with octanol and water, fluorescent octa-arginine and less efficient octa-ornithine moved after addition of laurylsulfate from the aqueous phase into the octanol layer. As the replacement of the amino functions of arginine with one or two methyl groups diminished the partitioning capacity, these results suggest the efficient formation of lipophilic ion pairs with abundant negatively charged groups, e.g. phospholipids, fatty acid salts and sulfates via bidentate hydrogen bonds^{70,71}, which are able to diffuse into the interior of the hydrophobic lipid bilayer. A recent molecular dynamics simulation with the RRP TAT stated that the interaction of TAT with the phosphate groups on both sides of an artificial lipid bilayer membrane (DOPC) was crucial for translocation⁹⁴.

The driving force for RRP to penetrate living cells was found to be membrane potential dependent. Incubation of living cells with isotonic K⁺-enriched buffer abolished uptake of arginine-rich CPPs^{38,69,70}, likewise pretreatment of cells with the membrane potential increasing antibiotic valinomycin led to higher intracellular concentration of octa-arginine⁷⁰. Hence, the model depicted in Fig 2C can be described as formation of lipophilic ion pairs and their diffusion along the membrane potential inside the cells. This would also imply that the transport is unidirectional and that internalized cargoes remain inside the cell. In addition, cargo-dependent differences in the uptake can be explained because the diffusion rate of higher molecular weight cargoes should be limited, if not prevented by structural constraints.

Likewise several observations of CPPs themselves and TAT fused to globular proteins suggest that the loss of tertiary structure enhances or permits translocation over the cell membrane. This would be equivalent to the import of cytosolic proteins into cell organelles, which also requires unfolding of the



protein to be translocated^{95,96}. The protein dihydrofolatereductase (DHFR) fused to the protein TAT was able to translocate into HeLa cells, but the import failed, when the tertiary structure of DHFR was stabilized by methotrexate, a folate-analogue⁹⁷. In agreement with this observation it was shown that the activity of a variety of proteins genetically fused to the CPP TAT depend on the purification protocol. For TAT-fusion proteins purified under denaturing conditions lower concentrations were sufficient to achieve the same effect than their natively extracted counterparts^{32,98}. For instance, the enzyme Cu-Zn superoxide dismutase fused to TAT was able to prevent paraquat-induced cell damage in a concentration dependent manner when

the purification scheme included denaturation in urea, but had no effect when purified natively⁹⁹. The requirement for unfolding for translocation through the membrane is more relevant for proteins fused to CPPs than for the CPPs themselves and/or fused to short peptides, as the total number of residues in the latter would permit, if at all, the formation of short secondary structures.

1.4. Toxicity of cell penetrating peptides (CPPs)

1.4.1. In vitro

A number of studies have assessed the toxicity of cell penetrating peptides *in vitro*. In general, comparative toxicity studies support the division of CPP into subgroups, namely RRP and amphipathic peptides. Thus, the induction of membrane leakage by amphipathic peptides could be correlated with the hydrophobic moment⁸⁶. The assessment of the toxicity of unmodified CPPs using a LDH-leakage, DiBAC₄(3)-(membrane depolarization) and hemolytic assay showed rather severe toxic effects of MAP and transportan 10 as representatives of the amphipathic CPPs, but only mild effects of the RRP TAT and penetratin¹⁰⁰. Using mouse myoblasts, oligoarginines consisting of minimal five and maximal 12 amino acids at different concentrations were analyzed for transduction and concomitant toxicological effects. Nona-arginine was identified as the oligoarginine of choice, combining high transduction frequencies with low short and long termed toxicological effects⁸⁵. Among the RRP the toxicity decreases in the series oligoarginine>penetratin>TAT^{101,102}. The toxicological properties can be dramatically changed also upon the attachment of low molecular weight cargoes, e.g. labels or other peptides^{101,103}. The toxicity of TAT fused to the anti-apoptotic Nemo-binding domain peptide as well as to the scrambled variant increased the detected toxicity in several cell types 100-fold¹⁰³. As the attachment of high molecular weight cargoes shifts the uptake mechanism to an endocytic pathway only, a reduction in toxicity in these cases most likely reflects the lower amount of bioavailable intracellular CPP-cargo^{37,38,101}.

1.4.2. In vivo

As with *in vitro* cell culture systems, *in vivo* data are difficult to compare due to the variety of CPPs used and the differences between the cargoes attached. In addition, the modes of administration of the CPP-cargoes to the animals and the type of animal used, further complicates a delineation of toxic effects. The RRPp TAT and penetratin alone were shown to reduce p38 mRNA levels in lung tissues after intracheal administration¹⁰⁴. The RRP (RXR)₄^{105,106} (X = 6-aminohexanoic acid) fused to a phosphorodiamidate morpholino oligomer (PMO) cargo was evaluated on the basis of mortality, changes in physical appearance, animal behaviour, body weight and serum biochemistry profile and appeared to be non-toxic below a concentration of 15 mg/kg in Sprague-Dawley rats when administered once by intravenous bolus injection¹⁰⁷. A Grb7 peptidic inhibitor fused to penetratin was intraperitoneally injected into BALB/c nu/nu mice every third day for 4 weeks at 100 mMol / kg and no clinically significant adverse effects as assayed by histological changes in the major tissues became apparent¹⁰⁸. Unfortunately, only few studies to date mention toxicological observations, in addition to the biological effect under study.

1.5 Applications of CPP-mediated intracellular delivery in molecular medicine

The non-invasive CPP-mediated delivery of hydrophilic compounds into living cells bears a tremendous potential for fundamental research as well as for therapeutics. Furthermore, this delivery method is virtually unlimited in the size of the shuttled cargo, provided that endocytically internalized cargoes can be released from endosomes efficiently. In this section, the versatile applicability of CPP-mediated delivery approaches is illustrated on the basis of selected examples.

1.5.1 Labeling and imaging

CPP-mediated delivery has proven useful in labeling cells or subcellular structures. TAT CPP coupled to magnetic nanoparticles was shown to be taken up by CD34⁺ cells^{34,109,110}, which, after intravenous injection into mice, could be tracked *in vivo*. Therefore, endocytic loading of nanoparticles connected to CPPs into particular cells *ex vivo* is a non-invasive cell labeling method allowing subsequent tracking of injected cells *in vivo*¹¹¹. Also TAT linked to the radiolabel ^{99m}Tc and injected intravenously into mice was detectable in all organs, although at higher levels in the liver and the urinary tract¹¹²⁻¹¹⁴. In addition to magnetic and radiolabel TAT-species, delivery of fluorescently labeled CPPs has been used for the visualization of tumor xenografts in mice¹¹⁵. In the latter study, the specific label of the tumor cells was achieved by release of the positively charged CPP from a negatively charged linked peptide via metalloproteinases presented by the tumor cells. Another interesting application of CPPs in animal imaging is the *in vivo* uptake via the skin of the low-molecular weight cargo luciferin coupled to an oligo-arginine CPP transporter into living transgenic mice expressing luciferase. Intracellular luciferin is converted by the luciferase to the photo-emitting form oxyluciferin, which can be detected with a cooled charge-coupled device camera in living animals²⁹.

Peptides fused to CPPs have also been used to specifically label subcellular structures in living cells. The deca-arginine itself was used as a cell permeable marker of the nucleolar compartment in a variety of cells⁶⁸ and the TAT CPP fused to a peptide derived from human ventricular myosin light chain 1 transduced into primary cardiomyocytes and highlighted sarcomeric structures¹¹⁶.

1.5.2 Modulation of intracellular function

1.5.2.1 Drug delivery

Only few groups have worked on the facilitation of delivery of synthetic macromolecules or therapeutics by CPPs. In a transport feasibility study TAT was shown to be able to shuttle a N-(2-hydroxypropyl)methacrylamide

(HPMA) copolymer and the anthracyclin doxorubicin into a human ovarian carcinoma cell line^{117,118}. The same drug and benzylpenicillin fused to the CPP SynB1 were able to cross the blood brain barrier as shown by an *in situ* rat brain perfusion technique after intravenous administration^{119,120}. Cyclosporin A connected to hepta-arginine applied within a lotion entered the epidermis and dermis of murine and human skin. Furthermore, a similar construct that releases cyclosporin A at physiological pH inhibited inflammation in mouse contact dermatitis²⁹.

1.5.2.2 Delivery of peptides and proteins

To date the vast majority of studies using CPP-mediated intracellular delivery, evaluated the uptake of either peptides or proteins into living cells and/or the corresponding effects on intracellular functions. Several studies have focused on their potential use as anti-tumor delivery agents, whereas others deal with their advantage to deliver protective agents in model systems of cellular damage (ischemia, neurodegeneration, etc.).

As a potential tumor therapy agent a peptidic inhibitor of growth factor receptor-bound protein 7, a factor highly expressed in metastatic pancreatic cancer, was fused to penetratin and after frequent intraperitoneal injections into mice containing pancreatic cancer cells, it was shown to diminish the number of metastatic nodules to 2%¹⁰⁸. Also the DNA replication licensing protein geminin shuttled by a novel PTD had an anti-proliferative effect in cultured cancer cells¹²¹. Another example of a potential anti-tumor approach consisted on the delivery of the apoptotic (KLAKLAK)₂, mitochondrial membrane disruptive peptide fused to hepta-arginine, which caused rapid cell death when injected subcutaneously into tumor xenografts in mice¹²².

On the other hand, a large number of studies showed cellular protective effects of various CPP-fusions. Delivery of TAT-BH4 protein and TAT-Bcl-xL peptides prevented apoptosis in models of sepsis¹²³, irradiation¹²⁴ and ischemia or reperfusion¹²⁵. Targeting the JNK pathway with a c-Jun inhibitory peptide fused to TAT minimized the lesion size in a rat model of ischemia. The same peptide was able to cross the blood-brain barrier after intraperitoneal injection¹²⁶. Another neuroprotective TAT-fusion to an isozyme specific

inhibitor of protein kinase C increased the number of microvessels and improved blood flow in a rat model of ischemia. In addition, prophylactic treatment reduced infarct size in hypertensive Dahl rats following an acute stroke. Another study used delivery of a TAT-Cu, Zn-superoxide dismutase to prevent injury caused by reactive oxygen species after transient forebrain ischemia in gerbils ¹²⁷. Besides its anti-inflammatory properties, Cavtratin – a chimera from penetratin and an hydrophobic peptide derived from caveolin-1 – that negatively regulates the activity of endothelial nitric oxide synthase – reduced microvessel permeability ¹²⁸. Intranasal delivery of a STAT-6 derived peptide fused to the CPP PTD₄ reduced lung inflammation in murine models of rhinitis and asthma inhibited many features of allergic airways disease ¹²⁹. Strikingly, frequent TAT-mediated intracellular delivery of the protein purine nucleoside phosphorylase rescued the immunodeficiency and neurodegenerative defects of the respective knock-out mice with no apparent toxicity ¹³⁰.

Finally, uptake of a striated muscle specific human ventricular light chain-1 peptide fused to TAT CPP into living adult rat primary cardiomyocytes and its localization to sarcomeric structures was measured. This cell permeable peptide was able to enhance muscle contractility without affecting the intracellular Ca^{2+} . These properties and the fact that this peptide only has targets in striated muscle, makes it a novel potential therapeutic tool to improve cardiac function ^{116,131}.

1.5.2.3 Delivery of oligonucleotides (ON)

Although CPP-mediated pinocytic delivery is independent of cargo size, the introduction of DNA or RNA seems to be technically more demanding. Due to the complexation of the intrinsically basic CPP with the negatively charged phosphate backbone of nucleic acids, the transducing moiety becomes less available for the interaction with negatively charged membrane constituents, which is crucial for the initiation of the internalization event ¹¹⁵.

Nevertheless, a 16-mer peptide nucleic acid (PNA) stably linked to the CPPs TAT, Transportan and Tp10 inhibited Tat-dependent trans-activation ¹³² and a

18-mer steric block oligonucleotide linked to the CPP R₆-Penetratin enhanced splice correction activity¹³³ in a HeLa cell reporter assay.

The usage of the RNA analogues phosphorodiamidate morpholino oligomers (PMO) replaces the phosphodiester- with a neutral phosphorodiamidate linkage and therefore results in a neutral nucleic acid compound that is resistant to nucleases and RNase H. Conjugated via a thioether linkage to several types of RRP s it redirected the splicing of targeted mRNAs in primary murine leukocytes¹⁹. With a similar alteration in pre-mRNA splicing the excision of a nonsense mutation in exon 23 was skipped in a mouse model of muscular dystrophy and functional dystrophin expression was restored¹³⁴.

Another innovative approach fused TAT to the RNA-binding domain of U1 small nuclear ribonucleoprotein as an adaptor moiety and used this shuttle for delivery of shRNA and si-RNA constructs into CHO cells¹³⁵. A further possibility to shuttle ONs is to use complexes of CPPs with ON at optimized ratios, e.g. to deliver si-RNA^{136,137} into cell culture systems.

1.5.2.4 Gene therapy

CPPs are also capable to aid viral mediated gene delivery *in vitro* and *in vivo*. Penetratin mixed with an adenoviral GFP expressing construct markedly enhanced the infectivity after luminal application into mouse carotid arteries¹³⁸. A recombinant TAT-M₂S (multisubunit DNA binding protein) was mixed with a therapeutical plasmid encoding α -galactosidase A (AGA) and injected into muscles of AGA-knockout mice, suffering from a lysosomal storage disease. This chimera significantly enhanced AGA expression in skeletal muscle in comparison to the DNA injected alone¹³⁹.

2. Results

2.1 Live cell analysis of cell penetration ability and toxicity of oligoarginines



Live-cell analysis of cell penetration ability and toxicity of oligo-arginines[†]

GISELA TÜNNEMANN,^a GOHAR TER-AVETISYAN,^a ROBERT M. MARTIN,^a MARTIN STÖCKL,^b ANDREAS HERRMANN^b and M. CRISTINA CARDOSO^{a*}

^a Max Delbrueck Center for Molecular Medicine, D-13125 Berlin, Germany

^b Institute of Biology/Biophysics, Humboldt University of Berlin, D-10115 Berlin, Germany

Received 9 July 2007; Revised 21 September 2007; Accepted 1 October 2007

Abstract: Cell penetrating peptides (CPPs) are useful tools to deliver low-molecular-weight cargoes into cells; however, their mode of uptake is still controversial. The most efficient CPPs belong to the group of arginine-rich peptides, but a systematic assessment of their potential toxicity is lacking. In this study we combined data on the membrane translocation abilities of oligo-arginines in living cells as a function of their chain length, concentration, stability and toxicity. Using confocal microscopy analysis of living cells we evaluated the transduction frequency of the L-isomers of oligo-arginines and lysines and then monitored their associated toxicity by concomitant addition of propidium iodide. Whereas lysines showed virtually no transduction, the transduction ability of arginines increased with the number of consecutive residues and the peptide concentration, with L-R9 and L-R10 performing overall best. We further compared the L- and D-R9 isomers and found that the D-isomer always showed a higher transduction as compared to the L-counterpart in all cell types. Notably, the transduction difference between D- and L-forms was highly variable between cell types, emphasizing the need for protease-resistant peptides as vectors for drug delivery. Real-time kinetic analysis of the D- and L-isomers applied simultaneously to the cells revealed a much faster transduction for the D-variant. The latter underlies the fact that the isomers do not mix, and penetration of one peptide does not perturb the membrane in a way that gives access to the other peptide. Finally, we performed short- and long-term cell viability and cell cycle progression analyses with the protease-resistant D-R9. Altogether, our results identified concentration windows with low toxicity and high transduction efficiency, resulting in fully bioavailable intracellular peptides. Copyright © 2007 European Peptide Society and John Wiley & Sons, Ltd.

Supplementary electronic material for this paper is available in Wiley InterScience at <http://www.interscience.wiley.com/jpages/1075-2617/suppmat/>

Keywords: arginine-rich peptides; cell cycle; cell penetrating peptides; cell viability; membrane integrity; membrane translocation; oligo-lysines; oligo-arginines

INTRODUCTION

Cell penetrating peptides (CPPs) possess the unique ability to shuttle linked cargoes such as drugs [1], peptides [2–6], proteins [7–9], peptide nucleic acids (PNAs) [10–12] and nanoparticles [13,14] across the plasma membrane which is otherwise virtually impermeable for hydrophilic compounds. CPPs can be subdivided into two major groups: model amphiphilic peptides (MAPs) [15,16] developed on the basis of spatial separation of positively charged and hydrophobic amino acid residues; and arginine-rich peptides (R-RPs) delineated from natively occurring minimal transduction domains of proteins, e.g. TAT from HIV-1 TAT protein [7,17–19] and penetratin from the homeobox of antennapedia protein [20–22]. However, plasma membrane translocation of MAPs structurally requires at

least four helical turns but does not depend on the positively charged amino acid residues [15], whereas the transduction ability of R-RPs depends on a minimum number of arginines [23,24], suggesting that the entry mechanisms of both types of CPPs are unrelated. The translocation ability of R-RPs does not seem to be solely a matter of charge, but has been proposed to reside in the guanidinium group of the arginine itself [25]. The formation of lipophilic ion pairs with abundant sulfate, phosphate or carboxylate groups of membrane constituents via the two amino functions of arginine provides a mechanistic framework for the translocation of a highly charged compound through the plasma membrane [26]. CPP-mediated delivery of cargoes into the cytoplasm can be achieved by at least two independent mechanisms: (i) adsorptive endocytosis and subsequent release of the enclosed compounds from endosomes or lysosomes [7,27–29]; and (ii) rapid crossing of the membrane by a seemingly energy-independent, not-well-understood mechanism referred to as transduction [5,30–32]. Whereas R-RPs coupled

*Correspondence to: M. Cristina Cardoso, Max Delbrueck Center for Molecular Medicine, Robert-Roessle-Str. 10, D-13125 Berlin, Germany; e-mail: cardoso@mdc-berlin.de

[†] This article is part of the Special Issue of the Journal of Peptide Science entitled "2nd workshop on biophysics of membrane-active peptides".

to high-molecular-weight cargoes are restricted to the endocytic mode of uptake [5,33,34], R-RPs themselves or interconnected to low-molecular-weight cargoes have both options. Above a certain concentration (transduction threshold), which varies between 1 and 10 μM depending on the cell type and the size of the cargo [5], R-RPs directly translocate across the plasma membrane into the cell. Several live-cell studies have shown that functional peptides attached to R-RPs exert biological effects after the transduction event [2–6]. Importantly, R-RP-mediated transduction circumvents the inefficient step of release from cytoplasmic vesicles after the endocytic uptake. However, a systematic evaluation of the cell penetration ability, in combination with an assessment of potential short- and long-term toxic effects of R-RPs, is lacking. In this study, we combined data on the membrane translocation abilities of oligo-arginines in living cells as a function of their chain length, concentration, stability and toxicity.

MATERIAL AND METHODS

Peptides

Consecutive arginines (5–12) and lysines (5–12) as L-isomers and TAMRA-R9 and Fluos-R10 also as D-isomers were synthesized and coupled directly to fluorescein (Fluos) or 5,6-TAMRA at the N-terminus by Peptide Specialty Laboratories GmbH (Heidelberg, Germany). The peptides were purified by HPLC and their appropriate masses confirmed by mass spectrometry. The isoelectric points (pI) were estimated using the freeware tool ProtParam.

Cells

All cell types were cultured in Dulbecco's modified Eagle medium (DMEM) with fetal calf serum (FCS) (Life Technologies, Inc., USA) at the following concentrations: C2C12 mouse myoblasts 20%, human HeLa cells 10%, MDCKII dog epithelial kidney cells 10% and BJ-hTERT human fibroblasts 10%. Primary cultures from male WKY rats aged 3 months were performed as described previously [35].

Transduction Experiments

As peptide transduction is influenced by the peptide-to-cell ratio [36], for all transduction experiments μ -Slide VI observation chambers were used (Ibidi, Martinsried, Germany), which guarantee a defined and equal liquid volume above the cells throughout the entire observation channel. The respective cell types were seeded at 70% confluency into the observation chambers and incubated overnight at 37 $^{\circ}\text{C}$ at 5% CO_2 . Special care was taken that cell densities were equal throughout sets of experiments. The oligo-arginines and oligo-lysines were diluted in DMEM medium without FCS to avoid precipitation of the peptides. For the chain-length-dependent transduction assay, 2 $\mu\text{g}/\text{ml}$ propidium iodide (PI) was added directly to the diluted peptide solution prior to the transduction experiment. The culture medium was gently

aspirated from the cells and exchanged against the respective peptide dilutions in a volume of 60 μl . The cells were kept for 1 h in the incubator until imaging at the microscope under the same conditions. For each peptide concentration, between 140 and 250 cells were analyzed and the experiments were performed in duplicate. The images were collected with two different laser settings, one set resulting in images without overexposed signals and one set with higher laser intensities, so that weaker signals could not be missed. The microscope settings per concentration and within these two sets were identical. Acquired images were analyzed visually, and cells unambiguously showing fluorescent signal inside the nucleus were scored as transduced. The graphics were generated using the Origin version 7.5 software (OriginLab Corp., Northampton, USA).

Cell Cycle and Viability Assays

For the modified (3-(4,5-dimethylthiazol-2-yl)-2,5 diphenyl-tetrazolium-bromide (MTT) assay, C2C12 cells were incubated for 2 h with different concentrations of the peptides D-R9 and L-R9. MTT was dissolved at 0.4 mg/ml in DMEM. Subsequently, the cells were washed once, followed by addition of 100 μl of the MTT solution and were returned to the incubator for 5 h. Cells were then analyzed by confocal laser scanning microscopy (CLSM). The transduction frequency was monitored by the fluorescence of the Fluos- or TAMRA-labeled peptides, respectively, and the formation of the blue-violet formazan complex was monitored by excitation with 488 nm and detection in the transmission channel. For each peptide concentration, five fields of view with a 40 \times objective corresponding to a total number of \sim 150 cells were collected. Cells with less formazan signal intensity than the control cells were counted as nonviable.

For the analysis of the plasma membrane integrity during and after transduction, we used 2 $\mu\text{g}/\text{ml}$ PI mixed together with the transducing peptides in DMEM to detect transient pore formation or membrane perturbations, and 0.5% (V/V) trypan blue to distinguish, after the transduction period of 2 h, the cells with permanently compromised membranes. Data were displayed by using Microsoft Excel.

To analyze relatively short-term effects on DNA condensation by the peptides, C2C12 cells were preincubated for 10 min with the DNA dye DRAQ5 (Biostatus Limited, UK) as described [37] and then incubated with different concentrations of the D-R9 peptide. Cells were imaged by CLSM before and after the treatment. Long-term effects on the cell cycle progression were determined by fluorescence activated cell sorting (FACS) analysis of PI-stained C2C12 cells. For this purpose, C2C12 cells were plated onto 150 mm diameter dishes and incubated with different concentrations of the respective peptides at a density of 40% in DMEM for 2 h. Then the medium was replaced by DMEM with 20% FCS and the cells were cultivated for further 16 h until they reached a density of 60%. For FACS analysis the cells were trypsinized, washed with PBS, fixed with ice-cold 90% EtOH, washed with PBS, treated with 0.1 mg/ml RNase and stained with 33 $\mu\text{g}/\text{ml}$ PI, and DNA content was measured with a FACSCalibur (Becton Dickinson). Data were analyzed and plotted with the flow cytometry software FLOWJO (Tree Star, Inc., USA).

Microscopy, Image Acquisition and Analysis

Confocal images were acquired with a Zeiss confocal laser scanning microscope, LSM510 Meta, mounted on an Axiovert 200M inverted microscope equipped with a live-cell microscope incubation cage (Okolab, Italy) using either a 40 \times plan-neofluar NA1.3 or a 63 \times plan-apochromat NA1.4 oil-immersion, phase-contrast objectives. For all settings the main beam splitter was HFT UV/488/543/633, and the specific parameters for the single fluorophores were as follows: Fluos, excited at 488 nm, detected with a 500–530 nm band-pass filter; TAMRA, excited at 543 nm, detected with 565–615 nm band-pass filter; and trypan blue, PI and DRAQ5, excited with 633 nm, detected with 650 nm long-pass filter. Phase contrast images were recorded with excitation at 488 nm and detection in the transmission channel. Laser power for observation was typically 1–5% (488 nm, 25 mW), 50–60% (543 nm, 1 mW) and 3–5% (633 nm, 5 mW) unless otherwise indicated. Settings were adjusted in a way that image pixels were not over- or underexposed with the range indicator function in the Zeiss LSM software version 3.2. To ensure that weak intracellular fluorescence signals of the peptides were not missed, a set of overexposed images were collected in addition.

RESULTS AND DISCUSSION

The decisive role of arginine clusters for translocation over the plasma membrane has been known for some time. Therefore, several studies were aimed at determining the optimal number of arginines or minimal structural requirements that permit efficient transduction. Surprisingly, most of them analyzed either fixed cells [23,24,38] and/or used FACS analysis without a protocol to efficiently remove the cationic peptides sticking to the extracellular side of the plasma membrane [39]. To exclude the above artifacts, we analyzed the transduction frequency of oligo-arginines and -lysines with chain length from 5 to 12 directly by CLSM of living cells. In addition, we compared only data from experiments using the same incubation times for all peptides and at the same cell density and varied only the concentrations for each peptide. Figure 1(A) displays the possible uptake phenotypes of C2C12 mouse myoblasts after addition of the fluorescent peptide for 1 h. The images on the left side, upper panel, show cells that endocytosed the L-R9 peptide incubated at a concentration of 10 μ M, where the fluorescence of the peptide solely resided in cytoplasmic vesicles, and no free cytoplasmic peptide was detectable by means of fluorescence microscopy. The images on the right side, upper panel, depict cells that incorporated L-R6 peptide added at a concentration of 50 μ M with fluorescence detected throughout the cytoplasm and nucleus, which we hereafter refer to as transduction. Cells with mixed phenotypes (Figure 1(A), lower panel) that show in addition to transduction vesicular uptake were also scored as transduced cells. Only the uptake mode of transduction yields peptide available in all intracellular

compartments and, therefore, is able to reach all potential targets. In order to detect any possible membrane perturbations or transient pore formation, the vital dye PI was added to mouse myoblast cultures simultaneously with the oligo-arginines (see scheme in Figure 1(A)). The plots in Figure 1(B) summarize the transduction results for all oligo-arginine peptides. None of the oligo-arginines tested (R5–R12) was able to transduce at a concentration of 0.5, 1 or 5 μ M in a total volume of 60 μ L. Transduction could be observed at 10 μ M for the peptides R8–R12, with frequencies over 50% for the peptides R10–R12. Whereas R5 did not transduce over the whole concentration range tested (between 0.5 to 100 μ M), R6 appeared intracellularly only in 4% of the cells at 50 μ M and 28% at 100 μ M. R7–R9 transduced between 18 and 42% of the cells at 50 μ M and reached frequencies between 75 and 90% at 100 μ M. The peptides R10–R12 transduced already to a level of 70–90% at 10 μ M concentration and the percentage of transduction increased only slightly at 5- or 10-fold higher concentration. In stark contrast, either no or very low frequency of cell penetration could be detected with all the oligo-lysines tested (K5–K12) at an even wider concentration range (data not shown). The uptake of PI by the oligo-arginine transduced cells (Figure 1(B)) indicated severe toxicity only with R8, R10, R11 and R12 at the highest peptide concentration tested (100 μ M) and for R11 and R12 already at 50 μ M. For the transducing peptides with lower chain length, the percentage of PI-stained cells in all cases was below 10%. At 10 μ M, except for R12 all transducing peptides caused no membrane damage that could be detected by simultaneous PI staining. Notably, PI was not observed inside transduced cells by peptides with a low number of arginines or at low concentrations. This fact argues against the formation of transient pores or strong membrane perturbations. Whereas previous studies found an optimum number of consecutive arginines for transduction [24,38], our results support a linear dependence of the transduction frequencies on the number of consecutive arginines. Considering also the PI uptake data, R9 or R10 peptides combine a medium to high transduction level associated with a tolerable toxicity. To verify and extend our live-cell analysis, we selected three oligo-arginine peptides (namely, R5, R7 and R9) and tested their uptake potential into artificial membranes. The R5 peptide was chosen, as it did not transduce into cells, whereas the R7 was able to transduce, albeit at a low level, and R9 was the most efficient while still retaining low toxicity. The 7-nitro-2-1,3-benzoxadiazol-4-yl (NBD) labeled peptides were applied to large unilamellar vesicles (LUVs) and the percentage of transduced peptide over time was measured with a spectrofluorometer after quenching the outer fluorescence with the NBD quencher, dithionite. The percentage of transduction rose with the number of consecutive arginines in a manner

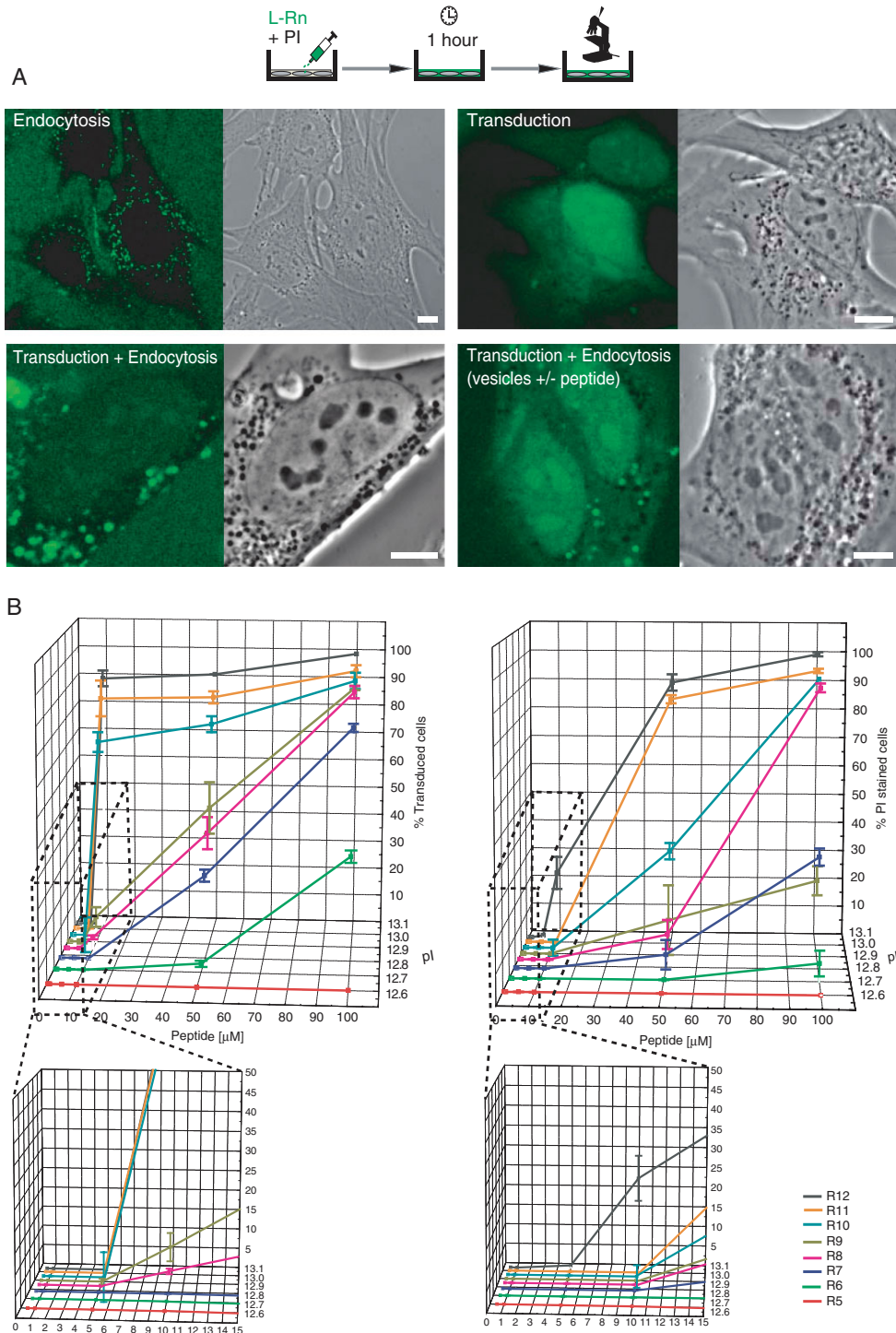


Figure 1 Assessment of dose-dependent transduction frequency of oligo-arginine peptides. (A) Confocal microscopy images displaying examples of endocytic uptake (upper, left panel, L-R9 at 10 μM) versus transduction (upper, right panel, L-R6 at 50 μM) of oligo-arginines (L-Rn; $n = 5-12$) into mouse C2C12 myoblasts. Two mixed forms of transduction + endocytosis are shown below: transduction and endocytic peptide vesicles (left panel L-R9 at 10 μM) versus transduction and peptide enclosed in endocytic vesicles (+) as well as excluded from endocytic vesicles (-) (right panel L-R6 at 50 μM). Scale bars 10 μm . The experimental procedure is shown above. Only cells showing the transduction mode of uptake (including the mixed phenotypes shown in the lower panels) were counted for the quantification in B. (B) The peptide transduction frequency shown as a fraction of C2C12 cells (in %) was scored as explained in A. Peptide transduction frequencies are shown plotted against peptide concentration (0.5, 1, 5, 10, 50, 100 μM) and corresponding estimated isoelectric point (pI). The fraction of PI-stained C2C12 cells (in %) within the transduced cell population is plotted similarly. The lower peptide concentration plots are also shown magnified for better visualization. Error bars display the standard deviation of two independent experiments. The total number of cells counted was between 140 and 250 for each experiment.

analogous to that in the living-cell uptake analyses (Supplementary Figure S1).

Octa-, nona- and deca-arginines have been shown to transduce successfully into living cells under noninvasive conditions and at lower concentrations [31,32,40], but different cell types as well as D- and L-isomers were used in those studies. Therefore, we next assessed the influence of D- and L-isomeric forms on the transduction efficiencies in different cell types. For that purpose, we incubated different cell types of various mammalian species and also primary cells with 10^{-6} M of the TAMRA-labeled D-isomer and the Fluos-labeled L-isomer of R9 and determined the percentage of transduced cells after 1 h incubation (Figure 2(A)). In general, the transduction frequencies for the L-form in all cell types were lower than that of the D-form, illustrating that peptide stability is an important issue for transduction. By calculating the index for the percentage of cells transduced by the L-isomer divided by the percentage of cells transduced by the D-isomer, we found characteristic values for individual cell types, which most

probably reflect their extracellular proteolytic activity [41]. Whereas diploid human fibroblasts were very inefficiently transduced, rat cardiomyocytes and mouse myoblasts showed higher levels of transduction for the L-form, approaching the level of the D-form. As the D-isomer of R9 reached transduction efficiencies of over 95% in all cell types, the isomer-specific differences cannot be due to cell-type-specific membrane composition. The loss of only one arginine from L-R9 would already reduce the transduction efficiency to half at a concentration of 10^{-6} M and lead to the disappearance of the transduction potential with further proteolysis (see plot in Figure 1(B)). To ensure that the different indices were not a result of the distinct fluorescent labels attached to the peptides, the same set of experiments was performed with Fluos-labeled D- and L-isomers of R10 with the same outcome (data not shown). The overview images of the different cell types after transduction also revealed that the fluorescence intensity varied between individual cells. This variation was not correlated to

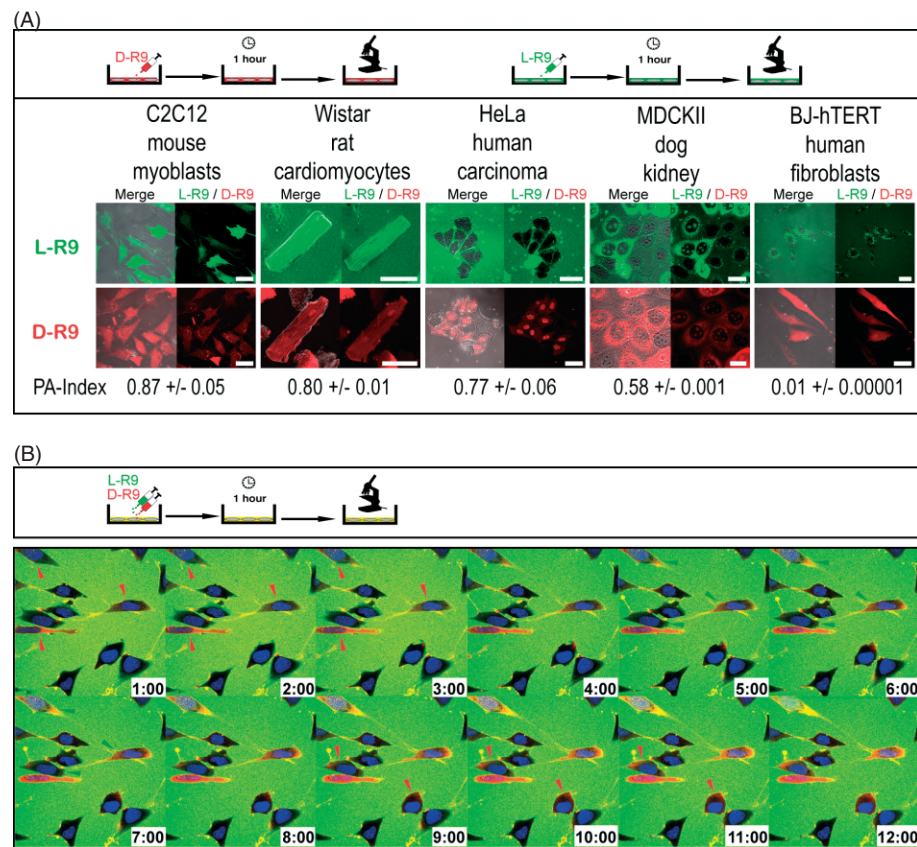


Figure 2 Cell-type-specific differences in transduction frequencies and kinetics of L- and D-isomers of R9. (A) Confocal microscopy sections of different cell types from various mammalian species 1 h after application of 10^{-6} M of the Fluos-labeled L-isomer (upper panel, green fluorescence) and the TAMRA-labeled D-isomer (lower panel, red fluorescence) of R9. For each cell type, merge images of phase contrast and fluorescence and fluorescence images alone are displayed. The index corresponds to the ratio (% transduced cells by L-isomer/% transduced cells by D-isomer) \pm standard deviation. (B) Confocal microscopy time lapse (minutes:seconds) of the transduction of the L- and D-isomers of R9 simultaneously applied to C2C12 mouse myoblasts at a concentration of 10^{-6} M each. Red and green arrowheads indicate the initial detection of the transduced corresponding peptides in intracellular compartments. The cells are counterstained with the live-cell DNA dye DRAQ5 (blue). Scale bar 50 μ m.

the size and, therefore, to the total accessible membrane surface of the transduced cells. Next, we tested whether kinetic differences between the transduction of D- and L-isomers occurred. For this, we applied 20 μM of a 1:1 mixture onto mouse myoblasts and monitored the uptake in real time by CLSM. Surprisingly, several cells selectively took up the TAMRA-labeled D-isomer but not the Fluos-labeled L-form, although some cells also showed yellow color seen in the overlay of the two fluorescence images (Figure 2(B) and Movie 1). Nevertheless, the kinetics of transduction was quite different for both isomers, even though after a certain time both species had been internalized. This result argues against the formation of mixed D- and L-isomers into multimeric assemblies. We can, however, not rule out the existence of single-species multimers. In addition, no change in the transduction efficiency of the individual D- or the L- chiral forms was observed, which would be expected from the higher total peptide concentration. Finally, these data clearly show the absence of membrane damage by the penetration of one peptide species since the other species in the same cell at the same time was not taken up concomitantly.

In view of the therapeutic potential of peptide vectors for the delivery of low-molecular-weight compounds and considering the relatively high transduction rate and low percentage of PI-stained cells (Figure 1(B) and 2), we selected the nondegradable D-isomer of R9 for further detailed analysis of toxicity on mouse myoblasts. Transduction was observed starting from a concentration threshold of 5 μM with a transduction frequency of about 10% (Figure 3(A)). Ten micromolar D-R9 was transduced into more than 50%, and 25 μM into 70% of the cells. For concentrations of 50 and 100 μM , transduction was nearly complete. Next, we examined the viability of mouse myoblasts after 2 h of incubation with different concentrations with D-R9. The ability of the cells to exclude the vital dye trypan blue was used to judge membrane integrity. Furthermore, we assessed by an MTT assay whether the transduction of D-R9 influences enzymatic activities inside the cells detected here by their ability to produce formazan [42]. Starting from the transduction threshold of 5 μM , a constant decrease in viability by both assays was observed, which was mild between 5 and 25 μM peptide concentration. At a concentration of 50 μM , about 17% of the cells stained positive for trypan blue, and 15% of the cells produced formazan to a lesser extent than the controls. Cell death in 60% of cells resulted from 100 μM of D-R9, and also the formazan levels of those cells were greatly reduced in comparison to the control cells. The slope of the trypan blue exclusion curve is steeper than that of the viability assayed by the MTT test, indicating that the membranes are the first location where massive damage occurs. Arginine-rich clusters can be found in RNA-binding proteins and are targeted to the nuclear compartment. To test long-term

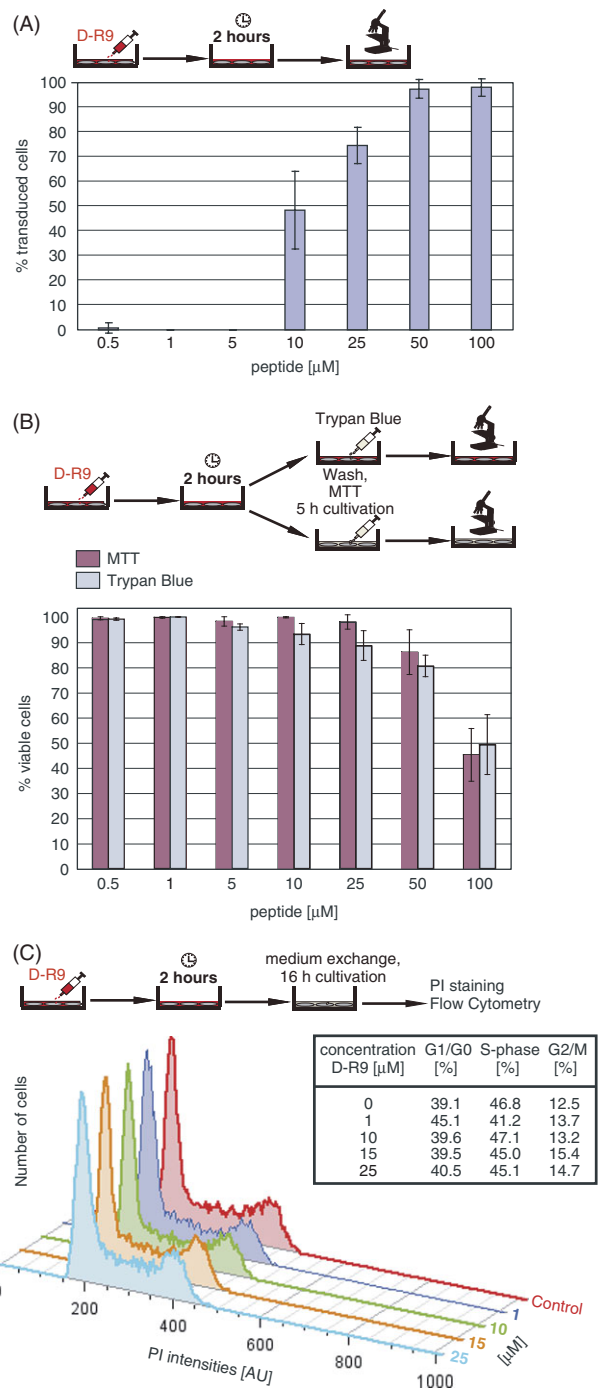


Figure 3 Short- and long-term dose-dependent effects of D-R9 transduction on cell viability and proliferation. (A) Transduction frequencies of D-R9 in C2C12 mouse myoblasts determined as in Figure 1. (B) Cell viability determined by trypan blue exclusion and enzymatic activity MTT assay after 2 h of incubation with different concentrations of D-R9. (C) Long-term effects on the cell cycle distribution assayed by flow cytometry analysis of DNA content stained with PI. The respective experiments are explained in the schemes. For (A) and (B) the error bars display the standard deviation of two independent experiments. The total number of cells counted was between 140 and 250 for each experiment. In (C), one example of three independent experiments is depicted.

effects on DNA replication and cell cycle progression, mouse myoblasts were incubated for 2 h with the D-R9 peptide, the medium was exchanged and they were kept in culture until the next day. Cultures were then fixed, DNA was stained with PI and the cell cycle distribution was analyzed by flow cytometry. The cell cycle profiles and the statistics are displayed in Figure 3(C) and show no concentration-dependent effect of the D-R9 peptide on the cell cycle. Altogether, the toxicological effects of the D-R9 peptide in a range of 5–25 μM can be classified as mild and cell proliferation was also not affected.

CONCLUSIONS

In summary, we evaluated the transduction frequency of the L-isoforms of oligo-arginines and monitored their associated toxicity. This risk-benefit analysis of transduction led us to the selection of R9 for further analysis. With its nondegradable counterpart D-R9, we established an assay that allows the quantification of the proteolytic activity of different cell types, and emphasize the need for protease-resistant peptides as vectors for drug delivery. Importantly, the D-isoform always showed a higher transduction as compared to the L-counterpart in all cell types. The transduction difference between D- and L-forms was highly variable between cell types. Finally, our toxicity results indicate concentration windows with low toxicity and high transduction efficiency, not requiring further treatments to force endocytic vesicle rupture.

Supplementary Material

Supplementary electronic material for this paper is available in Wiley InterScience at: <http://www.interscience.wiley.com/jpages/1075-2617/suppmat/>

Acknowledgements

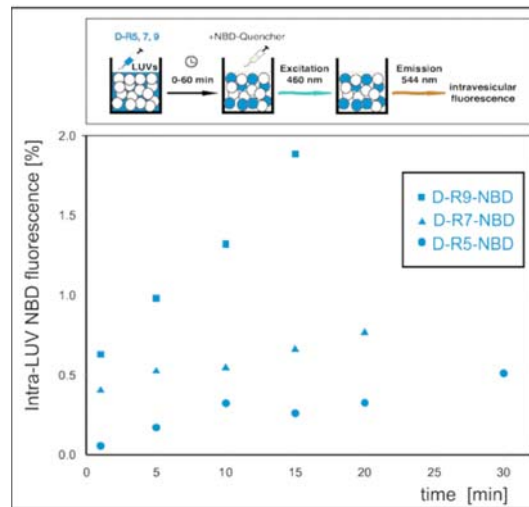
We thank I. Kocman for help with the flow cytometry, P. Domaing for excellent technical assistance and F. Witzel for her participation at the earlier stages of this project. G.T. was supported in part by the European Union (ESF Program). This work was funded by grants of the Deutsche Forschungsgemeinschaft and the Volkswagen Foundation to M.C.C.

REFERENCES

- Nori A, Jensen KD, Tijerina M, Kopeckova P, Kopecek J. Tat-conjugated synthetic macromolecules facilitate cytoplasmic drug delivery to human ovarian carcinoma cells. *Bioconjugate Chem.* 2003; **14**: 44–50.
- Chen CH, Gray MO, Mochly-Rosen D. Cardioprotection from ischemia by a brief exposure to physiological levels of ethanol: role of epsilon protein kinase C. *Proc. Natl. Acad. Sci. U.S.A.* 1999; **96**: 12784–12789.
- Choi M, Rolle S, Wellner M, Cardoso MC, Scheidereit C, Luft FC, Kettritz R. Inhibition of NF-kappaB by a TAT-NEMO-binding domain peptide accelerates constitutive apoptosis and abrogates LPS-delayed neutrophil apoptosis. *Blood* 2003; **102**: 2259–2267.
- Rohrbach S, Muller-Werdan U, Werdan K, Koch S, Gellerich NF, Holtz J. Apoptosis-modulating interaction of the neuregulin/erbB pathway with anthracyclines in regulating Bcl-xS and Bcl-xL in cardiomyocytes. *J. Mol. Cell. Cardiol.* 2005; **38**: 485–493.
- Tünnemann G, Martin RM, Haupt S, Patsch C, Edenhofer F, Cardoso MC. Cargo-dependent mode of uptake and bioavailability of TAT-containing proteins and peptides in living cells. *FASEB J.* 2006; **20**: 1775–1784.
- Tünnemann G, Karczewski P, Haase H, Cardoso MC, Morano I. Modulation of muscle contraction by a cell permeable peptide. *J. Mol. Med.* (in press). DOI: 10.1007/s00109-007-0238-6.
- Fawell S, Seery J, Daikh Y, Moore C, Chen LL, Pepinsky B, Barsoum J. Tat-mediated delivery of heterologous proteins into cells. *Proc. Natl. Acad. Sci. U.S.A.* 1994; **91**: 664–668.
- Nagahara H, Vocero-Akbani AM, Snyder EL, Ho A, Latham DG, Lissy NA, Becker-Hapak M, Ezhevsky SA, Dowdy SF. Transduction of full-length TAT fusion proteins into mammalian cells: TAT-p27Kip1 induces cell migration. *Nat. Med.* 1998; **4**: 1449–1452.
- Schwarze SR, Ho A, Vocero-Akbani A, Dowdy SF. *In vivo* protein transduction: delivery of a biologically active protein into the mouse. *Science* 1999; **285**: 1569–1572.
- Oehlke J, Wallukat G, Wolf Y, Ehrlich A, Wiesner B, Berger H, Bienert M. Enhancement of intracellular concentration and biological activity of PNA after conjugation with a cell-penetrating synthetic model peptide. *Eur. J. Biochem.* 2004; **271**: 3043–3049.
- Turner JJ, Ivanova GD, Verbeure B, Williams D, Arzumanov AA, Abes S, Lebleu B, Gait MJ. Cell-penetrating peptide conjugates of peptide nucleic acids (PNA) as inhibitors of HIV-1 Tat-dependent trans-activation in cells. *Nucleic Acids Res.* 2005; **33**: 6837–6849.
- Wolf Y, Pritz S, Abes S, Bienert M, Lebleu B, Oehlke J. Structural requirements for cellular uptake and antisense activity of peptide nucleic acids conjugated with various peptides. *Biochemistry* 2006; **45**: 14944–14954.
- Santra S, Yang H, Stanley JT, Holloway PH, Moudgil BM, Walter G, Mericle RA. Rapid and effective labeling of brain tissue using TAT-conjugated CdS:Mn/ZnS quantum dots. *Chem. Commun.* 2005; **25**: 3144–3146.
- Lewin M, Carlesso N, Tung CH, Tang XW, Cory D, Scadden DT, Weissleder R. Tat peptide-derivatized magnetic nanoparticles allow in vivo tracking and recovery of progenitor cells. *Nat. Biotechnol.* 2000; **18**: 410–414.
- Scheller A, Oehlke J, Wiesner B, Dathe M, Krause E, Beyer-mann M, Melzig M, Bienert M. Structural requirements for cellular uptake of alpha-helical amphipathic peptides. *J. Pept. Sci.* 1999; **5**: 185–194.
- Oehlke J, Scheller A, Wiesner B, Krause E, Beyer-mann M, Klauschen E, Melzig M, Bienert M. Cellular uptake of an alpha-helical amphipathic model peptide with the potential to deliver polar compounds into the cell interior non-endocytically. *Biochim. Biophys. Acta* 1998; **1414**: 127–139.
- Frankel AD, Pabo CO. Cellular uptake of the tat protein from human immunodeficiency virus. *Cell* 1988; **55**: 1189–1193.
- Green M, Loewenstein PM. Autonomous functional domains of chemically synthesized human immunodeficiency virus tat trans-activator protein. *Cell* 1988; **55**: 1179–1188.
- Vives E, Brodin P, Lebleu B. A truncated HIV-1 Tat protein basic domain rapidly translocates through the plasma membrane and accumulates in the cell nucleus. *J. Biol. Chem.* 1997; **272**: 16010–16017.
- Perez F, Joliot A, Bloch-Gallego E, Zahraoui A, Triller A, Prochiantz A. Antennapedia homeobox as a signal for the cellular internalization and nuclear addressing of a small exogenous peptide. *J. Cell Sci.* 1992; **102**: 717–722.

21. Joliot A, Le Roux I, Volovitch M, Bloch-Gallego E, Prochiantz A. Neurotrophic activity of a homeobox peptide. *Prog. Neurobiol.* 1994; **42**: 309–311.
22. Derossi D, Joliot AH, Chassaing G, Prochiantz A. The third helix of the Antennapedia homeodomain translocates through biological membranes. *J. Biol. Chem.* 1994; **269**: 10444–10450.
23. Suzuki T, Futaki S, Niwa M, Tanaka S, Ueda K, Sugiura Y. Possible existence of common internalization mechanisms among arginine-rich peptides. *J. Biol. Chem.* 2002; **277**: 2437–2443.
24. Futaki S, Goto S, Sugiura Y. Membrane permeability commonly shared among arginine-rich peptides. *J. Mol. Recognit.* 2003; **16**: 260–264.
25. Rothbard JB, Kreider E, VanDeusen CL, Wright L, Wylie BL, Wender PA. Arginine-rich molecular transporters for drug delivery: role of backbone spacing in cellular uptake. *J. Med. Chem.* 2002; **45**: 3612–3618.
26. Rothbard JB, Jessop TC, Wender PA. Adaptive translocation: the role of hydrogen bonding and membrane potential in the uptake of guanidinium-rich transporters into cells. *Adv. Drug Delivery Rev.* 2005; **57**: 495–504.
27. Ferrari A, Pellegrini V, Arcangeli C, Fittipaldi A, Giacca M, Beltram F. Caveolae-mediated internalization of extracellular HIV-1 tat fusion proteins visualized in real time. *Mol. Ther.* 2003; **8**: 284–294.
28. Wadia JS, Stan RV, Dowdy SF. Transducible TAT-HA fusogenic peptide enhances escape of TAT-fusion proteins after lipid raft macropinocytosis. *Nat. Med.* 2004; **10**: 310–315.
29. Richard JP, Melikov K, Brooks H, Prevot P, Lebleu B, Chernomordik LV. Cellular uptake of unconjugated TAT peptide involves clathrin-dependent endocytosis and heparan sulfate receptors. *J. Biol. Chem.* 2005; **280**: 15300–15306.
30. Ziegler A, Nervi P, Durrenberger M, Seelig J. The cationic cell-penetrating peptide CPP(TAT) derived from the HIV-1 protein TAT is rapidly transported into living fibroblasts: optical, biophysical, and metabolic evidence. *Biochemistry* 2005; **44**: 138–148.
31. Fretz MM, Penning NA, Al-Taei S, Futaki S, Takeuchi T, Nakase I, Storm G, Jones AT. Temperature-, concentration- and cholesterol-dependent translocation of L- and D-octa-arginine across the plasma and nuclear membrane of CD34+ leukaemia cells. *Biochem. J.* 2007; **403**: 335–342.
32. Duchardt F, Fotin-Mleczek M, Schwarz H, Fischer R, Brock R. A comprehensive model for the cellular uptake of cationic cell-penetrating peptides. *Traffic* 2007; **8**: 848–866.
33. Silhol M, Tyagi M, Giacca M, Lebleu B, Vives E. Different mechanisms for cellular internalization of the HIV-1 Tat-derived cell penetrating peptide and recombinant proteins fused to Tat. *Eur. J. Biochem.* 2002; **269**: 494–501.
34. Maiolo JR, Ferrer M, Ottinger EA. Effects of cargo molecules on the cellular uptake of arginine-rich cell-penetrating peptides. *Biochim. Biophys. Acta* 2005; **1712**: 161–172.
35. Alvarez J, Hamplova J, Hohaus A, Morano I, Haase H, Vassort G. Calcium current in rat cardiomyocytes is modulated by the carboxyl-terminal ahnak domain. *J. Biol. Chem.* 2004; **279**: 12456–12461.
36. Hallbrink M, Oehlke J, Papsdorf G, Bienert M. Uptake of cell-penetrating peptides is dependent on peptide-to-cell ratio rather than on peptide concentration. *Biochim. Biophys. Acta* 2004; **1667**: 222–228.
37. Martin RM, Leonhardt H, Cardoso MC. DNA labeling in living cells. *Cytometry A* 2005; **67**: 45–52.
38. Futaki S, Suzuki T, Ohashi W, Yagami T, Tanaka S, Ueda K, Sugiura Y. Arginine-rich peptides. An abundant source of membrane-permeable peptides having potential as carriers for intracellular protein delivery. *J. Biol. Chem.* 2001; **276**: 5836–5840.
39. Goun EA, Pillow TH, Jones LR, Rothbard JB, Wender PA. Molecular transporters: synthesis of oligoguanidinium transporters and their application to drug delivery and real-time imaging. *ChemBiochem* 2006; **7**: 1497–1515.
40. Martin RM, Tünnemann G, Leonhardt H, Cardoso MC. Nucleolar marker for living cells. *Histochem. Cell Biol.* 2007; **127**: 243–251.
41. Trehin R, Nielsen HM, Jahnke HG, Krauss U, Beck-Sickinger AG, Merkle HP. Metabolic cleavage of cell-penetrating peptides in contact with epithelial models: human calcitonin (hCT)-derived peptides, Tat(47–57) and penetratin(43–58). *Biochem. J.* 2004; **382**: 945–956.
42. Mosmann T. Rapid colorimetric assay for cellular growth and survival: application to proliferation and cytotoxicity assays. *J. Immunol. Methods* 1983; **65**: 55–63.

Supplementary figure 1

**Supplemental figure legend:****Supplementary Figure 1 Penetration of artificial membranes by oligo-arginines.**

LUVs (Large Unilamellar Vesicles) were prepared from a mixture from 70 mol% of DOPC (dioleoylphosphatidylcholine) and 30 mol% of DOPS (dioleoylphosphatidylserine). In total 1 μmol of lipids were mixed in chloroform. A dry lipid film was formed by solvent evaporation under a nitrogen stream. The dried lipids were resolubilized in 2 ml of PBS (pH 7.4) by 5 min of vortexing. To yield LUVs the lipid suspension was processed by freeze/thaw-cycles (5x) and extrusion through a 0.1 μm filter (10x). Consecutive arginines (R5, R7, R9) as D-isomers were synthesized and coupled directly to the NBD (7-nitro-2-1,3-benzoxadiazol-4-yl)-group at the N-terminus by Peptide Specialty Laboratories GmbH (Heidelberg, Germany). For the quenching assay 740 μl of PBS were mixed with 60 μl of LUV suspension and incubated with the NBD-labeled peptides at 5 μM for different time spans. NBD fluorescence from peptides remaining in the exterior of the LUVs was then quenched by adding 25 mM of the non membrane permeable sodium dithionite. Fluorescence was detected with a FluoroMax-4-spectrofluorometer (Horiba Jobin Yvon, Edison, USA). NBD was excited at 460 nm and the fluorescence was recorded at 544 nm. For measuring the maximal quenchable fluorescence of the peptides present in the exterior and also in the interior of the LUVs, 0.5 % Triton X-100 was added afterwards to dissolve the vesicles. Counts for total fluorescence and fluorescence after quenching were corrected by subtracting this non-quenchable fraction. The intravesicular peptide in LUVs was displayed as percentage of total fluorescence after dithionate quenching for the different NBD-peptides (\bullet) R5-NBD, (\blacktriangle) R7-NBD and (\blacksquare) R9-NBD. At a first glance the percentage of transduction as measured by the non-quenched intra-LUV peptide fluorescence seemed to be low in comparison to the experiments in living cells. However, under our experimental conditions the total volume of LUVs corresponded to about 0.2 % of the suspension volume assuming a LUV diameter of 100 nm and a surface area of lipids of 0.6 nm^2 . In the light of this estimate the results indicate an enrichment of peptides in the lumen of LUVs at least for R9.

2.2 Cell entry of arginine-rich peptides is independent of endocytosis

Cell Entry of Arginine-rich Peptides Is Independent of Endocytosis^{*[5]}

Received for publication, July 21, 2008, and in revised form, November 11, 2008. Published, JBC Papers in Press, December 1, 2008, DOI 10.1074/jbc.M805550200

Gohar Ter-Avetisyan[‡], Gisela Tünnemann[‡], Danny Nowak[‡], Matthias Nitschke[§], Andreas Herrmann[§], Marek Drab[¶], and M. Cristina Cardoso^{†||}

From the [‡]Max Delbrueck Center for Molecular Medicine, D-13125 Berlin, the [§]Department of Biology/Biophysics, Humboldt University Berlin, D-10115 Berlin, the [¶]Department of Molecular Biology, Max Planck Institute for Infection Biology, D-10117 Berlin, and the ^{||}Department of Biology, Technische Universität Darmstadt, D-64287 Darmstadt, Germany

Arginine-rich peptides are a subclass of cell-penetrating peptides that are taken up by living cells and can be detected freely diffusing inside the cytoplasm and nucleoplasm. This phenomenon has been attributed to either an endocytic mode of uptake and a subsequent release from vesicles or to direct membrane penetration (transduction). To distinguish between both possibilities, we have blocked endocytic pathways suggested to be involved in uptake of cell-penetrating peptides. We have then monitored by confocal microscopy the uptake and distribution of the cell-penetrating transactivator of transcription (TAT) peptide into living mammalian cells over time. To prevent side effects of chemical inhibitors, we used genetically engineered cells as well as different temperature. We found that a knock-down of clathrin-mediated endocytosis and a knock-out of caveolin-mediated endocytosis did not affect the ability of TAT to enter cells. In addition, the TAT peptide showed the same intracellular distribution throughout the cytoplasm and nucleus as in control cells. Even incubation of cells at 4 °C did not abrogate TAT uptake nor change its intracellular distribution. We therefore conclude that this distribution results from TAT peptide that directly penetrated (transduced) the plasma membrane. The formation of nonselective pores is unlikely, because simultaneously added fluorophores were not taken up together with the TAT peptide. In summary, although the frequency and kinetics of TAT transduction varied between cell types, it was independent of endocytosis.

The discovery that the transactivator of transcription (TAT)² protein of human immunodeficiency virus type 1 was able to

* This work was supported by grants from the Deutsche Forschungsgemeinschaft and the Volkswagen Foundation (to M. C. C.). The costs of publication of this article were defrayed in part by the payment of page charges. This article must therefore be hereby marked "advertisement" in accordance with 18 U.S.C. Section 1734 solely to indicate this fact.

Author's Choice—Final version full access.

[5] The on-line version of this article (available at <http://www.jbc.org>) contains supplemental Figs. S1–S5 and Movies 1–10.

¹ To whom correspondence should be addressed. Tel.: 49-6151-16-2377; Fax: 49-6151-16-2375; E-mail: Cardoso@bio.tu-darmstadt.de.

² The abbreviations used are: TAT, transactivator of transcription; BHK, baby hamster kidney; cav, caveolin; CHC, clathrin heavy chain; CPP, cell-penetrating peptide; DMEM, Dulbecco's modified Eagle's medium; FCS, fetal calf serum; FITC, fluorescein isothiocyanate; HIV, human immunodeficiency virus; KO, knockout; LMW, low molecular weight; PTD, protein transduction domain; RRP, arginine-rich peptide; TAMRA, 5,6-carboxytetramethylrhodamine; TAT-bt-SAv, TAT-biotin-streptavidin complex; tet, tetracycline; Tf, transferrin; tTA, transcriptional activator; WT, wild type.

traverse cellular membranes and subsequently affected gene transcription (1, 2) led to the emergence of a new research field on cell-penetrating peptides (CPPs), also known as protein transduction domains (PTDs) or membrane transduction peptides (3). CPPs opened up the possibility to effectively deliver cell-impermeable hydrophilic compounds into living cells. The cargos reported to be shuttled to intracellular compartments include drugs (4), fluorophores (5), peptides (6–8), nucleic acids (9), proteins (10–12), nanoparticles (13), and liposomes (14, 15). The exact mechanism of cellular entry of CPPs remained unknown, but it was thought to be receptor-, energy-, and temperature-independent. In 2003 this unique mode of uptake was refuted as a methodological artifact, and endocytosis was suggested as the main pathway of cellular uptake of CPPs in live cells (16, 17). Arginine-rich peptides (RRPs) were not only historically the first (TAT) (1, 2) type of CPPs described, but they combined high uptake ability with moderate toxicity (18). Some groups observed a nonendocytic internalization pathway (8, 18–21), whereas others assigned CPP uptake to endocytic pathways, as CPPs were internalized and stored inside the vesicles. Endocytosis is broadly subdivided into phagocytosis and pinocytosis. Whereas phagocytosis is restricted to specialized cells like macrophages and leukocytes, pinocytosis occurs in all eukaryotic (or mammalian) cell types through at least four different endocytic pathways (22). Three of them have been implicated as routes for internalization depending on the CPP sequence and cargo of the CPPs as follows: clathrin-mediated endocytosis (23), caveolae-mediated endocytosis (24, 25), macropinocytosis (26–28), as well as the involvement of more than one endocytic pathway (16, 19). However, most of the studies so far utilized chemical inhibitors to characterize the contribution of a distinct endocytic pathway and could not exclude inhibitor-associated side effects.

RRPs such as TAT linked to high molecular weight cargos (e.g. proteins) were taken up into cells solely by endocytosis. When conjugated to low molecular weight cargos (e.g. peptides) however, in addition to be present in vesicles, they could be found freely diffusing in the cytoplasm and the nuclear compartment (8). However, a consensus regarding the latter uptake mode has not been reached. Our translocation studies of oligoarginines and oligolysines of various chain lengths and concentrations into living cells demonstrated the coexistence of two uptake modes (8, 18). Whereas a subset of the intracellular peptide was found inside cytoplasmic vesicles (Fig. 1A), some of the peptide displayed a rather homogeneous distribution

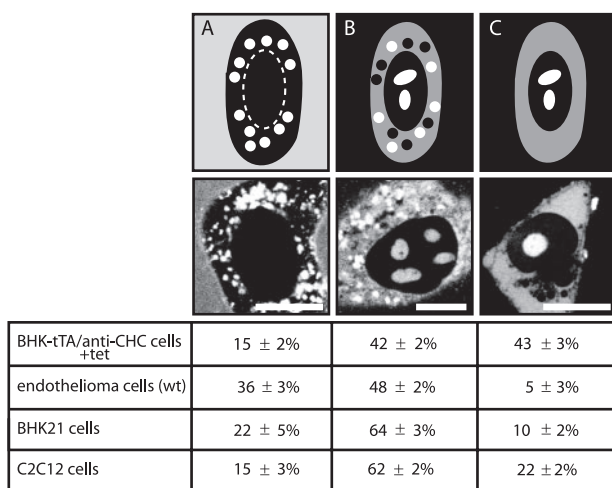


FIGURE 1. Schematic illustration (upper panel), corresponding representative cell images, and relative proportions of the observed intracellular distributions of TAT CPP in different cell types after 1 h of incubation. A, TAT peptide is present in the medium and in endocytic vesicles, but not freely available inside the cytoplasm or the nuclear compartment. B, TAT peptide reached all intracellular compartments and accumulated, in addition, in vesicles. C, TAT peptide is homogeneously distributed throughout the cytoplasm and accumulated in the nucleolus. Scale bar, 10 μ m.

throughout the cytoplasm and high accumulation inside the nucleolar compartment (Fig. 1, B and C). The latter is henceforth termed transduction. It is still unclear whether transduction reflects CPPs that enter living cells by a not yet defined mechanism and/or CPPs that are released from endo- or lysosomes after endocytosis. To understand if both intracellular phenotypes are two distinct intermediate stages of the same process or indicate different uptake routes, we monitored the cytoplasmic and nucleolar localization of RRP upon inhibition of endocytosis. In addition to TAT, we used the peptide PTD₄, which is an artificial, more amphipathic CPP with a reduced number of arginines and increased α -helical content compared with TAT (29). Most importantly, to suppress endocytic pathways, we restricted ourselves to the usage of genetically inducible systems, knock-out (KO) cell cultures, or physical methods, thus avoiding any potential side effects of chemical inhibitors of endocytosis.

EXPERIMENTAL PROCEDURES

Cells and Culture Conditions—The following cells were used: BHK21 (C-13) fibroblasts (baby hamster kidney clone 13, American Type Culture Collection), BHK21-tTA/anti-clathrin heavy chain (CHC) cell line (30), cav-1-KO and cav-1-wt mouse endothelioma cell lines (31), C2C12 mouse myoblasts (32), and 3T3 mouse fibroblasts (Invitrogen). The cells were cultured in Dulbecco's modified Eagle's medium (high glucose, with sodium pyruvate and L-glutamine) (PAA, Pasching, Austria) supplemented with 10 or 20% (the latter for C2C12 cells only) fetal calf serum (PAA, Pasching, Austria), 2 mM L-glutamine (Invitrogen), 50 μ g/ml gentamicin (PAA, Pasching, Austria). For the cav-1-KO and cav-1 wild type (WT) endothelioma cell lines, the growth media was additionally supplemented with 1% nonessential amino acids (Sigma), 1% sodium pyruvate (Invitrogen), and 2 mM 2-mercaptoethanol diluted in phosphate-buffered saline (Invitrogen). For the BHK21-tTA/anti-

CHC cell line, the following additives were added: 10% tetracycline-negative fetal calf serum (PAA, Pasching, Austria), 0.2 mg/ml geneticin (G418, Invitrogen), 0.5 μ g/ml puromycin (Sigma), 2 μ g/ml tetracycline (Sigma). For the induction of CHC antisense RNA expression, tetracycline was removed from the medium.

Peptides, Proteins, and Fluorophores—Peptides 5,6-carboxytetramethylrhodamine (TAMRA)-TAT (GRKKRRQRRR) and TAMRA-PTD₄ (YARAARQARA) (29) were synthesized as D-isomers and coupled directly to TAMRA at the N terminus (Peptide Specialty Laboratories GmbH, Heidelberg, Germany). Peptides and labels were diluted in RPMI 1640 medium without phenol red (PAA, Pasching, Austria) and applied at 10 μ M final concentration to the cells. At lower concentrations, as we have shown previously (8), only the endocytic mode of uptake was detected (supplemental Fig. S1). To monitor CHC expression and function, transferrin (Tf) conjugated to Alexa Fluor 633 (Invitrogen) was added as a marker for clathrin-dependent endocytosis. Nonreactive forms of the fluorophores FITC (fluorescein isothiocyanate) and TAMRA were generated by incubation with Tris buffer (indicated by an asterisk) and used as a small molecule to monitor the generation of pores during the transduction event. To control for the complete inhibition of endocytosis at 4 $^{\circ}$ C, the globular protein TAT-biotin-streptavidin (TAT-bt-SAv) labeled with the fluorophore cyanine dye was used as an additional marker for fluid-phase uptake (supplemental Fig. S2).

Live Cell Uptake Experiments—For all experiments either 8-well μ -slides or 35-mm μ -dishes (Ibidi, Martinsried, Germany) were used. The cells were seeded onto the observation chambers and incubated overnight at 37 $^{\circ}$ C with 5% CO₂. The peptides TAMRA-TAT and TAMRA-PTD₄ (10 μ M), the fluorophores FITC* and TAMRA* (10 μ M), and Tf (10 μ g/ml) were diluted in RPMI 1640 medium (PAA, Pasching, Austria) without phenol red and used at the indicated concentrations. Special care was taken to ensure that the volume of the peptide solution above the cells was comparable in the two different observation chambers and that the exchange against the appropriate peptide (label, marker) dilutions was performed very gently. Immediately after addition of the peptide (label, marker) to the cells, time lapses over 60 min (with time intervals of one image per min) were recorded. The experimental settings for the confocal microscope were identical for all experiments.

For the uptake experiments at 4 $^{\circ}$ C a custom-built cooling chamber was used. The height of this cooling chamber occupying the cooling flow and the radius of the loophole at the bottom were optimized to guarantee a constant temperature exchange between the 35-mm μ -dish observation chamber and the cool water flux. The temperature was regulated by a thermostat, and the exact temperature of 4 $^{\circ}$ C inside the medium above the cells was verified by measurements with a thermometer before and after the 1-h time lapses.

Microscopy, Image Acquisition, and Analysis—Confocal optical sections were acquired with a Zeiss confocal laser scanning microscope, LSM510 Meta, mounted on an Axiovert 200 M inverted microscope equipped with a live cell microscope incubation cage (Okolab, Ottaviano, Italy) using a 63 \times plan-apochromat NA1.4 oil immersion, phase-contrast objective.

TAT Transduction Occurs in the Absence of Endocytosis

The microscope incubation cage maintained a humidified atmosphere of 5% CO₂ and 37 °C, which was used throughout except for the low temperature experiments. For all settings the main beam splitter was HFT UV/488/543/633, and the specific parameters for the single fluorophores were as follows: FITC excited at 488 nm, detected with a 500–530-nm bandpass filter; TAMRA-TAT and TAMRA-fluorophore excited at 543 nm, detected with a 565–615-nm bandpass filter, transferrin-Alexa Fluor 633 excited with 633 nm, detected with a 650-nm long pass filter. Phase contrast images were recorded with excitation at 488 nm and detection in the transmission channel. The laser power for observation was 1% (488 nm, 25 milliwatts), 7% (543 nm, 1 milliwatt), and 25% (633 nm, 5 milliwatts). Settings were adjusted in a way that image pixels were not over- or underexposed with the range indicator function in the Zeiss laser scanning microscopy software version 3.2. To ensure that weak intracellular fluorescence signals of the peptides were not missed, a set of overexposed images was additionally collected.

For the quantification of transduction, 100–150 cells per transduction experiment were evaluated to obtain the percentage of transduced cells (indicated by nucleolar appearance of the labeled peptide), and the kinetics of TAT transduction was further characterized by the earliest time point when transduction could be detected within a field of view (initiation time of transduction).

Western Blotting—For Western blot analysis of the cav-1-KO and WT cells, half a million cells were counted, resuspended in 100 μ l of phosphate-buffered saline, and boiled in Laemmli sample buffer for 10 min, and cell lysates were analyzed by SDS-PAGE followed by blotting onto polyvinylidene difluoride membranes. Signals were detected with the following primary antibodies: rabbit anti-Cav-1 polyclonal antibody (LifeSpan BioSciences, Inc., Seattle, WA) and mouse anti-Cav-2 and anti-Cav-3 monoclonal antibodies (1:2000 dilution, BD Transduction Laboratories). Anti-rabbit IgG-HRP (Sigma) and anti-mouse IgG-HRP (enhanced chemiluminescence, Amersham Biosciences) were used as secondary antibodies. Immunoreactive signals were visualized using enhanced chemiluminescence plus detection solution (Amersham Biosciences) and recorded using a luminescence imager (Luminescent Image Analyzer LAS-1000, FUJI Photo Film, Tokyo, Japan).

RESULTS

Because of their particularly high transduction ability, which solely depends on a minimal number of arginines, RRP play a special role among CPPs (18, 33–35). To clarify the role of endocytosis in the uptake mode of CPPs with low molecular weight (LMW) cargos into living cells, we investigated the occurrence and extent of transduction of TAT and PTD₄ as CPPs with high and low transduction frequency, respectively (8). The intracellular distribution of peptides in living cells was analyzed by laser scanning confocal microscopy. To unravel the relevance of endocytic routes for the uptake and intracellular distribution of peptides, endocytic pathways were specifically inhibited by genetic approaches or were blocked in ensemble by incubation of cells at low temperature.

Role of Clathrin-mediated Endocytosis in CPP Uptake—Clathrin-dependent endocytosis represents a major endocytic

pathway. For example, transferrin is taken up exclusively by this route, and several enveloped viruses (36), such as equine arteritis virus (37), exploit this route (38). As an early step of this route, upon binding of an extracellular ligand to specific cell-surface receptors, clathrin together with other adapter proteins builds an endocytic coat at the plasma membrane (Fig. 2A). The coated membrane buds and pinches off to form a cargo-filled vesicle (Fig. 2A).

Clathrin-dependent endocytic uptake of TAT has been repeatedly reported as a possible mechanism for CPP entry (23, 39, 40). To clarify the contribution of clathrin-dependent endocytosis in the uptake mode of arginine-rich CPPs, we used the BHK21-tTA/anti-CHC (30) cell line. This cell line expresses antisense CHC RNA under the control of a tetracycline-responsive element (Fig. 2B). More specifically, the transcription activator (tTA) is composed of the DNA binding domain of tetracycline repressor protein and a C-terminal activation domain of VP16 (herpes simplex virus protein) that functions as a strong transcription activator (41). The presence of tetracycline prevents binding of the transactivator tTA to the operator sequence and thus transcription of antisense RNA. In the absence of tetracycline the transactivator tTA binds to its operator sequence and activates the transcription of antisense RNA. As a consequence, the synthesis and functionality of CHC protein is significantly reduced, thereby suppressing clathrin-dependent endocytosis (30). The absence of tetracycline for 2 days was reported to inhibit 90% of transferrin internalization, and the expression of the CHC protein was reduced to 10% over 6 days in the absence of tetracycline (30). Therefore, to explore to what extent transduction of TAT depends on clathrin-dependent endocytosis, uptake of TAMRA-tagged TAT and PTD₄ was investigated in the presence (+tet) and absence (–tet) of tetracycline over 6 days. To simultaneously control the level of clathrin-dependent endocytosis, internalization of Alexa Fluor 633-labeled transferrin was monitored (Fig. 2C).

The control cells (+tet cells) are shown on the *left panel* of Fig. 2C and supplemental Fig. S3. TAT was homogeneously distributed throughout the cytoplasm and accumulated in the nucleolus (Fig. 2C, *arrowheads*) and therefore displayed the uptake mode of transduction. In addition, the labeled peptide was also present in cytoplasmic vesicles.

PTD₄ applied at the same concentration and monitored at identical confocal microscope settings did not show any transduction-associated cytoplasmic localization comparable with TAT. However, we observed the presence of PTD₄-containing vesicles (Fig. 2C, *left side, lower panel*). Fluorescent transferrin was internalized at high rates and enriched in the trans-Golgi network (42).

Inhibition of the clathrin-dependent endocytic pathway in –tet cells (Fig. 2C and supplemental Fig. S3A, *right panel*) was verified by the suppression of uptake of transferrin. TAT displayed the same intracellular distribution regarding the vesicular uptake as well as transduction, indicated by similar intensities inside the nucleolar compartment compared with the control (+tet) cells (Fig. 2C and supplemental Fig. S3). Similar to the control cells, no diffuse intracellular occurrence was observed for PTD₄, but in contrast to +tet cells the vesicular internalization of PTD₄ was almost completely abolished.

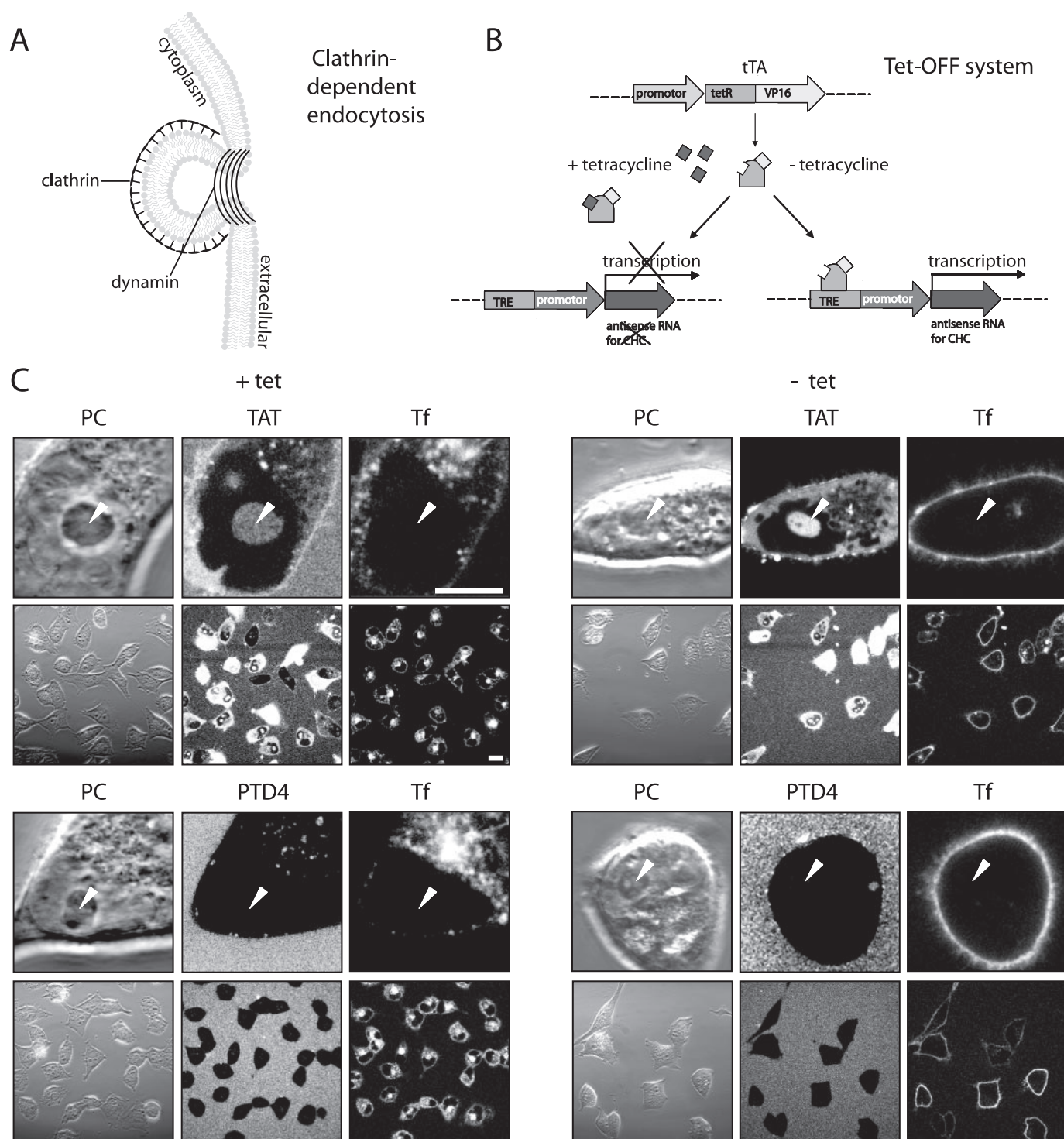


FIGURE 2. Transduction of TAT is independent of clathrin-mediated endocytosis. *A*, schematic diagram illustrating clathrin-dependent endocytosis. The clathrin coat is required for membrane invagination, and for the scission of clathrin-coated vesicles dynamin is needed. *B*, schematic representation of the Tet-OFF system, allowing a conditional knockdown of CHC in the BHK21-tTA/anti-CHC cell line. The binding of the transcriptional activator tTA to an operator sequence in the absence of tetracycline (–tet) results in activation of transcription of CHC-antisense RNA and thereby repression of the CHC mRNA translation. *C*, confocal optical sections of living cells during incubation with the fluorescent CPPs TAT (*upper panel*) or PTD₄ (*bottom panel*) in the presence of the transferrin (Tf) as a marker for clathrin-dependent endocytosis. Each panel displays high magnification images of the phase contrast (PC) and the fluorescently labeled compound to show the details of their intracellular distribution and low magnification images to highlight the frequency of CPP transduction and Tf internalization (see also supplemental Fig. S3). *Arrowheads* mark the position of nucleoli. Transduction experiments were performed in the presence (*left panel*) and absence (*right panel*) of tetracycline. Although uptake of Tf is nearly abolished after tetracycline removal over a period of 6 days, the TAT CPP is still capable of reaching all intracellular compartments (diffuse, nonvesicular fluorescence, and accumulation inside nucleoli), indicating that this mode of uptake is not influenced by clathrin-dependent endocytosis. Vesicular uptake of the CPP TAT was still detected under –tet conditions albeit at reduced levels. Scale bar, 10 μ m for high and 20 μ m for low magnification images.

TAT Transduction Occurs in the Absence of Endocytosis

We confirmed that TAT transduction was observed in most cells by acquiring low magnification images (Fig. 2C and supplemental Fig. S3). To control for any potential side effects of tetracycline, the parental BHK21 cells (43, 44) were incubated with the CPPs and transferrin in the presence and absence of tetracycline. However, no difference of peptide transduction and vesicle formation was observed (data not shown). Therefore, we conclude that clathrin-dependent endocytosis is not required for transduction of the RRP TAT fused to an LMW cargo.

Role of Caveolin-mediated Endocytosis in CPP Uptake—Besides the classical clathrin-mediated endocytic pathway, caveolae-mediated endocytosis is one of the main endocytic entry routes into living cells (22, 45). For example, it is exploited by bacterial toxins and by simian virus 40 (36). Caveolae are flask-shaped, small (50–70 nm diameter) invaginations in the plasma membrane (Fig. 3A) that constitute membrane domains enriched in cholesterol and sphingolipids, called lipid rafts (46). Caveolae are characterized by the presence of the integral membrane protein caveolin-1 and are involved in the intracellular transport of lipid raft-associated molecules (47). This pathway has been repeatedly reported as an uptake route for CPPs into the cells (24, 25). Former studies used fluorescently labeled β -subunit of cholera toxin as a marker to monitor caveolar uptake. However, the pathway chosen by cholera toxin subunit β depends on the cell type (48) and hence may not be a faithful indicator for a single internalization pathway. To specifically inhibit only the caveolin-dependent route and to prevent the potential side effects caused by chemical inhibitors of endocytosis, we made use of an endothelial heart cell line generated from a knock-out (KO) mouse deficient for caveolin (cav-1) and the respective wild type (WT) cell line. As reported previously (31), in the absence of caveolin-1, caveolin-2 protein is degraded. This was corroborated by Western blot analysis (Fig. 3B). In contrast to WT cells, no cav-1 and cav-2 were detected in the KO cells, and in addition, antibodies directed against muscle cell-specific cav-3 gave a much weaker signal in the extract of KO cells compared with those from wild type cells.

To elucidate if caveolae-dependent endocytosis plays a role in the uptake mode of TAT with the LMW TAMRA, we applied TAT (Fig. 3C, upper panel, and supplemental Fig. S4) and PTD₄ (Fig. 3C, middle panel) to the medium of wild type cells and cav-1-KO cells. To control whether the tagged fluorophore supports peptide internalization, the uptake of TAMRA* alone at the same concentration as the peptides was studied (Fig. 3C, bottom panel). For each experiment confocal optical sections are displayed at high and low magnification. Because of the large size of these cells, it was not possible to show a higher number of cells per field and at the same time keep imaging parameters constant throughout all experiments. No difference of TAT transduction between WT and cav-1-KO cells was found. TAT also became internalized by an endocytic route, as indicated by the punctated intracellular fluorescence. This signal was still present in the caveolin-deficient cells. In contrast to TAT, the PTD₄ peptide entered the cells only by the endocytic mode and could not be detected freely inside the cyto- and nucleoplasm and the nucleolus (Fig. 3C, middle panel, arrow-

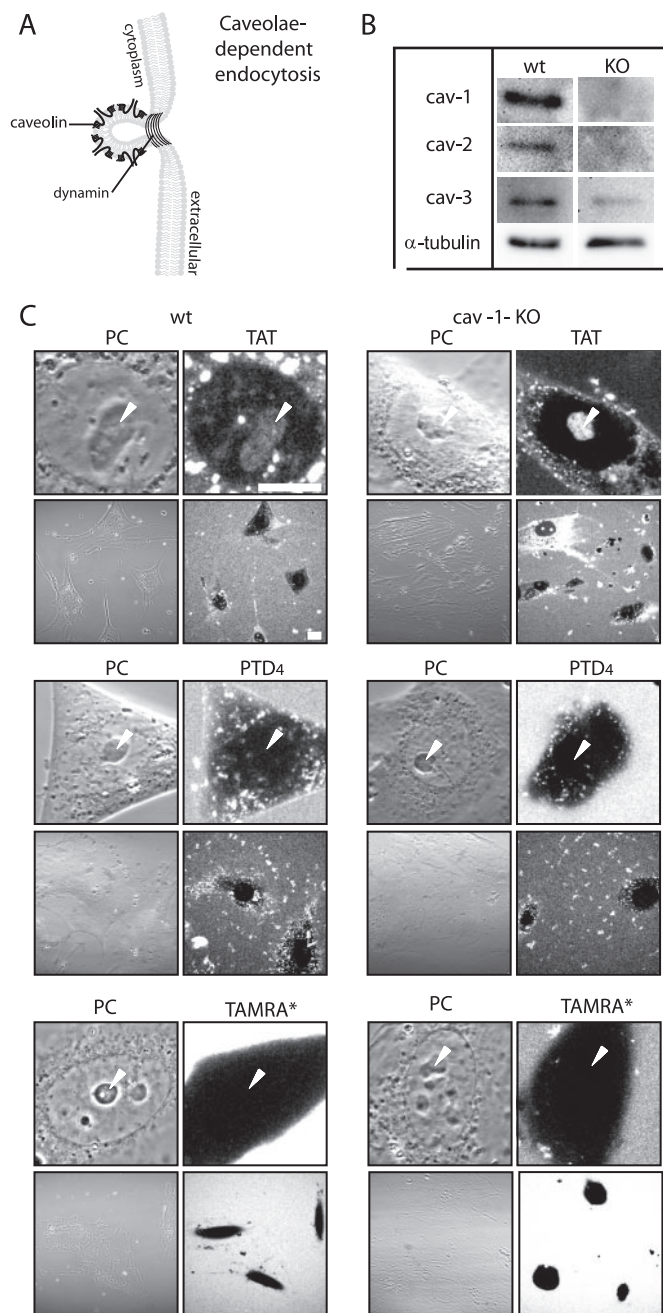


FIGURE 3. Transduction of TAT is independent of caveolin-mediated endocytosis. *A*, schematic diagram illustrating structural features of flask-shaped caveolae, which are lined by caveolin. Caveolae-mediated endocytosis is driven by a coat made of the integral membrane proteins caveolin-1, -2, or -3. Dynamin is required for the scission of caveolae. *B*, Western blot analysis of the integral membrane proteins caveolin (cav) -1, -2, and -3 in WT and caveolin 1 KO endothelial cells. α -Tubulin is used for loading. *C*, confocal optical sections of living cells during incubation with the fluorescent CPPs TAT (upper panel) or PTD₄ (mid panel) and the fluorophore TAMRA* (bottom panel). Each panel displays images of the phase contrast (PC) and the peptide or fluorophore fluorescence at high and low magnification to display their intracellular distribution and at low magnification to highlight the frequency of CPP transduction in WT and cav-1-KO cells (see also supplemental Fig. S4). Whereas the amphipathic control peptide PTD₄ and the fluorophore TAMRA* were not transduced, the CPP TAT was homogeneously distributed in the cytoplasm, and it reached the nucleus where it accumulated inside the nucleolar compartment (marked by arrowheads). Both CPPs displayed vesicular uptake in WT and cav-1-KO cells. Scale bar, 10 μ m for high and 20 μ m for low magnification images.

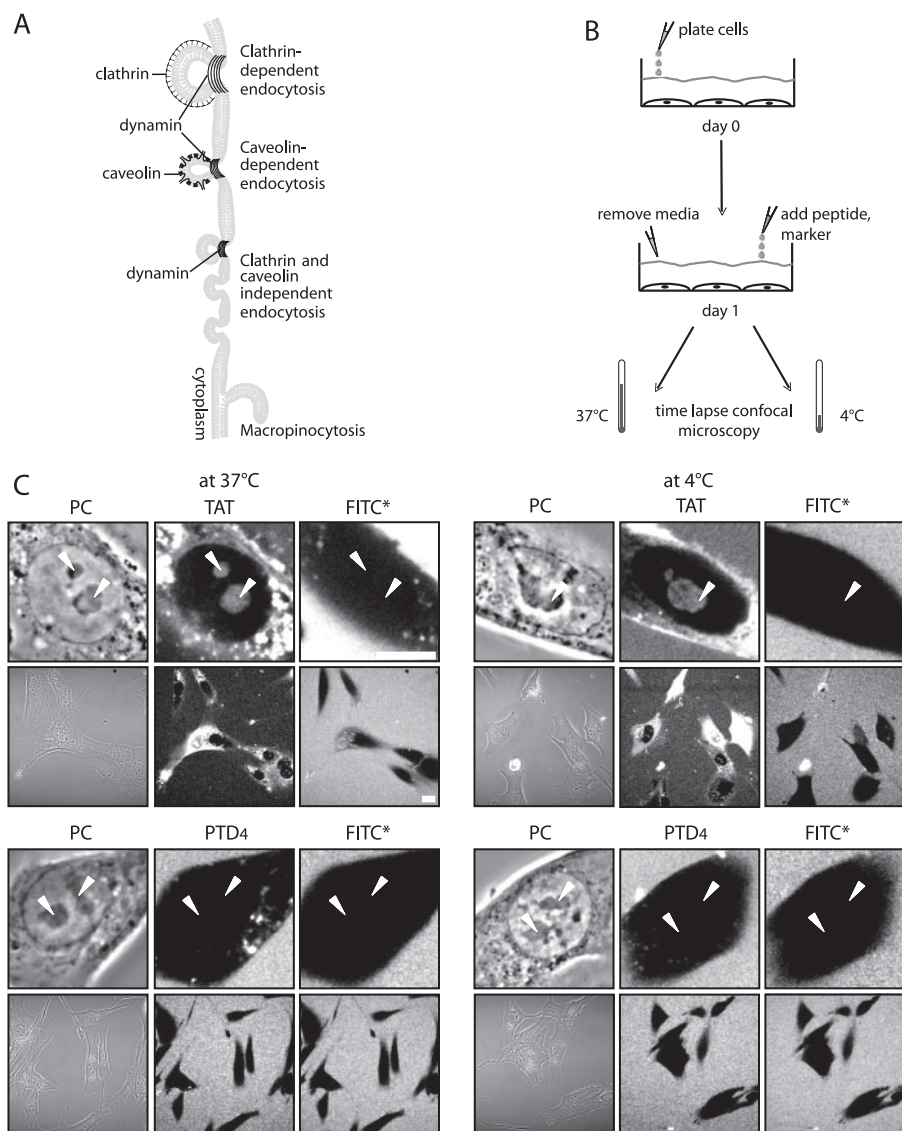


FIGURE 4. Transduction of TAT is independent of endocytosis. *A*, schematic overview of the different pathways of endocytic internalization that are suppressed at 4 °C: clathrin- and caveolin-dependent endocytosis, clathrin- and caveolin-independent endocytosis, and macropinocytosis. *B*, experimental strategy for transduction experiments performed at 37 and 4 °C. *C*, confocal optical sections of living cells during incubation with the fluorescent CPPs TAT (*upper panel*) or PTD₄ (*lower panel*) in the presence of the fluorophore FITC* as a small molecule marker to control for membrane pores or damage. Each panel displays high magnification images of the phase contrast (PC) and the fluorescently labeled peptide or fluorophore to show their uptake and intracellular distribution and low magnification images to highlight the frequency of transduction at 37 and 4 °C (see also supplemental Fig. S5). *Arrowheads* mark the position of nucleoli. The transduction experiments were performed in BHK21 cells kept at 37 and 4 °C. Although no intracellular vesicles were found at 4 °C, the transduction of TAT (nonvesicular, diffuse fluorescence with accumulation inside nucleoli) remained unchanged both at 37 and 4 °C. In contrast, the amphipathic control peptide PTD₄ and fluorophore FITC* were not transduced at 37 °C nor at 4 °C. *Scale bars* are 10 μm for high and 20 μm for low magnification images.

heads). TAMRA was excluded from the cytoplasm and intracellular compartments providing strong evidence that peptide uptake is not aided by the fluorophore. Based on these results, we conclude that caveolae-mediated endocytosis is not involved in the uptake mode of transduction of TAT conjugated to an LMW cargo.

Uptake of CPPs upon Shutting Off Endocytic Pathways—Because neither clathrin- nor caveolin-dependent endocytosis inhibits CPP uptake and in both cases we could still find TAT-containing vesicles concomitantly with freely available cyto-

plasmic TAT peptide, we tried next to inhibit all endocytic pathways simultaneously.

For this purpose, we followed the internalization of TAT and PTD₄ at low temperature, 4 °C. Fig. 4*A* depicts all potential endocytic uptake routes in cells that are expected to be inhibited under such conditions. Previous reports addressing the uptake of arginine-rich CPPs with LMW cargos into living cells are inconsistent. Although some reports insisted on the inability of CPPs to penetrate cells at low temperature and hence endocytosis would be required for internalization (49), according to other reports, CPP uptake is not inhibited at 4 °C (14, 19, 20). Fig. 4*B* displays the experimental setup for assessing the transduction ability of TAT and PTD₄ in C2C12 mouse myoblasts (data not shown) and in BHK21 hamster fibroblasts in the presence (37 °C) and absence (4 °C) of endocytosis by time-lapse confocal microscopy. To make sure that potential membrane lesions generated by low temperature conditions would not corrupt the transduction assay, the fluorophore FITC* was applied simultaneously with the TAMRA-labeled peptides to the cells. In case of severe membrane damage or pore formation induced by the peptides, the 389-Da-sized FITC* molecule should also be detectable intracellularly. Our observations displayed as high and low magnification images in Fig. 4*C* and supplemental Fig. S5 reveal that even at 4 °C TAT entered living cells and distributed over the cytoplasm and nucleus, where it accumulated inside nucleoli. At the same time the fluorophore FITC* did not gain access to intracellular compart-

ments indicating that the plasma membrane was not compromised. The complete obstruction of endocytosis was further confirmed by the absence of fluorescently labeled vesicles at 4 °C. Vesicles were not observed for the CPP TAT nor for PTD₄. Furthermore, uptake of the globular TAT fusion protein TAT-bt-SAV that is restricted to endocytosis (8) was also blocked on the level of the plasma membrane at 4 °C (supplemental Fig. S2). These results prove unambiguously that arginine-rich CPPs like TAT are capable of reaching intracellular compartments of living cells by a mechanism that is independent of

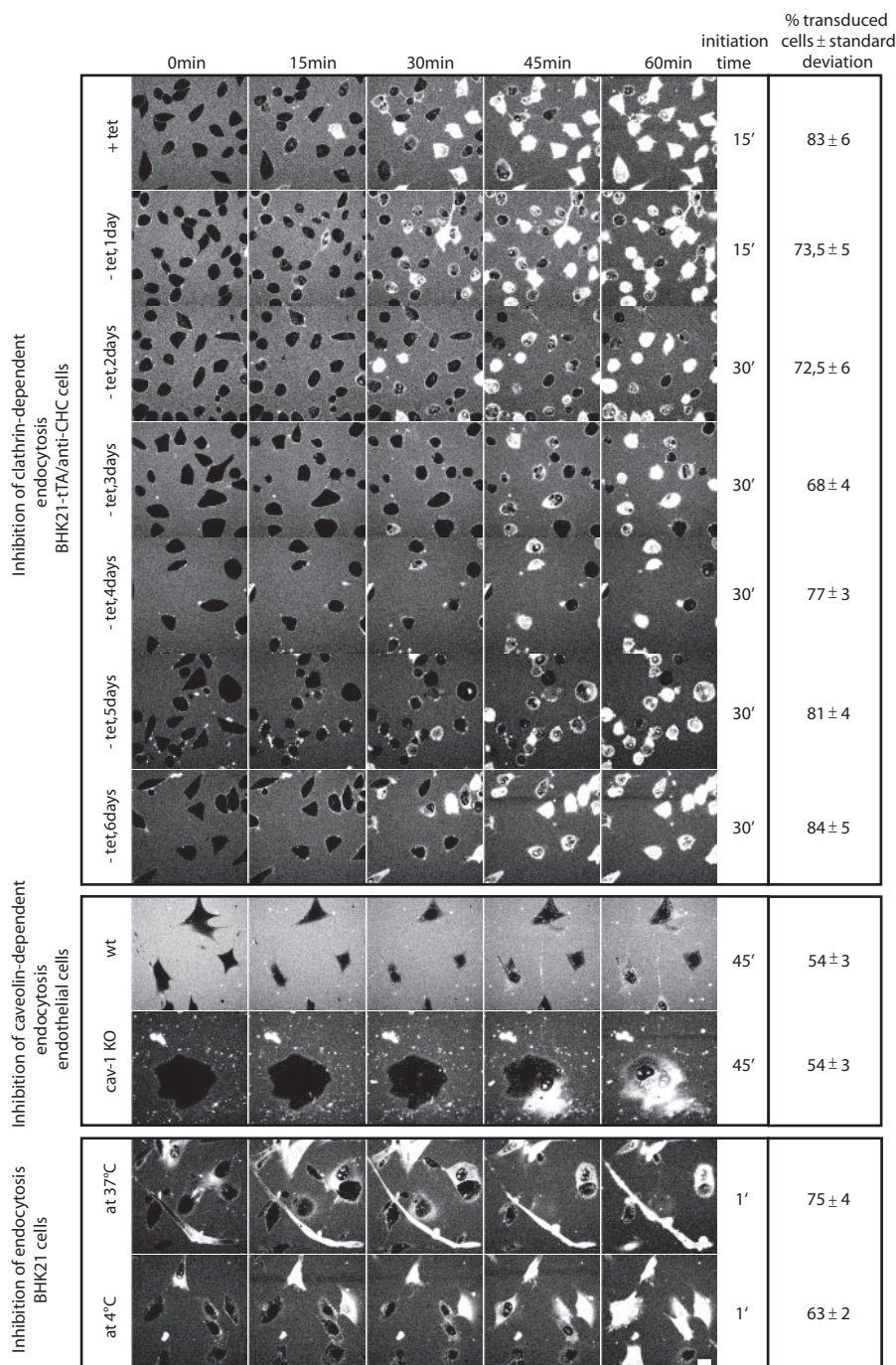


FIGURE 5. Kinetic and quantitative analysis of transduction. Assembly of confocal optical sections of living cells with time intervals of 15 min derived from the 60-min time lapses (see supplemental movies S1–S10) displaying the kinetics of TAT uptake in the different cell lines. All cell lines showed an unchanged transduction behavior in the control cells and the cells that were inhibited for a distinct or all pinocytic events. But the average entry time point of the TAT peptide is cell type-specific. The last column summarizes the transduction frequencies of TAT after 60 min of incubation in cells, where distinct or all endocytic pathways were suppressed. Transduction frequency was scored by counting the percentage of cells showing the intracellular freely available peptide (see Fig. 1, B and C). Scale bar, 10 μ m.

endocytosis. However, the data also clearly show that a minimal number of arginines is crucial to permit transduction.

Frequency and Initiation Time of TAT Transduction—To quantify our results on the transduction ability in the absence of a distinct pathway or all pathways of endocytosis, we evaluated the percentages of transduced cells after 60 min of incubation

with the CPP TAT and the initiation time of transduction (Fig. 5 and supplemental movies S1–S10). The control cells (+tet, day 0) showed a transduction frequency of 83%. While over the first 3 days after induction of the conditional knock-down of CHC (–tet) the transduction percentages were reduced to 68%, they recovered back to 84% transduction frequencies by day 6, although the internalization of fluorescently labeled transferrin was reduced by 90%. The frequency of transduced cells was identical in cav-1-deficient and isogenic WT cells (54%), although in these cells it was lower than in the BHK21-tTA/anti-CHC cells. Finally, the inhibition of all potential pinocytic pathways at 4 °C determined in BHK21 fibroblasts revealed that the transduction of the TAT peptide is diminished about 12% in comparison with transduction occurring in cells kept at 37 °C, but still 63% of the cells displayed nucleolar accumulation of TAT.

In BHK21-tTA/anti-CHC cells, the transduction mode of uptake initiated between 15 and 30 min of peptide addition after CHC knock-down as well as in control cells. The kinetics of peptide uptake in cav-1-KO and wild type cells displayed an uptake initiation at 45 min after application of TAT. The fastest uptake of TAT occurred in BHK21 fibroblasts within 1 min of addition to the medium and independent of temperature. A summary of the uptake kinetics of TAT peptide in all conditions tested is presented in Fig. 5.

In conclusion, the frequency and initiation time of TAT transduction was unchanged within a given cell type independent of endocytosis. However, both parameters were cell type-specific, suggesting that the membrane composition influences

the velocity of transduction.

DISCUSSION

Despite the controversy and uncertainty regarding the uptake mechanism, the property of CPPs to deliver nonpermeable molecules into living cells makes them attractive vectors to

be used in biological sciences as well as in medicine and biotechnology. Former studies used chemical inhibitors of endocytosis to assign the uptake of CPPs to a particular endocytic pathway. However, the potential side effects and lack of specificity of such inhibitors make these studies difficult to interpret. Either the chemical compounds affect more than one specific pathway, like methyl- β -cyclodextrin that affects both lipid raft (26) and caveolin-coated vesicle formation (50) hence also caveolin-dependent endocytosis, or they have other side effects that may impact the import of RRP, e.g. chlorpromazine was shown to interface with a number of Ca^{2+} -dependent signaling pathways (51) and to bind to dopamine receptors (19, 52). Thus, we have used genetically modified systems or physical methods to clarify the role of endocytosis in the translocation of RRP.

The different phenotypes shown in Fig. 1 permit at least two explanations for the occurrence of free RRP inside the cytoplasm and nucleoplasm. Either RRP become endocytosed and a portion of the peptide stored in vesicles gets released into the cytoplasm or a second nonendocytic entry route that allows RRP to directly cross the plasma membrane has to be considered.

Earlier reports associated uptake of RRP with and without attached cargos to distinct endocytic pathways (16, 23–28, 39, 40, 49). However, our results unambiguously demonstrate that the transduction of TAT into living cells is not dependent on any endocytic or pinocytic events. We could exclude the pathway of clathrin-mediated endocytosis by a carefully controlled knockdown experiment. Also caveolin-mediated endocytosis was not involved in TAT translocation, because caveolin knock-out cells showed an identical transduction frequency to the wild type cells. Most importantly, TAT was not excluded from cells that were gently transferred to 4 °C, a state where all potential endocytic pathways are inhibited.

It is noteworthy to mention that the amount of TAT transduced into a cell varies between cells within a single experiment, but its intracellular distribution does not. This phenomenon was observed in every cell type and was independent of which endocytic route was down-regulated. (Fig. 2–5 and supplemental Fig. S3–S5).

Comparing the transduction frequencies of the specific cell types, a variation from 68 to 84% for the BHK21-tTA/anti-CHC cell line, over 63–75% in BHK21 cells, and to 54% in the mouse endothelioma cells can be found, suggesting that the particular membrane composition of different cell types impacted on transduction (Fig. 5). This was further corroborated by the observation that the average initiation time of transduction was cell type-specific, but it did not change upon the inhibition of endocytosis within a given cell type. All experiments were conducted in addition to PTD₄ as a representative CPP (29) with a reduced number of arginines compared with TAT. At the same concentration, this peptide did not gain access to the intracellular compartments in a freely diffusing form and was internalized exclusively by endocytosis. This could be explained by the fact that a minimal number of six arginines is required to permit transduction (18). Instead, PTD₄ was predominantly internalized by the clathrin-dependent pathway. Although not capable of performing transduction, the CPP PTD₄ was endocytosed

more efficiently than non-CPP compounds added to the medium, e.g. the fluorophore TAMRA* alone (Fig. 3C).

Recent mechanistic studies with artificial membrane systems described the formation of pores as a consequence of the interaction with intermediate concentrations of the RRP TAT (53). However, the fluorophore FITC*, concomitantly applied to the cells together with the TAT peptide, remained outside of the cells, whereas TAT transduced selectively into the cells (Fig. 4C), arguing against the formation of nonselective pores.

In summary, our data indicate that TAT CPP internalization is independent of endocytosis and occurs without disruption of the cell membrane. These properties and its high intracellular bioavailability make TAT CPP a very effective tool to deliver small compounds into living cells.

Acknowledgments—We thank Kirsten Sandvig for the generous gift of the BHK-tTA/anti-CHC cell line. We are indebted to our colleagues Petra Domaing for help in the cell culture, Robert Martin and Jeff Stear for fruitful discussions and support with microscopy, and Sebastian Haase for advice in the image analysis.

REFERENCES

- Frankel, A. D., and Pabo, C. O. (1988) *Cell* **55**, 1189–1193
- Green, M., and Loewenstein, P. M. (1988) *Cell* **55**, 1179–1188
- Dietz, G. P., and Bahr, M. (2007) *Methods Mol. Biol.* **399**, 181–198
- Nori, A., Jensen, K. D., Tijerina, M., Kopeckova, P., and Kopecek, J. (2003) *Bioconjugate Chem.* **14**, 44–50
- Mann, D. A., and Frankel, A. D. (1991) *EMBO J.* **10**, 1733–1739
- Shibagaki, N., and Udey, M. C. (2002) *J. Immunol.* **168**, 2393–2401
- Tunnemann, G., Karczewski, P., Haase, H., Cardoso, M. C., and Morano, I. (2007) *J. Mol. Med.* **85**, 1405–1412
- Tunnemann, G., Martin, R. M., Haupt, S., Patsch, C., Edenhofer, F., and Cardoso, M. C. (2006) *FASEB J.* **20**, 1775–1784
- Astriab-Fisher, A., Sergueev, D., Fisher, M., Shaw, B. R., and Juliano, R. L. (2002) *Pharmacol. Res.* **19**, 744–754
- Fawell, S., Seery, J., Daikh, Y., Moore, C., Chen, L. L., Pepinsky, B., and Barsom, J. (1994) *Proc. Natl. Acad. Sci. U. S. A.* **91**, 664–668
- Nagahara, H., Vocero-Akbani, A. M., Snyder, E. L., Ho, A., Latham, D. G., Lissy, N. A., Becker-Hapak, M., Ezhevsky, S. A., and Dowdy, S. F. (1998) *Nat. Med.* **4**, 1449–1452
- Schwarze, S. R., Ho, A., Vocero-Akbani, A., and Dowdy, S. F. (1999) *Science* **285**, 1569–1572
- Lewin, M., Carlesso, N., Tung, C. H., Tang, X. W., Cory, D., Scadden, D. T., and Weissleder, R. (2000) *Nat. Biotechnol.* **18**, 410–414
- Iwasa, A., Akita, H., Khalil, I., Kogure, K., Futaki, S., and Harashima, H. (2006) *Biochim. Biophys. Acta* **1758**, 713–720
- Torchilin, V. P., Rammohan, R., Weissig, V., and Levchenko, T. S. (2001) *Proc. Natl. Acad. Sci. U. S. A.* **98**, 8786–8791
- Drin, G., Cottin, S., Blanc, E., Rees, A. R., and Tamsamani, J. (2003) *J. Biol. Chem.* **278**, 31192–31201
- Richard, J. P., Melikov, K., Vives, E., Ramos, C., Verbeure, B., Gait, M. J., Chernomordik, L. V., and Lebleu, B. (2003) *J. Biol. Chem.* **278**, 585–590
- Tunnemann, G., Ter-Avetisyan, G., Martin, R. M., Stockl, M., Herrmann, A., and Cardoso, M. C. (2008) *J. Pept. Sci.* **14**, 469–476
- Duchardt, F., Fotin-Mleczek, M., Schwarz, H., Fischer, R., and Brock, R. (2007) *Traffic* **8**, 848–866
- Fretz, M. M., Penning, N. A., Al-Taei, S., Futaki, S., Takeuchi, T., Nakase, I., Storm, G., and Jones, A. T. (2007) *Biochem. J.* **403**, 335–342
- Ziegler, A., Nervi, P., Durrenberger, M., and Seelig, J. (2005) *Biochemistry* **44**, 138–148
- Mayor, S., and Pagano, R. E. (2007) *Nat. Rev. Mol. Cell Biol.* **8**, 603–612
- Richard, J. P., Melikov, K., Brooks, H., Prevot, P., Lebleu, B., and Chernomordik, L. V. (2005) *J. Biol. Chem.* **280**, 15300–15306
- Ferrari, A., Pellegrini, V., Arcangeli, C., Fittipaldi, A., Giacca, M., and Bel-

TAT Transduction Occurs in the Absence of Endocytosis

- tram, F. (2003) *Mol. Ther.* **8**, 284–294
25. Fittipaldi, A., Ferrari, A., Zoppe, M., Arcangeli, C., Pellegrini, V., Beltram, F., and Giacca, M. (2003) *J. Biol. Chem.* **278**, 34141–34149
26. Kaplan, I. M., Wadia, J. S., and Dowdy, S. F. (2005) *J. Controlled Release* **102**, 247–253
27. Nakase, I., Tadokoro, A., Kawabata, N., Takeuchi, T., Katoh, H., Hiramoto, K., Negishi, M., Nomizu, M., Sugiura, Y., and Futaki, S. (2007) *Biochemistry* **46**, 492–501
28. Wadia, J. S., Stan, R. V., and Dowdy, S. F. (2004) *Nat. Med.* **10**, 310–315
29. Ho, A., Schwarze, S. R., Mermelstein, S. J., Waksman, G., and Dowdy, S. F. (2001) *Cancer Res.* **61**, 474–477
30. Iversen, T. G., Skretting, G., van Deurs, B., and Sandvig, K. (2003) *Proc. Natl. Acad. Sci. U. S. A.* **100**, 5175–5180
31. Drab, M., Verkade, P., Elger, M., Kasper, M., Lohn, M., Lauterbach, B., Menne, J., Lindschau, C., Mende, F., Luft, F. C., Schedl, A., Haller, H., and Kurzchalia, T. V. (2001) *Science* **293**, 2449–2452
32. Yaffe, D., and Saxel, O. (1977) *Nature* **270**, 725–727
33. Futaki, S., Suzuki, T., Ohashi, W., Yagami, T., Tanaka, S., Ueda, K., and Sugiura, Y. (2001) *J. Biol. Chem.* **276**, 5836–5840
34. Rothbard, J. B., Kreider, E., VanDeusen, C. L., Wright, L., Wylie, B. L., and Wender, P. A. (2002) *J. Med. Chem.* **45**, 3612–3618
35. Suzuki, T., Futaki, S., Niwa, M., Tanaka, S., Ueda, K., and Sugiura, Y. (2002) *J. Biol. Chem.* **277**, 2437–2443
36. Marsh, M., and Helenius, A. (2006) *Cell* **124**, 729–740
37. Nitschke, M., Korte, T., Tievesch, C., Ter-Avetisyan, G., Tunnemann, G., Cardoso, M. C., Veit, M., and Herrmann, A. (2008) *Virology* **377**, 248–254
38. Martin-Acebes, M. A., Gonzalez-Magaldi, M., Sandvig, K., Sobrino, F., and Armas-Portela, R. (2007) *Virology* **369**, 105–118
39. Kawamura, K. S., Sung, M., Bolewska-Pedyczak, E., and Garipey, J. (2006) *Biochemistry* **45**, 1116–1127
40. Vendeville, A., Rayne, F., Bonhoure, A., Bettache, N., Montcourrier, P., and Beaumelle, B. (2004) *Mol. Biol. Cell* **15**, 2347–2360
41. Gossen, M., and Bujard, H. (1992) *Proc. Natl. Acad. Sci. U. S. A.* **89**, 5547–5551
42. Bennett, E. M., Lin, S. X., Towler, M. C., Maxfield, F. R., and Brodsky, F. M. (2001) *Mol. Biol. Cell* **12**, 2790–2799
43. Feng, Y., Press, B., and Wandinger-Ness, A. (1995) *J. Cell Biol.* **131**, 1435–1452
44. Press, B., Feng, Y., Hoflack, B., and Wandinger-Ness, A. (1998) *J. Cell Biol.* **140**, 1075–1089
45. Soldati, T., and Schliwa, M. (2006) *Nat. Rev. Mol. Cell Biol.* **7**, 897–908
46. Anderson, R. G. (1998) *Annu. Rev. Biochem.* **67**, 199–225
47. Simons, K., and Ikonen, E. (1997) *Nature* **387**, 569–572
48. Torgersen, M. L., Skretting, G., van Deurs, B., and Sandvig, K. (2001) *J. Cell Sci.* **114**, 3737–3747
49. Zorko, M., and Langel, U. (2005) *Adv. Drug Delivery Rev.* **57**, 529–545
50. Saalik, P., Elmquist, A., Hansen, M., Padari, K., Saar, K., Viht, K., Langel, U., and Pooga, M. (2004) *Bioconjugate Chem.* **15**, 1246–1253
51. Marshak, D. R., Lukas, T. J., and Watterson, D. M. (1985) *Biochemistry* **24**, 144–150
52. Seeman, P. (2002) *Can. J. Psychiatry* **47**, 27–38
53. Herce, H. D., and Garcia, A. E. (2007) *Proc. Natl. Acad. Sci. U. S. A.* **104**, 20805–20810

SUPPLEMENTARY FIGURES

Figure S1

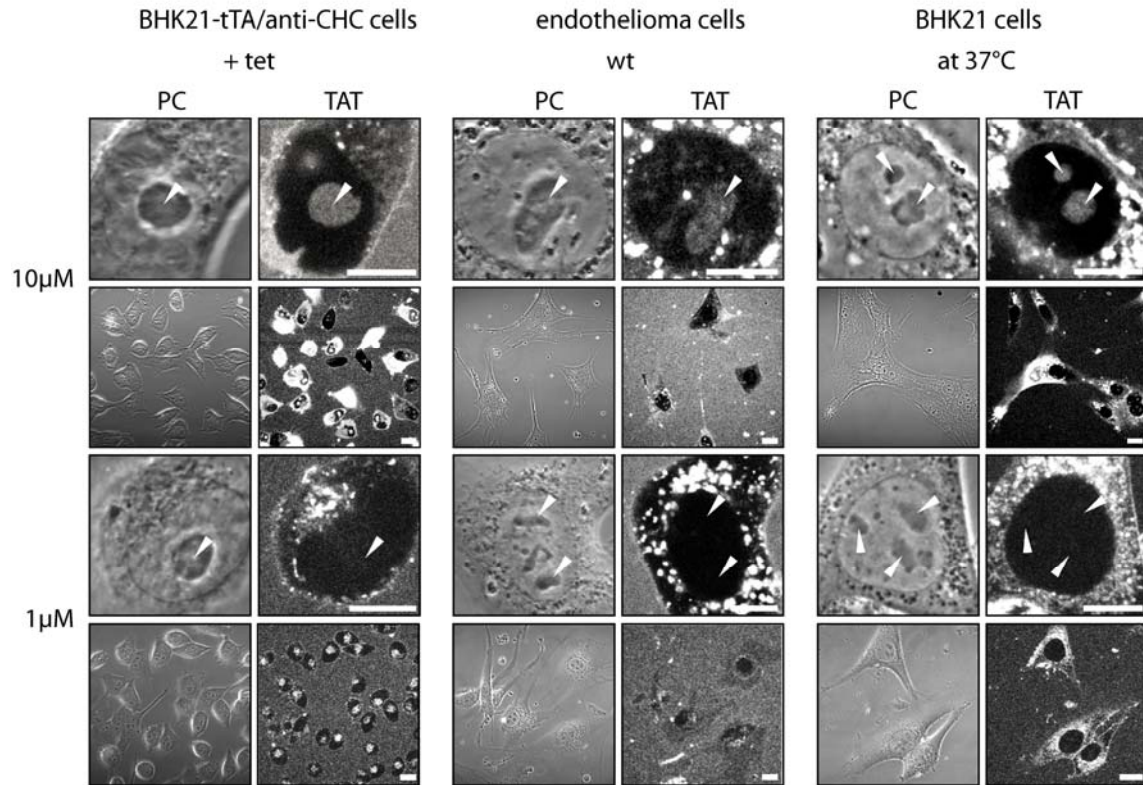


Fig. S1. Concentration-dependent mode of uptake of TAT CPP. TAT was incubated with the cells indicated at 1 and 10 μM concentration for one hour. Confocal optical sections of living cells are displayed with phase contrast (PC) and fluorescence images to show the uptake mode and intracellular distribution of TAT. Each panel contains high and low magnification images. Below a certain threshold concentration, transduction of TAT CPP, (visualized by the presence of peptide freely available in the cytoplasm and accumulation in the nucleolus (arrowheads) as shown in Fig. 1-5) does not occur whereas endocytosis of the TAT CPP persists as shown here. Scale bar 10 μm for high and 20 μm for low magnification images.

Figure S2

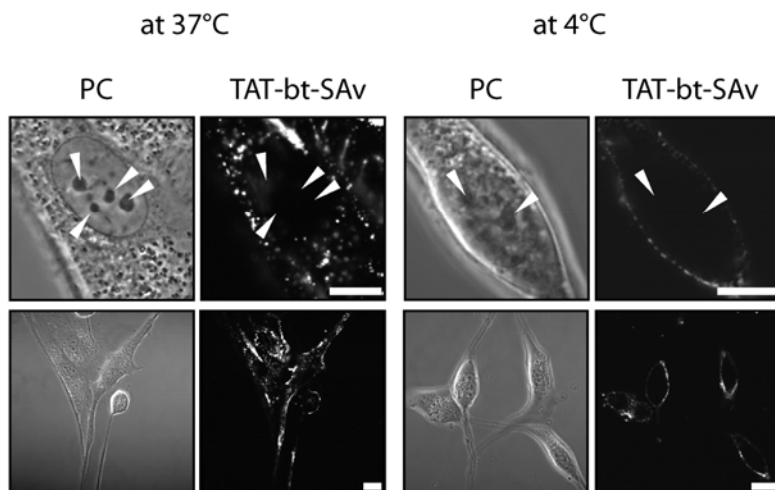


Fig. S2. Low temperature incubation abrogates all endocytic pathways. Mouse fibroblasts were incubated at 37°C and 4° C with the globular protein TAT-biotin-streptavidin-Cy5 (TAT-bt-SAv) as an additional fluid phase marker to the peptide PTD₄ and the fluorophore FITC* shown in Fig. 4. Confocal optical sections of living cells are shown as high and low magnifications after one hour incubation with the globular TAT-fusion protein. Arrowheads mark the nucleoli. Protein uptake was blocked at the level of the plasma membrane at a temperature of 4°C, whereas at 37°C the protein became rapidly internalized into vesicles. Scale bar 10µm for high and 20 µm for low magnification images.

Figure S3

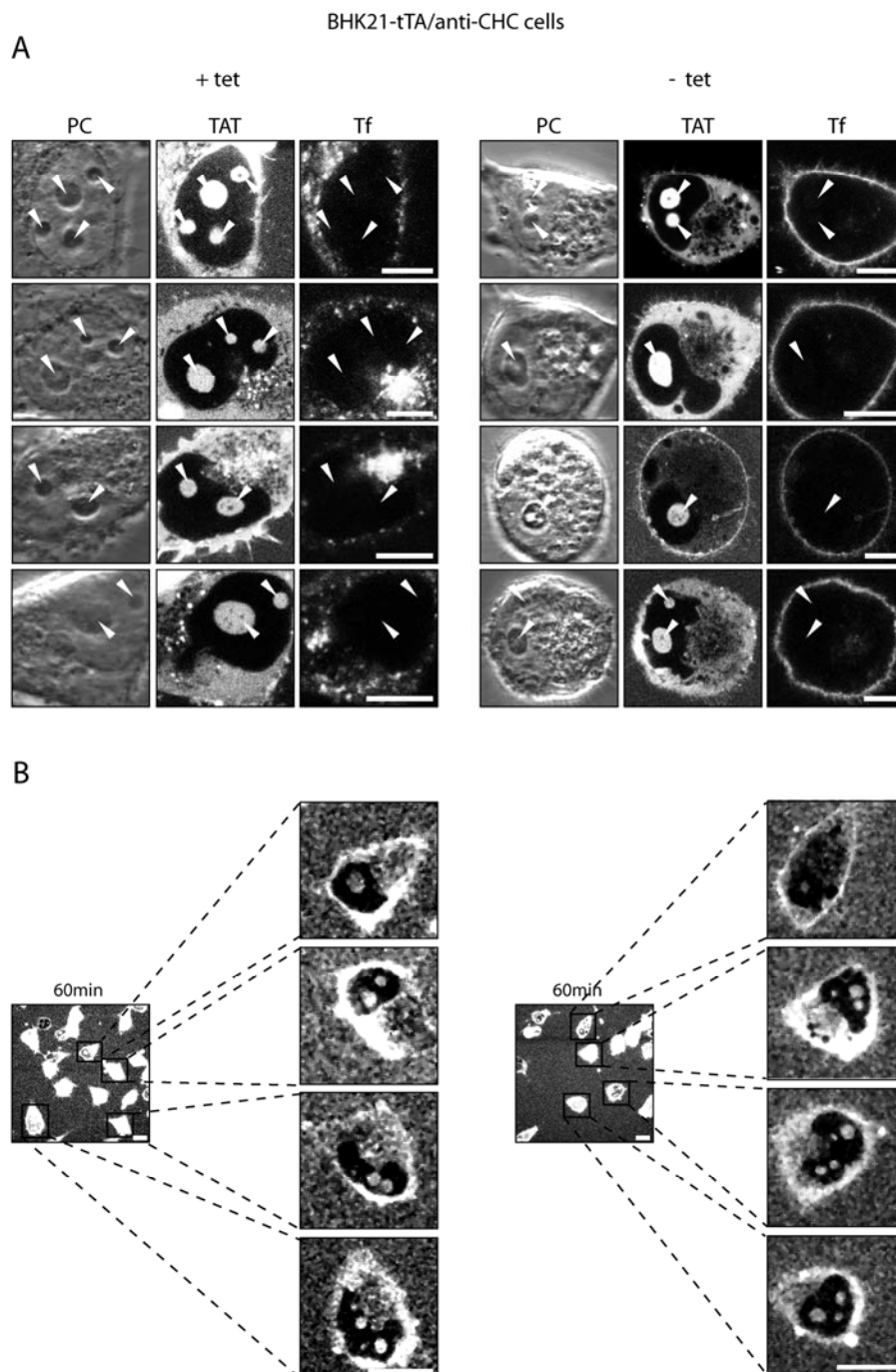


Fig. S3. Transduction of TAT is independent of clathrin-mediated endocytosis. Additional examples to the ones depicted in Fig. 2 are shown as high magnification images (A) and images magnified from the online supplementary movies S1 and S7 (B) after incubation with the TAT peptide for 60 minutes. Confocal optical sections of living cells during incubation with the fluorescent CPP TAT in the presence of transferrin (Tf) as a marker for clathrin-dependent endocytosis (only A). The control cells (left panel) and the cells after knockdown of the clathrin heavy chain (right panel) are shown as images of the phase contrast (PC) and the peptide (A) or of the peptide alone (B). Arrowheads mark the position of nucleoli (A). While uptake of Tf is nearly abolished after tetracycline removal over a period of six days (A) and vesicular uptake of TAT is reduced, the TAT CPP is still capable of reaching all intracellular compartments (non-vesicular, cytoplasmic and nucleolar fluorescence), indicating that this mode of uptake is not influenced by clathrin-dependent endocytosis. Scale bar 10 μm .

Figure S4

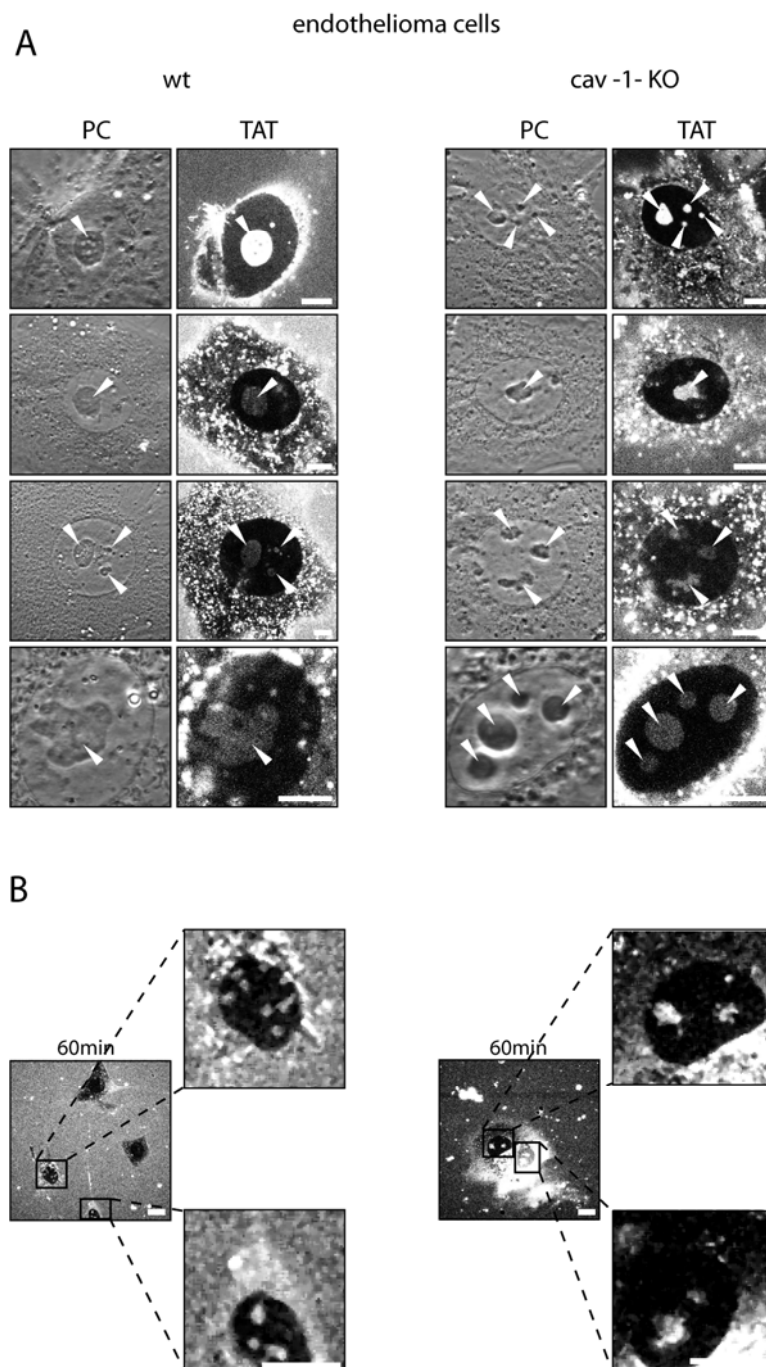


Fig. S4. Transduction of TAT is independent of caveolin-mediated endocytosis. Additional examples to the ones depicted in Fig. 3 are shown as high magnification images (**A**) and images magnified from the online supplementary movies S8 and S9 (**B**) after incubation with the TAT peptide for 60 minutes. Confocal optical sections of the wild type (left panel, wt) and caveolin-1 knockout (right panel, cav-1-KO) cells during incubation with the fluorescent CPP TAT. **A**-panels display images of the phase contrast (PC) and the peptide, **B**-panels only the peptide fluorescence images. Neither vesicular uptake of the CPP TAT nor the amount of TAT that was homogeneously distributed in the cytoplasm and accumulated inside the nucleolar compartment (marked by arrowheads), was different in both cases. Scale bar 10 μ m.

Figure S5

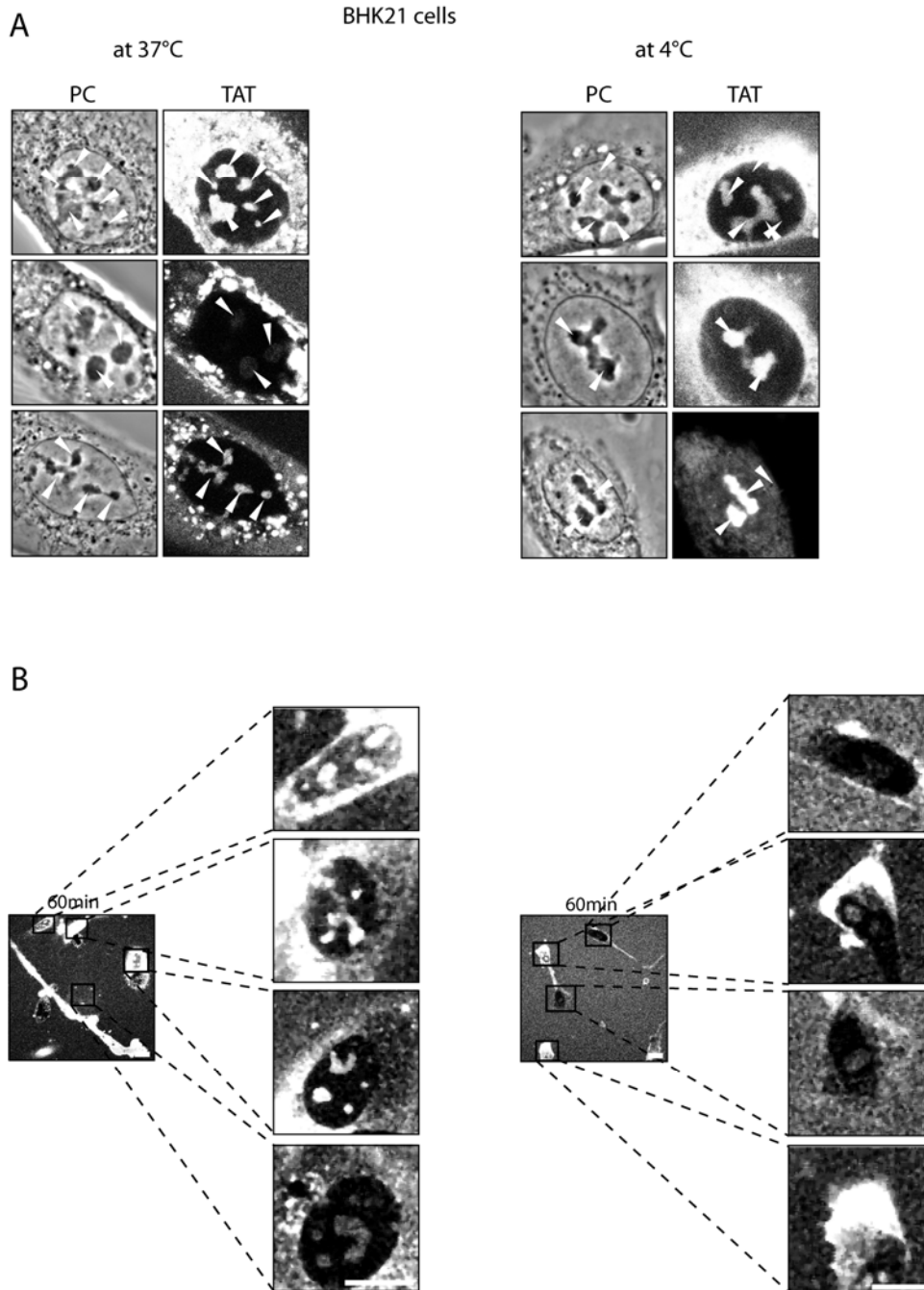


Fig. S5. Transduction of TAT is independent of endocytosis. Additional examples to the ones depicted in Fig. 4 are shown as high magnification images (A) and images magnified from the online supplementary movie S10 (B) after incubation with the TAT peptide for 60 minutes at 37°C (left panel) and at 4°C (right panel). In A each panel displays the phase contrast (PC) and the fluorescently labelled peptide. Arrowheads mark the position of nucleoli as unambiguous sign of freely diffusing intracellular TAT. In B the fluorescence of the labelled TAT-peptide is displayed. The transduction experiments were performed in BHK21 cells kept at the indicated temperatures before and during the experiment. Whereas there was no vesicle formation at 4°C (A) the transduction of TAT remained unchanged both at 37°C and 4°C (A and B). Scale bar 10 μ m.

2.3 Circularization and charge clustering promotes cellular uptake of arginine-rich cell penetrating peptides (Manuscript in preparation)

Circularization and charge clustering promotes cellular uptake of arginine-rich cell penetrating peptides (Manuscript in preparation)

Gisela Tünnemann¹, Joachim Behlke¹, Manuel Prinz², Daniel Hoffmann², Caroline Palm³, Ingo Morano¹ and M. Cristina Cardoso^{1,4}.

¹Max Delbrueck Center for Molecular Medicine, Robert-Roessle-Str. 10, 13125 Berlin, Germany. ²Center for Medical Biotechnology, University of Duisburg-Essen, Universitaetsstr.1-5, 45117 Essen, Germany. ³Department of Neurochemistry, Stockholm University, Svante Arrheniusväg 21A, SE-10691 Stockholm, Sweden. ⁴Darmstadt University of Technology, Department of Biology, 64287 Darmstadt, Germany.

Little is known about the mechanism enabling hydrophilic cell penetrating peptides to traverse biological membranes in a non-endocytic mode termed transduction. Here we demonstrate that transduction not only requires arginines but its efficiency depends on their clustering. Consequently, a cyclic TAT showed enhanced kinetics of uptake relative to its linear counterpart. We propose that the rigid geometry of arginine side chains in the cyclic TAT increases membrane contacts thus enhancing cell penetration.

Beginning with the observation in 1988 that the protein HIV-1 TAT crossed membranes of living cells and altered gene expression^{1,2}, a variety of so called protein transduction domains (PTDs) or cell penetrating peptides (CPPs) have been identified and utilized to introduce attached cargoes into living cells, organs or animals. For CPPs containing a low number of arginines³ or carrying large globular cargoes⁴, the mode of cellular uptake is restricted to endocytosis. The well studied CPPs TAT and artificial oligoarginines belong to the class of arginine-rich CPPs (RRPs) and have, in addition, the option to reach the intracellular space in an immediately bioavailable⁴ and non-toxic⁵ manner, hereafter referred to as transduction. RRP facilitate the delivery of low molecular weight cargoes via this mechanism, e.g. peptides up to 30 amino acids, and thus are appealing tools to modulate protein function in living cells. Nonetheless, it has remained poorly understood which characteristics of RRP permit their transduction over the plasma membrane in view of their hydrophilicity.

In this study, we applied laser scanning confocal microscopy of cellular uptake of fluorescently labeled peptides and analytical ultracentrifugation to delineate sequence and structural requirements for transduction. First, the transduction abilities and frequencies of several CPPs (Table S1), as well as the RRP TAT fused to different peptide cargoes and the respective cargoes alone were studied in a live-cell transduction assay. From the class of CPPs three RRP, namely the well studied CPP TAT^{6,7}, ten consecutive arginines R10^{8,9} and a cyclic variant of the native TAT sequence cTAT, were selected. PTD₄ was chosen in addition as a CPP with an assumed higher alpha-helical content¹⁰. In stark contrast to PTD₄

with 0.5 % transduction frequency all RRP transduced with efficiencies over 96 % (Fig. 1A, i). To further define which isoelectric properties allow for the transduction of peptides, we tested next a peptide without positive charges NBD (Nemo-binding domain)¹¹ (iv), a peptide containing four lysines VLC-1 (iii), one containing a bipartite nuclear localization sequence consisting of two lysines and five arginines (p21 peptide) (ii), as well as their corresponding TAT-fusion peptides. None of the TAT-free peptides was able to cross the plasma membrane whereas upon fusion to TAT these peptides translocated into living cells in the same manner as the TAT alone, albeit with lower transduction frequencies in the range of 75-85 %. In Fig. 1C i) the transduction frequencies of the peptides as a function of their pI are plotted and clearly demonstrate that positive charge is necessary but not sufficient for a peptide to be able to transduce. Furthermore, the fact that VLC-1 with four lysines but no arginines as well as nona-lysine (K9, Fig. S2) were not able to transduce into cells implies that arginines are essential and additional lysines, as present in p21, cannot substitute for a suboptimal number and/or arrangement of arginines.

Next we asked whether structural features could explain the high transduction efficiencies of TAT and oligoarginines compared to the other peptides devoid of TAT. All peptides from the transduction assay (Fig. 1A) were subjected to a sedimentation velocity analytical ultracentrifugation experiment. The frictional ratio f/f_0 determined by this analysis allowed the estimation of the gross conformation and dimensions of the peptides (Fig. 1B; see supplementary information and Table S2 for all parameters). Frictional ratios around 1 imply sphere-like particles and with increasing values the macromolecules can be modeled to more extended and rigid structures. Interestingly, all TAT-containing peptides and R10 exhibited a f/f_0 between 1.29 and 1.55 and thus appeared to be extended and rigid, whereas the values found for the non-transducing peptides (without TAT) range from 1.00 to 1.16 and hint towards a globular shape (Fig. 1B). Only the non-transducing p21 peptide exhibited a f/f_0 of 1.40 indicating elongated shape, which was though less extended than the corresponding TAT-fusion counterpart. The fact that this peptide sediments with a high frictional ratio equivalent to the one from the transducing peptides but was not able in itself to transduce into living cells (Fig. 1A, ii) suggests that the extended conformation is not *per se* sufficient. Corroborating this conclusion, the f/f_0 value for cyclic TAT was significantly reduced (1.14) compared to the linear TAT (1.39) and similar to the value for non-transducing peptides although both TAT peptides transduced into living cells.

To understand if rigidity and elongated structure are correlated with the pI the f/f_0 was plotted as a function of the pI (Fig.1C, ii). NBD with an acidic pI and VLC-1 with a slightly basic pI have a f/f_0 around 1, all other peptides form a basic cluster with pI ranging from 11.70 to 12.95 and corresponding frictional ratio varying between 1.14 and 1.55. TAT (8+) and R10 (10+) are both 10 amino acids long and, thus, the difference of 0.10 in the frictional ratio should reflect the number of evenly charged residues. Although the frictional ratio did not perfectly reflect the pI, above a certain basic charge, the peptides exhibited a stretch conformation. We conclude that a stretched conformation should be an intrinsic

structural property for RRP and other equally charged peptides but both features do not ensure transduction ability.

Therefore, we checked whether transduction ability was correlated with the number and density of charge (arginines) within the peptides. Indeed, the cyclic form of TAT was not only able to translocate into living cells with comparable frequencies as the linear TAT (Fig. 1A and C, iii) but even exhibited enhanced transduction kinetics (Fig. 2, supplementary movie 1), which is in contrast to a cyclic form of penetratin that lost most of its translocation capacity¹². Although both forms were identically charged, the cyclic TAT variant entered living cells on average 15 minutes earlier than the linear form and the concentration of peptide was higher inside the cells (Fig. 2). As both peptides harbor eight positive charges, the kinetic uptake difference can be attributed to different clustering of charges (Fig. 1C, iii). The gradual and steady increase of peptide inside the cell (Fig. 2A) argues against the formation of transient pores as suggested by a molecular dynamics simulations¹³.

The molecular dimensions determined by analytical ultracentrifugation (Fig. 1B) describe cTAT as a disk-like structure and linear TAT as a thin rod-like structure. We and others have previously reported a concentration threshold for transduction^{4,14} and an enrichment of RRP on the membrane surface¹⁵⁻¹⁷. The planar shape accompanied by increased clustering of arginines in cTAT might facilitate the formation of RRP assemblies on the cell membranes initiating transduction earlier.

In summary, we show that the non-endocytic mode of entry by RRP termed transduction depends solely on the number and clustering of arginines. We propose that the stable and outwards geometrical orientation of arginine side chains in one plane within the cyclic TAT create optimal interfaces to the negatively charged membrane surface constituents and results in a higher transduction efficiency. This finding will lead to the development of a new generation of more efficient delivery vectors in the future.

References

1. Frankel, A.D. & Pabo, C.O. *Cell*. **55**, 1189-93 (1988).
2. Green, M. & Loewenstein, P.M. *Cell*. **55**, 1179-88 (1988).
3. Rothbard, J.B. et al. *J Am Chem Soc*. **126**, 9506-7 (2004).
4. Tunnemann, G. et al. *FASEB J*. **20**, 1775-84 (2006).
5. Tunnemann, G. et al. *J Pept Sci*. **14**, 469-76 (2008).
6. Fawell, S. et al. *Proc Natl Acad Sci U S A*. **91**, 664-8 (1994).
7. Vives, E., Brodin, P. & Lebleu, B. *J Biol Chem*. **272**, 16010-7 (1997).
8. Futaki, S. et al. *J Biol Chem*. **276**, 5836-40 (2001).
9. Martin, R.M. et al. *Histochem Cell Biol*. **127**, 243-51 (2007).
10. Ho, A. et al. *Cancer Res*. **61**, 474-7 (2001).
11. Choi, M. et al. *Blood*. **102**, 2259-67 (2003).
12. Fischer, P.M. et al. *J Pept Res*. **55**, 163-72 (2000).

13. Herce, H.D. & Garcia, A.E. *Proc Natl Acad Sci U S A.* **104**, 20805-10 (2007).
14. Duchardt, F. et al. *Traffic.* **8**, 848-66 (2007).
15. Afonin, S. et al. *Chemphyschem.* **7**, 2134-42 (2006).
16. Mishra, A. et al. *Angew Chem Int Ed Engl.* (2008).
17. Ziegler, A. et al. *Biochemistry.* **44**, 138-48 (2005).

Figure legends

Fig. 1: Comparison of live-cell transduction ability of RRP as a function of their charge and shape:

(A) RRP-containing peptides transduced into living mouse myoblast cells after incubation for one hour at 15 μ M in a volume of 200 μ l. Representative transmission images of the phase contrast (PC) and confocal optical sections of the fluorescent peptides are shown. Scalebars = 10 μ m. Sequences are indicated, with D-amino acids as small letter and L-amino acids as capital letters. Linker sequences are underlined. Fl = fluorescein, R = tetramethyl-rhodamine. (B) Results from the sedimentation velocity ultracentrifugation experiments and subsequent analysis: f/f_0 : frictional ratio, d: diameter, edge length. (C) Results of the Replica Exchange Molecular Dynamics (REMD) Simulations displayed as the number of structures in clusters, histogram of the distance distribution of peptide termini, 3D-structure from the cluster with the highest frequency. (D) Correlations between transduction frequencies, pI and charge distribution. Filled diamonds denote transducible peptides. pI was estimated with ProtParam (www.expasy.ch) and charge clustering was derived from the number of positive charges divided by the length taken from the ultracentrifugation analysis.

Fig. 2: Kinetic uptake characteristics of a linear and cyclic form of TAT:

(A) Mean fluorescence intensity of fluorescein-labeled linear and cyclic TAT inside the nucleolus was monitored over 95 minutes at a frame rate of one image every 80 seconds. Curves display the mean of 22 and 30 cells for cyclic and linear TAT, respectively, from two experiments. Error bars show the standard deviation.

(B) Selected confocal optical sections of timelapse movies (see movie S1) show the uptake of fluorescently labeled linear and cyclic TAT (20 μ M). Arrowheads indicate the appearance of fluorescence in nucleoli albeit with weak intensities, which is better visualized in the contrast stretched images shown in the insets. Scalebar = 10 μ m. Average uptake initiation times from three timelapses including 40 cells total are indicated with the standard deviation.

Acknowledgements

We thank Heinrich Leonhardt for scientific discussions and critical reading of the manuscript. This work was supported by grants from the German Research Council and the Volkswagen Foundation to M.C.C.

Author Contributions

G.T. designed experiments, performed the live-cell confocal microscopy assays, and analyzed data. J.B. performed the analytical ultracentrifugation experiments and analyzed the respective data. C.P. synthesized some of the peptides. I.M. was involved in the ultracentrifugation analysis. G.T. and M.C.C. designed the project and wrote the manuscript.

Fig. 1

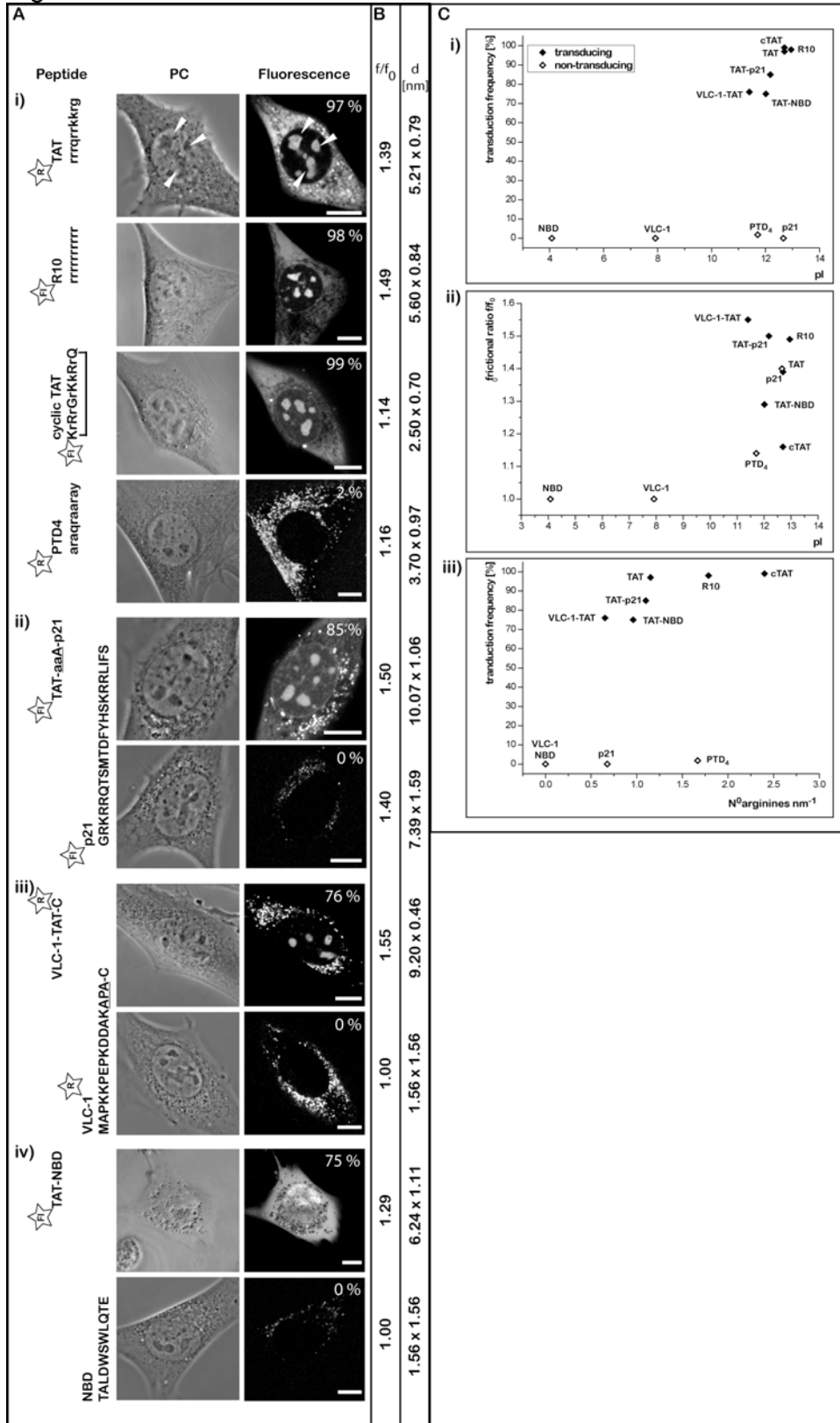
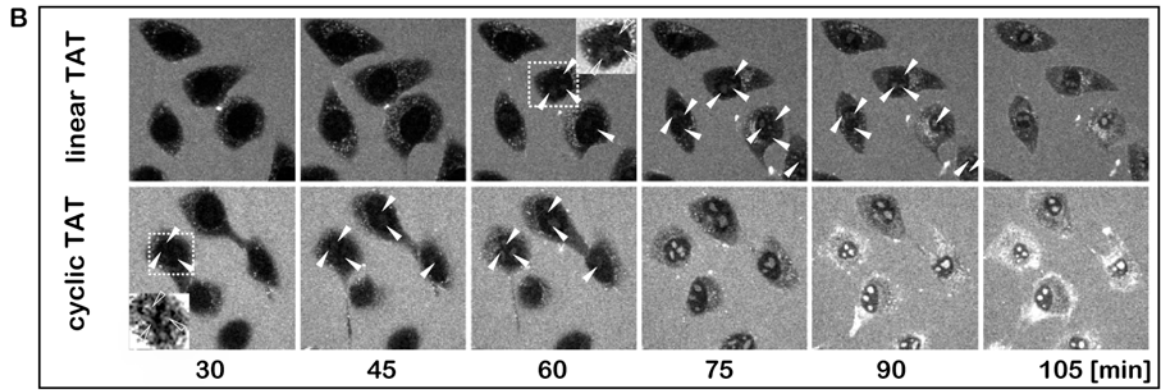
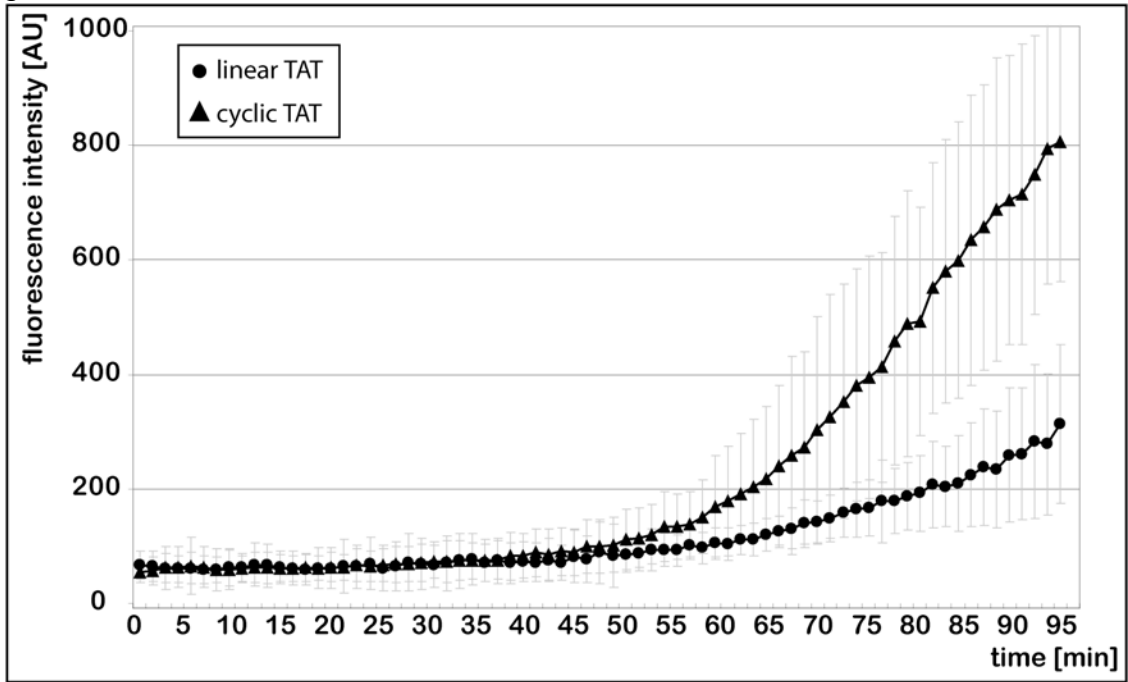


Fig. 2



Supplementary information

1. Cells, transduction experiments, microscopy and image analysis

C2C12 mouse myoblasts were seeded at 70% confluency into 8-well microscope observation chambers (ibidi, Martinsried, Germany) and the growth medium (Dulbecco's modified Eagle medium; PAA, Pasching, Austria) supplemented with 20% fetal calf serum (Life Technologies Inc.; Grand Island, NY, USA) and gentamycin was exchanged against the peptide solutions. The peptides (Table S1) were synthesized using standard Fmoc-chemistry (Peptide Specialty Laboratories, Heidelberg, Germany; BioTez, Berlin,

Germany). The circularization of the cTAT peptide was realized between an additional lysine and glutamic acid, which results in a TAT-ring with the same overall charge as in the native linear form (Fig.1A). Peptides were diluted to 15 μ M final concentration in 200 μ l phosphate buffered saline, pH 7.4 (PBS) and incubated with the cells for 60 minutes at 37 °C. Subsequently, the peptide solution was gently exchanged against growth medium. For the timelapse microscopy over a time of 110 minutes the cells were treated as described above, with the exception that the peptides were diluted in DMEM without FCS to a final concentration of 20 μ M.

Peptide	Sequence	Label (linker)	MW [kDa]
TAT	rrrqrkkrg	(Ahx)	1396.6
TAT	rrrqrkkrg	FI (Ahx)	1866.0
TAT	rrrqrkkrg	FITC (Ahx)	1897.0
TAT	rrrqrkkrg	TAMRA (Ahx)	1921.1
cTAT	KrRrGrKkRrq	FI (K1)	1866.0
R10	rrrrrrrrrr	FI(Ahx)	1692.1
R10	rrrrrrrrrr	FI	2050.2
PTD4	YARAARQARA	Biotin (Ahx)	1542.8
PTD4	araqraaray	TAMRA (Ahx)	1615.5
TAT-p21	rrrqrkkrgaaAGRKRRQTSMTDFYHSKRRLIFS	FII	4914.6
p21	GRKRRQTSMTDFYHSKRRLIFS	FI	3327.7
VLC-1-TAT	MAPKKPEPKDDAKAP <u>AGRKKRRQRRRC</u>		3175.7
VLC-1	MAPKKPEPKDDAKAP <u>AC</u>		1737.1
VLC-1-TAT	MAPKKPEPKDDAKAP <u>AGRKKRRQRRRC</u>	TAMRA	3856.9
VLC-1	MAPKKPEPKDDAKAP <u>AC</u>	TAMRA	1737.1
TAT-NBD	YGRKKRRQRRRTALDWSWLQTE		2891.7
TAT-NBD	YGRKKRRQRRRTALDWSWLQTE	FI (Ahx)	3559.7
NBD	TALDWSWLQTE		1348.7
NBD	TALDWSWLQTE	FI (Ahx)	1819.8
K9	KKKKKKKKK	FI	1528.9

Table S1: Summary of peptides used. Lower case letters indicate D- and upper case letters L-amino acids. The labeled form of PTD4 as well as several other peptides were synthesized in the retro-inverso (retro-all D) form. Linker sequences are underlined. The fluorophores are given together with the amino acid or chemical compound used for coupling at the N-terminus.

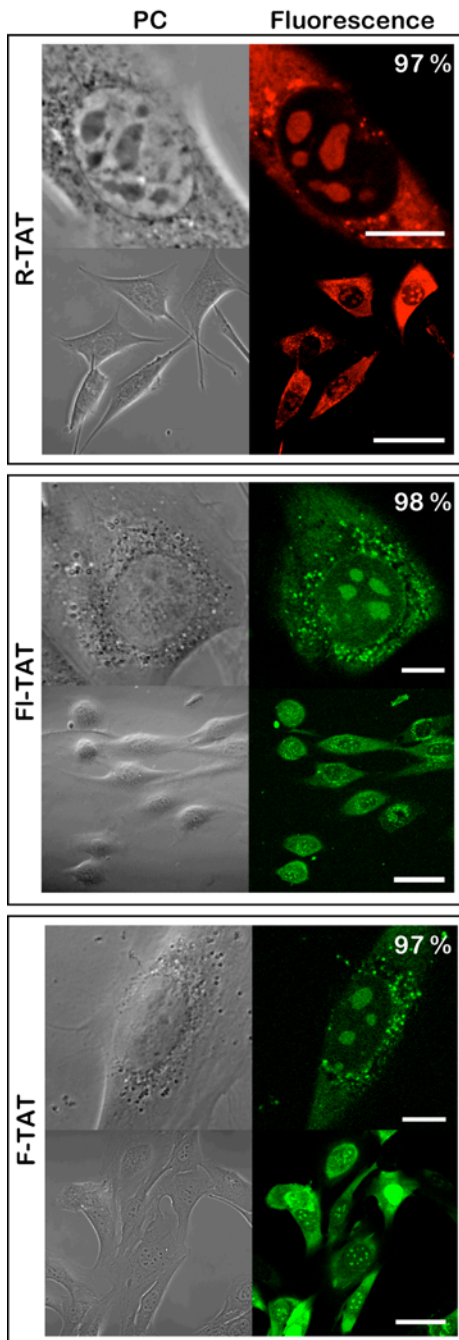


Figure S1:
Fluorescent labels have no effect on CPP uptake and distribution.

Different fluorophores attached to linear TAT transduced with similar efficiencies (given as % total cells in the images) and exhibited the same intracellular distribution. PC: phase contrast, R: TAMRA, FI: fluorescein, F: FITC. Scalebars = 10 μm for high and 50 μm for low magnification images.

To ensure, that different labels did not influence the transduction assay, TAT (amino acids (aa) 48-57 from the transactivator of transcription of the human HIV-1 protein) coupled to several variations of fluorophores used in the experiments was tested for its transduction frequencies and localization (Fig. S1). Confocal microscopy images were acquired with a LSM510 Meta system mounted on an Axiovert 200M inverted microscope and using a 63 x phase contrast plan apochromat oil objective NA1.4 (Zeiss, Jena, Germany). The microscope was equipped with a live-cell incubation chamber maintaining a humidified atmosphere of 5% CO_2 and 37 $^\circ\text{C}$ (Okolab, Ottaviana (NA), Italy). For all settings the main beam splitter was HFT UV/488/543/633, and the specific parameters for the single fluorophores were as follows: TAMRA (R) labeled peptides were excited at 543nm, detected with 565–615 nm band-pass filter and FITC (F) or fluorescein (FI) labeled peptides were excited at 488 nm and detected with a 500–530 nm band-pass filter. Phase contrast images were recorded with excitation at 488 nm and detection in the transmission channel. Laser power for observation was 1%, 488 nm, 25mW and 50 %, 543 nm, 1mW. Settings were adjusted in a way that image pixels were not over or underexposed with the range indicator function in the Zeiss LSM software version 3.2. The macro 'Multi Time Series Rev. 3.2m (Zeiss, Jena, Germany) was used to record in parallel the uptake of the linear and cyclic variants of TAT in two different wells of the observation chambers. This methodology guaranteed an identical peptide to cell ratio for the measurement, which is crucial for transduction experiments. Movies of the collected images over time were generated with the macro 'Concatenate Macro for LSM 3.2'¹⁸. For the analysis of transduction kinetics the movies were cropped to the size of single cells using the open source program suite ImageJ and the cells were aligned with the help of the plugin 'Stack reg'¹⁹. Subsequently, the increase in intensity after peptide application was graphed as average intensity over a square of 20 x 20 pixels inside the nucleolar compartment over a time of 110 minutes. 22 and 30 cells for cyclic and linear TAT, respectively, from two different experiments were evaluated. For the transduction comparison of the linear and cyclic forms of TAT the respective peptides

were normalized to their peptide content via UV-spectroscopy at 280 nm, leading to slight differences in the detected intensity by laser scanning fluorescence microscopy, as the peptide to label ratio differed. However, the transduction characteristics did not change, when the intensity levels were normalized after acquisition.

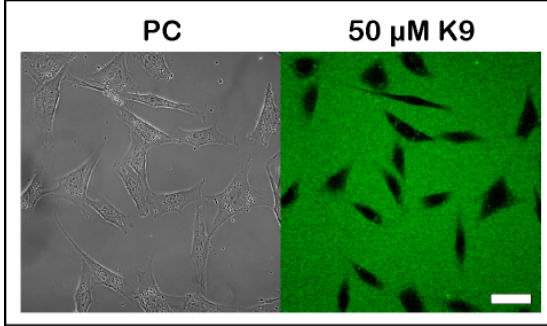


Fig. S2: Oligolysines refuse to transduce:

Incubation C2C12 mouse myoblast with 50 μM of fluos-labeled K9 for two hours. Confocal analysis did not detect K9 freely diffusing intracellularly. Scalebar = 50 μm

2. Sedimentation velocity ultracentrifugation analysis

The shape parameters of the peptides listed in the Table S2 were determined by analytical ultracentrifugation. Molecular mass studies were carried out using an analytical ultracentrifuge XL-A (Beckmann, Palo Alto, Ca, USA). About 400 μl of the peptides dissolved in 4 mM phosphate buffer, pH 7.45, containing 0.3 M NaCl were centrifuged in standard double sector cells at 50,000 rpm and at 20 $^{\circ}\text{C}$. From the moving boundary the following parameters sedimentation (s) and diffusion (D) coefficients were calculated using the program LAMM²⁰. Together with the partial specific volumes the molecular masses were determined via the Svedberg equation and corresponded in all cases to the expected values for the monomeric peptides. Surprisingly, the hydrodynamic mobilities of the TAT fusion peptides were despite of their longer sequences clearly lower than those of the fusion peptides alone. Therefore, as an estimate for the gross conformation, the frictional ratio (f/f_0) was calculated.

$$f/f_0 = 10^{-8} \left(\frac{1 - p\bar{v}}{\sigma\Delta\bar{v}} \right)^{1/3} \quad (1)$$

(f/f_0) is influenced by the two unknown variables shape and hydration. Assuming an average hydration of about 0.3 g bound water per g peptide, a hydration-dependent fraction (f/f_0)_{hy} can be obtained using

$$(f/f_0)_{\text{hy}} = 10^{-8} ((1 - w)/\bar{v}\rho)^{1/3} \quad (2)$$

where w is the portion of bound water. Division of f/f_0 by the factor (f/f_0)_{hy} yields a shape dependent frictional ratio (f/f_0)_{shape}, that permits the rough estimation of the molecular dimensions. With the knowledge of M and the dry volume (V) can be calculated according to equation (eq 3), with the Avogadro number N_A :

$$V = (M \cdot \bar{v}) / N_A \quad (3)$$

The dry volumes of the peptides were calculated based on the formulas 4 and 5 for the description of sphere-like molecules

$$V = 1.33\pi \cdot r^3 \quad (4)$$

with the particle radius corresponding to

$$r = \left(\frac{0.75V}{\pi} \right)^{1/3} \quad (5)$$

formula 6 for rod-like shaped molecules assuming a prolate ellipsoids of revolution with the half axis a and b ($a > b$) or in case of the TAT_{circ} an oblate ellipsoid of revolution with the half axis a and b ($a > b$)

$$V = 1.33 ab^2 \quad (6)$$

and using the a/b ratios derived from the Oncley-diagram²¹ the dry volumes of the peptides were determined.

Construct	$S_{20,W}$	$D_{20,W}$ [$10^7 \text{ cm}^2 \text{ s}^{-1}$]	$M_{\text{exp.}}$ [kDa]	(f/f_0) shape	V_{dry} [nm^3]	d_{sphere} [nm]	d_a [nm]	d_b [nm]	shape
TAT	0.291	18.6	1.445	1.39	1.71	1.48	5.21	0.79	rod
TAT (R)	0.416	20.21	1.899	1.28	2.21	0.808	3.65	1.07	rod
R10	0.303	16.83	1.692	1.49	2.08	1.58	5.60	0.84	rod
PTD ₄	3.75	21.55	1.542	1.16		1.158	3.70	0.98	rod
cTAT (FI)	0.368	19.99	1.87	1.14	2.31	1.64	2.50	0.70	ellipsoid
TAT-p21 (FI)	0.606	10.97	4.843	1.50	5.92	2.24	10.00	1.06	rod
P21 (FI)	0.521	13.30	3.081	1.40	3.76	1.55	7.39	0.98	rod
VLC-1-TAT	0.410	12.43	3.135	1.55	4.07	1.00	9.20	0.46	rod
VLC-1	0.420	24.26	1.626	1.00	2.00	1.56	1.56	1.56	sphere
TAT-NBD	0.539	14.80	3.274	1.29	3.97	1.96	6.24	1.11	rod
NBD	0.397	25.96	1.349	1.00	1,61	1.45	1.45	1.45	sphere

Table S2: Measured and calculated parameters determined by analytical ultracentrifugation with s - sedimentation coefficient, D - diffusion coefficient, MW - molecular weight, V - volume and d - diameter.

Movie S1

Timelapse confocal microscopy of the uptake of linear and cyclic TAT CPP into C2C12 mouse myoblasts. For details see Fig.2.

Supplementary references

18. Rabut, G. & Ellenberg, J. *J Microsc.* **216**, 131-7 (2004).
19. Thevenaz, P., Ruttimann, U.E. & Unser, M. *IEEE Trans Image Process.* **7**, 27-41 (1998).
20. Behlke, J. & Ristau, O. *Biophys Chem.* **95**, 59-68 (2002).
21. Oncley, J.L. *Ann N Y Acad Sci.* **41**, 121-156 (1941).

2.4 Nucleolar marker for living cells

Nucleolar marker for living cells

Robert M. Martin · Gisela Tünnemann ·
Heinrich Leonhardt · M. Cristina Cardoso

Accepted: 10 November 2006
© Springer-Verlag 2006

Abstract In the recent molecular and cell biological research, there is an increasing need for labeling of subcellular structures in living cells. Here, we present the use of a fluorescently labeled cell penetrating peptide for fast labeling of nucleoli in living cells of different species and origin. We show that the short peptide with ten amino acids was able to cross cellular membranes and reach the nucleolar target sites, thereby marking this subnuclear structure in living cells. The treatment of cells with actinomycin D and labeling of B23 protein and fibrillar protein provided evidence for a localization to the granular component of the nucleolus. The fluorescently conjugated nucleolar marker could be used in combination with different fluorophores like fluorescent proteins or DNA dyes, and nucleolar labeling was also preserved during fixation and staining of the cells. Furthermore, we observed a high stability of the label in long-term studies over 24 h as well as no effect on the cellular viability and proliferation and on rDNA transcription. The transducible nucleolar marker is therefore a valuable molecular tool for cell biology that allows a fast and easy labeling of this structure in living cells.

Electronic supplementary material The online version of this article (doi:10.1007/s00418-006-0256-4) contains supplementary material, which is available to authorized users.

R. M. Martin · G. Tünnemann · H. Leonhardt ·
M. C. Cardoso (✉)
Max Delbrück Center for Molecular Medicine,
Robert-Roessle-Str. 10, 13125 Berlin, Germany
e-mail: cardoso@mdc-berlin.de

H. Leonhardt
Department of Biology II, Ludwig Maximilians University
Munich, 82152 Planegg-Martinsried, Germany

Keywords Cell penetrating peptides · Fluorescence microscopy · Living cells · Nucleolus · Transducible nucleolar marker

Abbreviations

AMD	Actinomycin D
DRAQ5	Deep red fluorescing anthraquinone Nr. 5
DMEM	Dulbecco's modified eagle medium
FACS	Fluorescence activated cell sorting
FCS	Fetal calf serum
FITC	Fluorescein isothiocyanate
FU	Fluorouridine
GFP	Green fluorescent protein
HEPES	<i>N</i> -2-hydroxyethylpiperazine- <i>N'</i> -2-ethanesulfonic acid
HIV	Human immunodeficiency virus
mRFP	Monomeric red fluorescent protein
PI	Propidium iodide
PCNA	Proliferating cell nuclear antigen
TAT	Transactivator of transcription

Introduction

The nucleolus is the most prominent substructure in the cell nucleus and it was first described in 1836 by Gabriel Gustav Valentin (Franke 1988). It took more than one century to establish its role in ribosome biogenesis (Brown and Gurdon 1964; Perry 1962). The nucleolus is a very dynamic structure and it forms around the rDNA loci (Andersen et al. 2005). The inner nucleolar structure is organized into fibrillar centers (FC, where rDNA is located and at the periphery of which transcription takes place) surrounded by the dense fibrillar component (DFC, into which nascent

transcripts migrate) and all around the granular component (GC), which is filled with ribosomal precursors (Cheutin et al. 2002; Derenzini et al. 2006; Scheer and Hock 1999). Long ago, it has been noted that the nucleolus size reflects the cellular activity, proliferation and differentiation (Hernandez-Verdun 2006). Furthermore, the nucleolus bears the hallmark of other subnuclear compartments, in that is not delimited by membranes, as is the case for cytoplasmic organelles.

Owing to its higher density and refractility in comparison to the surrounding nucleoplasm, the nucleolus can be visualized with phase contrast or differential interference contrast microscopy. However, the three-dimensional volume and localization within the nucleus as well as its exact borders are hard to identify by contrast microscopy alone and require a fluorescence label (Lam et al. 2005). In addition, such a marker would facilitate high throughput analysis to sort nuclear proteins according to their intranuclear localization. Finally, the development of new high-resolution optical techniques allows for the first time optical analysis down to the nanometer scale but require fluorescent labels. This gain in information could help to elucidate the functional nuclear and genome organization in relation to the nucleolus in the three-dimensional nuclear structure. Specific antibodies to nucleolar proteins or the transfection of cells with plasmids encoding for fluorescent fusions of nucleolar proteins allow the visualization of the nucleolus by fluorescence microscopy. However, these methods require either fixation of the sample and immunostaining in the case of antibodies or transfection of cells and expression of the fluorescence marker in the case of fluorescent proteins. The latter strategy has the advantage of allowing live-cell microscopy but is first time consuming and second restricted to transfectable cells, which is not the case of most primary cells. Furthermore the analysis of drug effects on the nucleolar organization and function could be simplified by using a fast nucleolar label for living cells. A membrane-permeable fluorescent label for the nucleoli, which is fast and easy to apply on living cells, would therefore be a very useful molecular tool for diagnostics and cell biological research.

The ability of certain peptides and proteins with concentrated basic charges to cross cellular membranes was earlier discovered in 1988 for the HIV TAT protein (Frankel and Pabo 1988; Green and Loewenstein 1988), and the peptide domain responsible for membrane transduction was mapped a decade later (Vives et al. 1997). Further comparison of native and artificial membrane transducing peptides indicated that arginines are superior to lysines in transduction potential (Mitchell et al. 2000; Thoren et al. 2003). Independent studies found that peptide sequences present in several

viral and cellular proteins containing a stretch of 6–10 basic amino acids could serve as a targeting sequence for the nucleus and the nucleolus (Dang and Lee 1989; Hatanaka 1990). In this work we reasoned that if both properties, membrane transduction ability and nucleolar targeting signal, could be combined in the same peptide made of a series of basic amino acids we could exploit these independent biological functions to directly label the nucleolus in living cells.

Materials and methods

Peptides and plasmids

Amino-terminal fluorescein labeled deca-arginine peptide (FITC-R₁₀) was synthesized with D-amino acids by Peptide Specialty Laboratories (Heidelberg, Germany), dissolved in ddH₂O and, for application on living cells, further diluted in growth medium.

The mRFP-PCNA expression construct was described before (Sporbert et al. 2005).

Cell culture and transfection

Human HeLa cells as well as Flp 3T3 mouse fibroblast cells were cultivated in DMEM with 10% FCS + 5 mM L-glutamine and 5 µg/ml Gentamycine. C2C12 mouse myoblasts were grown in DMEM with 20% FCS and the same additives. Transfection of C2C12 cells with mRFP-PCNA was carried out by CaPO₄ precipitation method as described (Cardoso et al. 1997). For live cell microscopy the cells were plated onto 4- or 8-well Lab-Tek coverglass chambers (NalgeNunc) or 8-well Ibidi chambers (Ibidi). Adult ventricular cardiomyocytes were enzymatically isolated by retrograde perfusion from excised adult male Wistar rat hearts at a constant flow of 6 ml per min with a Ca²⁺-free HEPES solution containing collagenase (Worthington type II, 60 IU per ml). The freshly dissociated cells were kept at physiological solution with 0.3 mM Ca²⁺ and 0.5% bovine serum albumin at room temperature (Alvarez et al. 2004). DRAQ5 (Biostatus Ltd) staining of DNA in living cells was as described (Martin et al. 2005).

Transduction assays

All peptide transduction experiments were performed with living cells plated on 4- or 8-well coverglass chambers. Before observation, the medium was removed and growth medium with the different peptide concentrations was directly applied to the cells. To remove the background fluorescence of extracellular peptides a

washing step with PBS was included after 30 min of incubation followed by incubation in growth medium without peptide. For the concentration dependent uptake (Fig. 3a) the cells were incubated with the peptides for 1 h before washing with PBS while for the continuous time series to study the uptake dynamics (Fig. 3b) no washing step was performed. The uptake of the marker peptide was studied under a fluorescence microscope for 1 h starting with the peptide application. After observation and imaging of the nucleolar label the cells were returned to the incubator and further image collection was performed 24 h later. Transduction efficiencies were determined in two independent experiments by counting the number of transduced cells with nucleolar label directly on the fluorescence microscope in ten fields of view ($n = 130\text{--}180$ cells).

Cell viability and proliferation assay

Cell viability and label stability after nucleolar marker application were monitored by the ability of the cells to undergo complete mitotic cell cycles and grow to

confluency as well as monitoring the label intensity in the nucleoli 24 h after application.

The membrane integrity was ascertained by the trypan blue exclusion assay. Into each well of a 4-well LabTek chamber with 400 μl medium 2 μl trypan blue solution (Sigma) was added and mixed by pipetting up and down. The number of trypan blue positive cells was counted at 30 min and in separate samples at 24 h.

The impact of the nucleolar marker on cell viability and cell cycle progression was assayed by plating equal number of cells and 1 day later adding or not 10 μM FITC-R₁₀ to the media for 1 h followed by a washing step in PBS and incubation in growth medium. The next day, cells were trypsinized, fixed with methanol for 20 min and stained with 50 μM propidium iodide (PI) (Sigma) for 1 h in the presence of 0.1 mg/ml RNase A (Sigma). DNA content was analyzed by flow cytometry (Becton Dickinson FACSVantage using 488 nm laser excitation and 675/20 nm bandpass filter for detection) as a measure of cell cycle progression (Plander et al. 2003). Five sets of 1×10^4 cells and five sets of 2×10^4 cells were analyzed, and all the data sets were used for the calculation of mean values of cells in

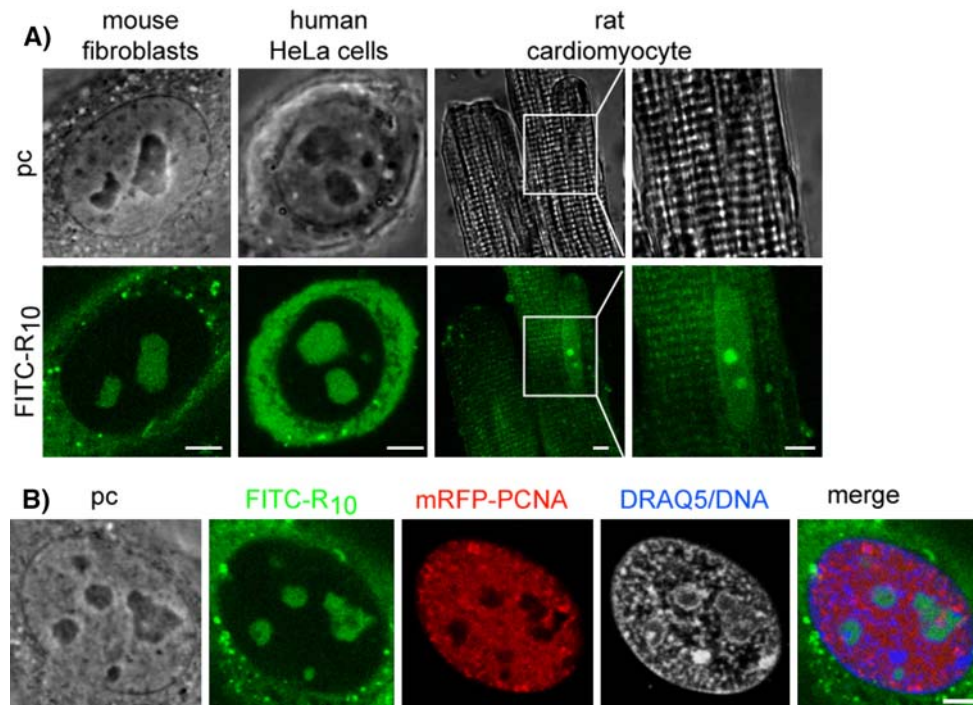


Fig. 1 Transducible nucleolar marker uptake into different cell types and in combination with other fluorophores **a** This figure shows the fluorescently labeled nucleolar marker taken up into cells of different species and origin, which are either from cultured cell lines (fibroblasts, mouse; HeLa, human) or primary cells that are terminally differentiated (adult cardiomyocyte, rat). The cells were incubated with a medium containing the transducible nucleolar marker for 30 min and then washed in PBS and supplied with

the medium. In both cases the marker transduced fast into the cells where it accumulated in the nucleoli and thereby marked this sub-nuclear structure. **b** Displays a C2C12 mouse myoblast transfected with a plasmid coding for mRFP-PCNA (red) and with DNA stained by DRAQ5 (blue). The transducible nucleolar marker labeled with FITC (green) can be used in combination with fluorescent protein labels like mRFP as well as fluorescent dyes such as the live cell DNA stain DRAQ5. Scalebar: 5 μm

G1, S and G2/M phase for FITC-R₁₀ labeled and control cells using ModFit 3.0 software.

In situ transcription assay and inhibition with actinomycin D

Cells were grown on glass coverslips and 1 day later incubated with FITC-R₁₀ for 1 h or 24 h in a 12-well plate. Actinomycin D (AMD) treatment was performed at 0.04 mg/l for 2 h before adding FITC-R₁₀ at 10 μ M to the same growth medium or for 2 h after the incubation of cells with FITC-R₁₀ for 1 h. For the labeling of nascent RNA cells were incubated with 1.5 mM FU in growth medium for 10 min and washed in PBS.

After the incubation schemes cells were fixed in 3.7% formaldehyde in PBS for 10 min and permeabilized with 0.25% (0.5% for AMD experiments) Triton X100 in PBS for 10–12 min. The samples were immunostained with anti-B23 mouse monoclonal antibody (clone FC82291; Sigma) followed by detection with donkey anti-mouse IgG antibody conjugated with TexasRed (Jackson) and #346 anti-fibrillar human autoantibody (kind gift from P. Hemmerich, FLI Jena) followed by donkey anti-human IgG biotin SP (Lot: 47441 Jackson) and streptavidin-Cy5 (Amersham). Fluorouridine incorporated into RNA was detected with anti-BrdU rat monoclonal antibody (clone BU1/75; Harlan Sera Lab) followed by incubation with donkey anti-rat IgG antibody conjugated with Cy5 (Jackson). For the labeling of DNA cells were counterstained with TOPRO-3 at 1.3 μ M final concentration in PBS (Molecular Probes) and mounted with Moviol.

Microscopy, image acquisition and analysis

Live cell microscopy was performed with a Zeiss LSM510Meta confocal setup mounted on an Axiovert 200 M inverted microscope using a 63 \times phase contrast plan-apochromat oil objective NA 1.4 heated to 37°C. For all acquisition settings the main beam splitter was HFT UV/488/543/633 and the parameters specific for each fluorochrome are listed below:

Fluorochrome	Ex (nm)	Em (nm)
FITC	488	BP500–530
mRFP, L-Rhodamine	543	BP565–615
DRAQ5, Cy5	633	LP650

Imaging of AMD treated cells was done at a Leica TCS SP5 confocal setup mounted on a Leica DMI 6000 CS inverted microscope using a 63 \times HCX plan-

apochromat DIC oil objective NA 1.4. The image acquisition was done sequentially to minimize potential crosstalk between the fluorophores. The trypan blue exclusion was determined with brightfield illumination on the Zeiss LSM510 microscope setup. The uptake kinetics analysis (Fig. 3b) was performed by selecting ten nucleoli in ten individual cell nuclei in the image of the last time point and determining their mean fluorescence intensity (FI) at each time point. The fluorescence intensity data for all individual nucleoli were averaged and plotted against the time-scale. Labeling of nascent RNA by FU was analyzed by selecting 60 nuclei from confocal images and determining the mean fluorescence intensity. Background correction was done by applying a threshold according to the mean fluorescence intensity in images from control cells without primary antibody (anti-BrdU). Image analysis was performed with Zeiss LSM Image examiner 3.2 (Zeiss) and Origin 7.5 software (Origin Lab Corp.).

Results and discussion

Our goal was to develop an easy to use live cell fluorescent marker for the nucleolus. Therefore, we tested whether nucleolar targeting ability could be combined with cell penetrating ability in one peptide. The latter would allow non-invasive application to all sorts of cells. We chose a peptide composed of 10 arginines, which had been shown to efficiently transduce into cells (Wender et al. 2000). To prevent proteolytic degradation the peptide was synthesized with D-amino acids. The fluorescent label (FITC) was added to the N-terminal end.

First, we tested the ability of this peptide (FITC-R₁₀) to be taken up by different cells and its intracellular localization. We selected different cell types (fibroblasts, epithelial, muscle) from different species (mouse, rat, human) and not only cell lines (Flp 3T3, HeLa) but also primary cultures (cardiomyocytes). FITC-R₁₀ was diluted in growth medium and applied directly to the cells for 30 min. After the incubation time the cells were washed and analyzed by confocal microscopy. In all cells tested (Fig. 1a) the fluorescence label was found accumulated in the nucleoli identified by the phase contrast images (except in cardiomyocytes where the nucleoli cannot be detected due to the sarcomeric structures) and also diffusely distributed in the cytoplasm. The transfection of the cells with an S-phase marker (mRFP-PCNA; Sporbert et al. 2005 and simultaneous DNA labeling with DRAQ5 Martin et al. 2005) indicated that uptake of the peptide was not cell

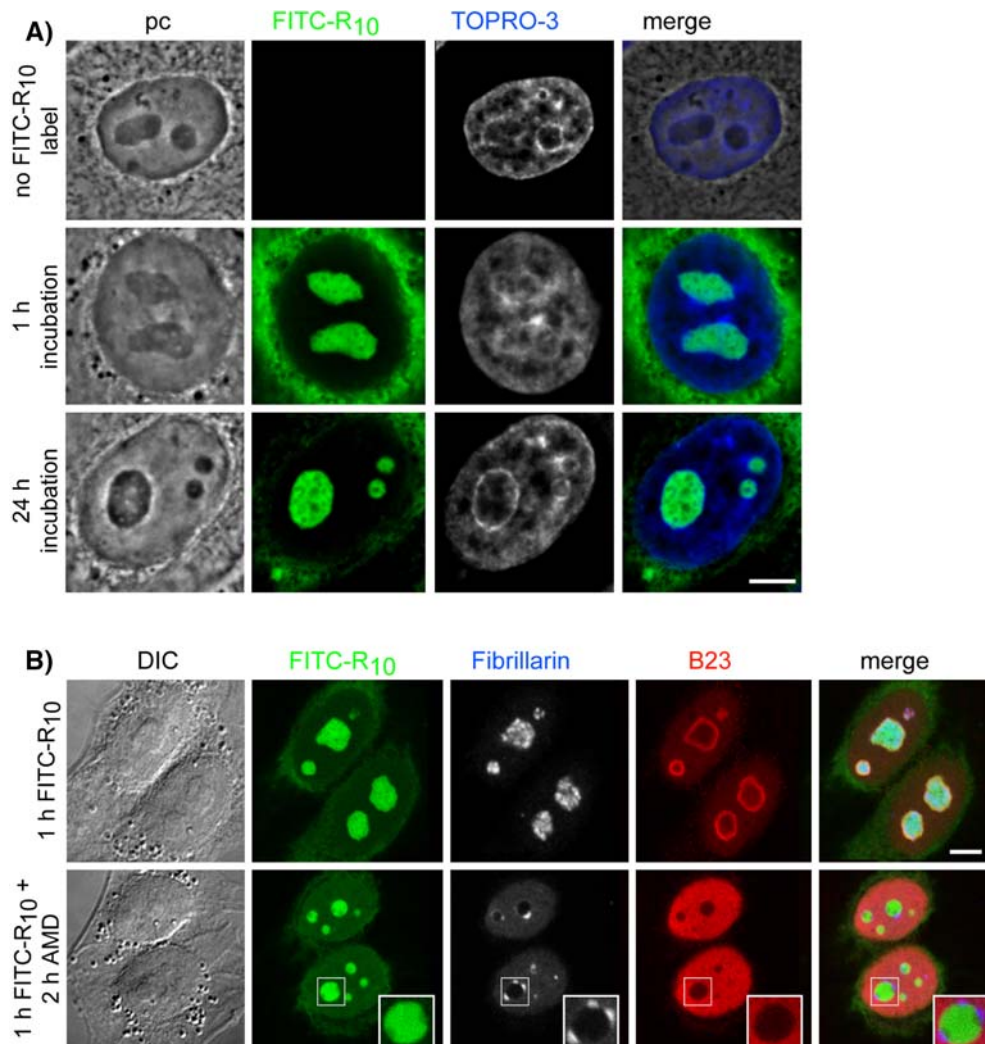
cycle dependent. Indeed, cells in different stages of the S-phase as well as in G1/G2 exhibited nucleolar labeling and also mitotic cells had taken up the marker although the nucleus and the nucleoli are not present (Fig. 1b and data not shown). These data also indicate that combinations with other fluorochromes (e.g., live cell DNA staining with DRAQ5) and fluorescent proteins (e.g., mRFP) are possible. Since any other fluorescent label can be selected for the nucleolar marker peptide, this allows multiple combinations with other fluorochromes.

The FITC-R₁₀ label colocalized with the dark structures in the phase contrast images, which were surrounded by dense chromatin detected by TOPRO-3 staining (Fig. 2a). To confirm the nucleolar localization of FITC-R₁₀ we performed colocalization studies with nucleophosmin/B23 (Fig. 2b), a protein present in the granular component of the nucleolus and fibrillarin localized in the dense fibrillar component (reviewed in Olson and Dundr 2005). The FITC-R₁₀ label

colocalized with the B23 antibody signal at the periphery of the nucleoli and filled the nucleolar interior showing a decreased concentration in the dense fibrillar components labeled by fibrillarin (Fig. 2b). This demonstrated that the FITC-R₁₀ peptide possesses intracellular nucleolar targeting ability and furthermore localizes to the granular component of the nucleolus.

To further test the exclusion of FITC-R₁₀ from fibrillar components we treated cells with AMD. Exposure of cells to this transcription inhibitor leads to a separation of fibrillar and granular components into distinct caps (Reynolds et al. 1964; Chen et al. 1999). The AMD treatment of cells before or after (data not shown) labeling the nucleoli with FITC-R₁₀ showed the persistent localization of FITC-R₁₀ to the granular component remnant separated from the caps formed by the fibrillar components without FITC-R₁₀ (Fig. 2b). In contrast to B23, the nucleolar marker did not redistribute throughout the nucleoplasm after AMD

Fig. 2 Intracellular localization of the FITC-R₁₀. **a** HeLa cells incubated for 1 and 24 h with 10 μM FITC-R₁₀ as well as unlabeled controls were fixed in 3.7% formaldehyde in PBS and stained with TO-PRO-3 to label the DNA. The FITC-R₁₀ label colocalize with the nucleoli identified in the phase contrast during short- and long-term incubation of the cells. **b** The HeLa cells were immunolabeled for B23/nucleophosmin to highlight the granular component of the nucleolus and fibrillarin to label the dense fibrillar components. One sample was treated with actinomycin D (AMD), which leads to a stop in rDNA transcription and the formation of nucleolar caps containing the fibrillar components. The FITC-R₁₀ label was still localized to the nucleolar interior unlike B23, which was redistributed to the nucleoplasm and excluded from the nucleoli. The nucleolar marker does not colocalize with the fibrillarin labeled caps in AMD treated cells. Scalebar: 5 μm



treatment indicating that it interacts with other molecules of the granular component. Thus, the FITC-R₁₀ can also be used in cells where rDNA transcription was stopped to label the granular components of disassembled nucleoli.

Furthermore, these immunostaining experiments after live cell application of FITC-R₁₀ demonstrated that fixation and further treatments could be performed without losing the label or changing its localization (Fig. 2 and suppl. Fig. 1A). When FITC-R₁₀ was applied to pre-fixed samples though, it did not stain the nucleolus (suppl. Fig. 1A).

The kinetics of uptake of the peptide into cells was then studied by time-lapse confocal microscopy. The time series analysis is shown in Fig. 3b and in the supplementary online movie. The images at the first and last timepoints display the accumulation of the marker over time inside the cells and on the cell membrane. The graph represents the fluorescence increase in the nucleoli of 10 different cells. The peptide was rapidly internalized and labeling of the nucleoli started around 20 min and reached the equilibrium at 40 min. Earlier nucleolar labeling could have been missed due to the strong extracellular fluorescence of non-internalized peptides.

In a separate set of experiments we performed a dose response uptake analysis. Different concentrations of the marker in the growth medium were applied for 1 h

to HeLa cell cultures. A threshold minimal concentration for nucleolar labeling was found at 2.5 μM . Lower peptide concentration (1 μM) resulted in no uptake of the marker into the cells (Fig. 3a). A possible explanation for this finding is that a certain concentration of the basic CPP on the cell membrane needs to be reached to enable the membrane transduction process (Dietz and Bdeltahr 2004; Tunnemann et al. 2006). Alternatively, the fluorescence detection method used might not be sensitive enough to detect very low concentrations of fluorescent peptide over the background signal.

Next, we wanted to test the intracellular stability of the marker and its localization. This was examined by applying the transducible fluorescent nucleolar marker to living C2C12 myoblasts for 30 min, which as before resulted in nucleolar accumulation, removing the excess extracellular fluorescent peptide by a washing step with PBS and analyzing the cells by confocal microscopy 24 h later. The fluorescent nucleolar label was surprisingly stable showing very bright nucleolar signal 1 day later without detectable decrease in fluorescence intensity or the number of cells marked (Fig. 3c). No proteolytic degradation or intracellular recycling of the FITC-R₁₀ was observed within this time period. In addition, the morphology of the cells was not changed, and the cultures grew to confluency indicating no overt effect of the nucleolar marker on cell cycle progression and mitotic division. The structure

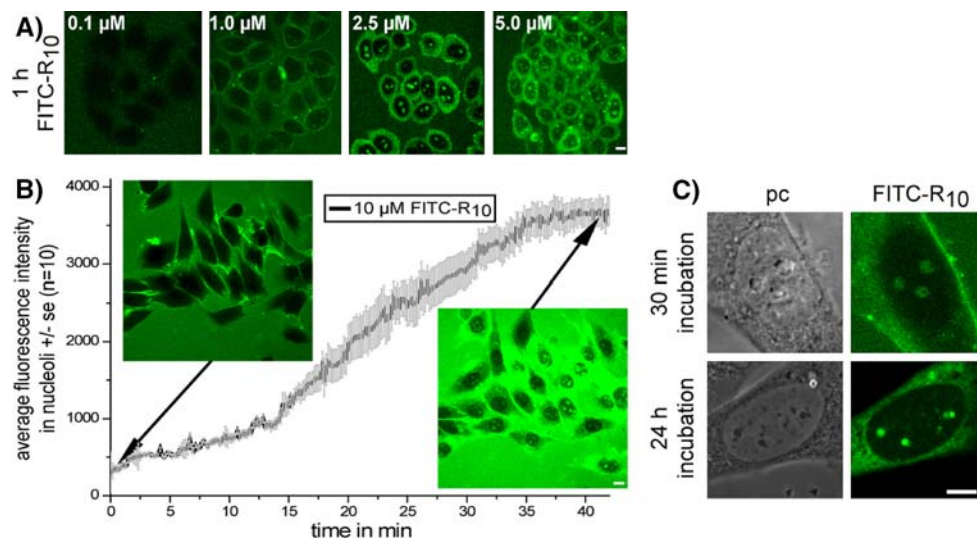


Fig. 3 Kinetics of uptake and intracellular stability of the nucleolar marker The images in **a** show the concentration dependent labeling of the nucleoli in HeLa cells with a threshold at a concentration of 2.5 μM FITC-R₁₀. The kinetics of uptake in **b** display the increase of the fluorescent label in the nucleoli directly after application of 10 μM FITC-R₁₀ in medium to living C2C12 cells without a washing step. The uptake started immediately after the application of the nucleolar marker and was clearly visible after

20 min. A maximum of the nucleolar label was reached 40 min after the start of the experiment (see supplementary movie). **c** C2C12 cells were incubated for 30 min with FITC-R₁₀ in a medium followed by washing in PBS and imaged 24 h later. Representative images are shown and demonstrate the stability of the transducible nucleolar marker over the 1 day period tested (see also Fig. 2a). Scalebar: 5 μm

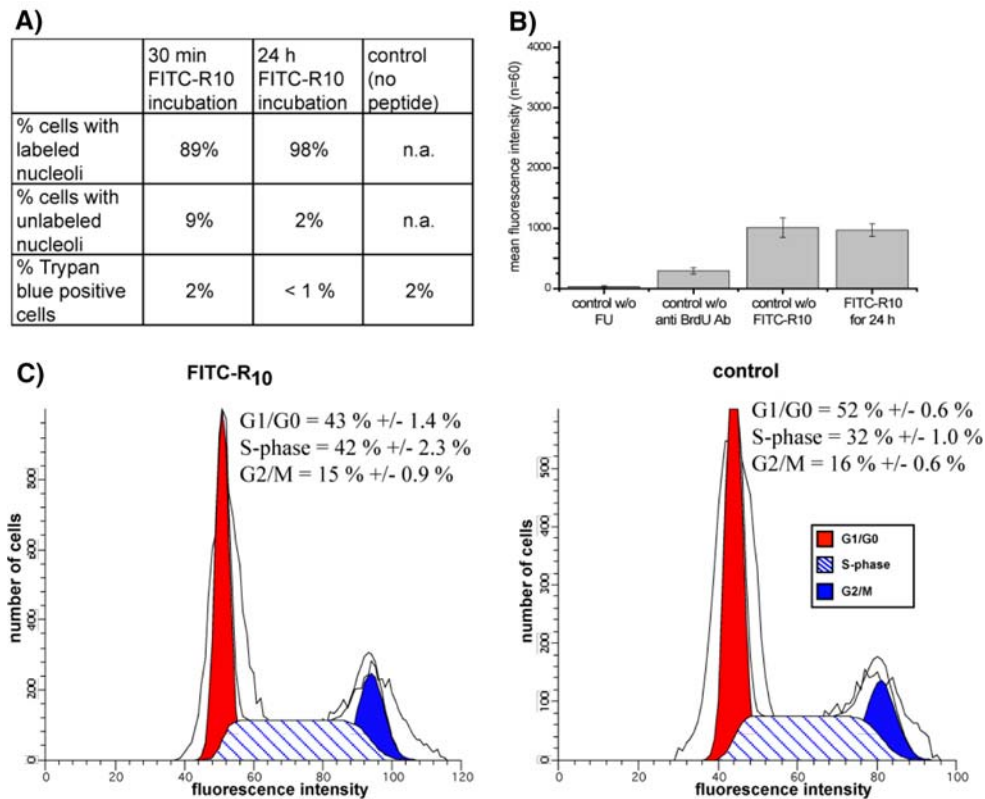


Fig. 4 Effect of the nucleolar marker on the cellular viability, proliferation and rDNA transcription. The table in **a** summarizes the percentage of cells with labeled or unlabeled nucleoli and the trypan blue exclusion test after short- and long-term incubation of living cells with 5 μ M FITC-R₁₀. In both cases a small number of cells remained unlabeled, whereas the majority of cells showed nucleolar labeling after 30 min and also after 24 h incubation with the nucleolar marker. The quantity of trypan blue positive cells during short- and long-time incubation is comparable to the control cells. The diagram in **b** displays in each bar the mean intensity

of fluorescently labeled FU incorporated into rRNA from 60 nuclei measured in confocal images. The signals of labeled rRNA in FITC-R₁₀ labeled or unlabeled control cells differed only a little and within the range of the standard deviation. In **c** the histograms represent fitted curves of flow cytometry measurements. HeLa cells were incubated or not with the transducible nucleolar marker for 1 h following a washing step in PBS and staining with PI in the presence of RNase. The percentage of cells in the respective cell cycle stage, and the standard errors were calculated from ten measurements each

and localization of components of the granular component visualized by antibody labeling of B23 was also not altered between untreated cells and samples labeled for 1 and 24 h with FITC-R₁₀ (Fig. 2a and data not shown).

To measure the efficiency of nucleolar labeling we determined the percentage of labeled cells at different times after application. Nearly 89% of the cells showed nucleolar fluorescence after 30 min and the number even increased to 98% at 24 h (Fig. 4a). Having FITC-R₁₀ in the growth medium for the initial 30 min or during the entire 24 h period yielded no difference in the nucleolar label and the cellular viability (Fig. 4a and data not shown). To further investigate the impact of the peptide transduction on membrane integrity we used the trypan blue exclusion test. No difference was measured between labeled and unlabeled control cells in the number of trypan blue positive cells, which was 1–2% (Fig. 4a).

Next, cells labeled for 24 h with FITC-R₁₀ were incubated for 10 min with fluorouridine (FU), which is preferentially incorporated into rRNA, and the incorporated nucleotide was detected by immunostaining to determine the amount of synthesized RNA in comparison to cells without nucleolar marker (Boisvert et al. 2000). The diagram in Fig. 4b displays the mean fluorescence intensity of 60 nuclei measured from low magnification confocal images. FU labeled cells with and without FITC-R₁₀ exhibited no difference in the level of incorporated nucleotide, i.e., no effect was detected on rDNA transcription.

Finally, to assess potential effects of FITC-R₁₀ on cell proliferation, we subjected HeLa cells with labeled nucleoli and unlabeled control cells to PI staining and flow cytometric analysis of cellular DNA content. The cells were incubated for 1 h with 10 μ M FITC-R₁₀ and then washed in PBS and grown at 37°C for 24 h. After

this incubation scheme the labeled and untreated control cells were methanol fixed and stained with PI including RNase treatment to measure the DNA amount for cell cycle distribution analysis. The control cells showed a cell cycle profile with 52% of cells in G1/G0, 32% in S-phase and 16% in G2/M. In comparison the cells incubated with 10 μ M of the nucleolar marker for 1 h showed some deviations from the control cell cycle profile 24 h post-labeling. The quantity of cells in G1/G0 was decreased to 43%, whereas the cells in S-phase increased to 42% concomitantly. The fraction of G2/M cells remained similar to the control cells (15%; Fig. 4c). These data suggest some delay in cells proceeding through S-phase indicated by an increase and a corresponding decrease of cells in G1/G0. The quantity of cells that exit the S-phase and continued to G2 and the mitotic division was stable also under the influence of the nucleolar marker, which fits the observation of increased confluency in cultures after 24 h.

Altogether, no major effect of the nucleolar marker on either membrane integrity, cell viability and proliferation, RNA synthesis or distribution of nucleolar components was observed at short- or long-incubation times.

Such a label is totally non-invasive and importantly works well in combination with other fluorochromes such as autofluorescent proteins or various dyes. Moreover, most cells not only established cell lines but also non-transfectable primary cultures were transduced with 90% or higher efficiency, and the nucleolar labeling needed only about 20 min to be readily visualized. Curiously, always a few cells remained unlabeled, which could be due to genetic or epigenetic differences in gene expression among the cells in the culture (Tyagi et al. 2001).

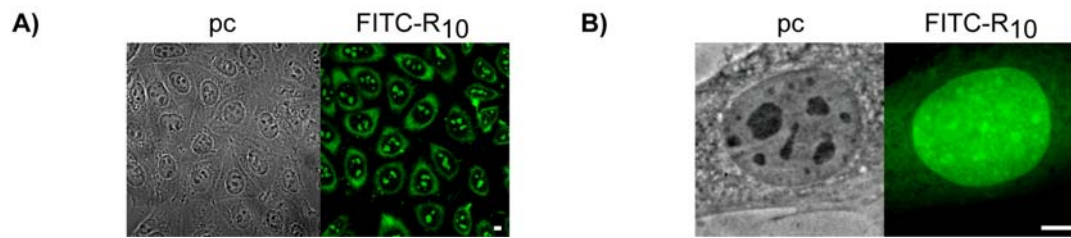
We conclude that the FITC labeled deca-arginine peptide does not interfere with major cellular processes at the concentrations tested. The combination of membrane permeability and nucleolar targeting in one peptide makes this transducible fluorescent marker for the nucleoli applicable to most mammalian cells and a novel and non-invasive tool for live cell microscopy.

Acknowledgments We thank H.-P. Rahn and P. Pierschalek for technical help. GT was supported by the European Union (ESF Program). This work was funded by grants from the Deutsche Forschungsgemeinschaft to HL and MCC.

References

- Alvarez J, Hamplova J, Hohaus A, Morano I, Haase H, Vassort G (2004) Calcium current in rat cardiomyocytes is modulated by the carboxyl-terminal ahnak domain. *J Biol Chem* 279:12456–12461
- Andersen JS, Lam YW, Leung AK, Ong SE, Lyon CE, Lamond AI, Mann M (2005) Nucleolar proteome dynamics. *Nature* 433:77–83
- Boisvert FM, Hendzel MJ, Bazett-Jones DP (2000) Promyelocytic leukemia (PML) nuclear bodies are protein structures that do not accumulate RNA. *J Cell Biol* 148:283–292
- Brown DD, Gurdon JB (1964) Absence of ribosomal RNA synthesis in the anucleolate mutant of *Xenopus laevis*. *Proc Natl Acad Sci USA* 51:139–146
- Cardoso MC, Joseph C, Rahn HP, Reusch R, Nadal-Ginard B, Leonhardt H (1997) Mapping and use of a sequence that targets DNA ligase I to sites of DNA replication in vivo. *J Cell Biol* 139:579–587
- Chen HK, Pai CY, Huang JY, Yeh NH (1999) Human Nopp140, which interacts with RNA polymerase I: implications for rRNA gene transcription and nucleolar structural organization. *Mol Cell Biol* 19:8536–8546
- Cheutin T, O'Donohue MF, Beorchia A, Vandelaer M, Kaplan H, Defever B, Ploton D, Thiry M (2002) Three-dimensional organization of active rRNA genes within the nucleolus. *J Cell Sci* 115:3297–3307
- Dang CV, Lee WM (1989) Nuclear and nucleolar targeting sequences of c-erb-A, c-myc, N-myc, p53, HSP70, and HIV tat proteins. *J Biol Chem* 264:18019–18023
- Derenzini M, Pasquinelli G, O'Donohue MF, Ploton D, Thiry M (2006) Structural and functional organization of ribosomal genes within the mammalian cell nucleolus. *J Histochem Cytochem* 54:131–145
- Dietz GP, Bdeltahr M (2004) Delivery of bioactive molecules into the cell: the Trojan horse approach. *Mol Cell Neurosci* 27:85–131
- Franke WW (1988) Matthias Jacob Schleiden and the definition of the cell nucleus. *Eur J Cell Biol* 47:145–156
- Frankel AD, Pabo CO (1988) Cellular uptake of the tat protein from human immunodeficiency virus. *Cell* 55:1189–1193
- Green M, Loewenstein PM (1988) Autonomous functional domains of chemically synthesized human immunodeficiency virus tat trans-activator protein. *Cell* 55:1179–1188
- Hatanaka M (1990) Discovery of the nucleolar targeting signal. *Bioessays* 12:143–148
- Hernandez-Verdun D (2006) Nucleolus: from structure to dynamics. *Histochem Cell Biol* 125:127–137
- Lam YW, Trinkle-Mulcahy L, Lamond AI (2005) The nucleolus. *J Cell Sci* 118:1335–1337
- Martin RM, Leonhardt H, Cardoso MC (2005) DNA labeling in living cells. *Cytometry A* 67:45–52
- Mitchell DJ, Kim DT, Steinman L, Fathman CG, Rothbard JB (2000) Polyarginine enters cells more efficiently than other polycationic homopolymers. *J Pept Res* 56:318–325
- Olson M.O, Dundr M (2005) The moving parts of the nucleolus. *Histochem Cell Biol* 123:203–216
- Perry RP (1962) The cellular sites of synthesis of ribosomal and 4s RNA. *Proc Natl Acad Sci USA* 48:2179–2186
- Plander M, Brockhoff G, Barlage S, Schwarz S, Rothe G, Knuechel R (2003) Optimization of three- and four-color multiparameter DNA analysis in lymphoma specimens. *Cytometry A* 54:66–74
- Reynolds RC, Montgomery PO, Hughes B (1964) Nucleolar “Caps” produced by actinomycin D. *Cancer Res* 24:1269–1277
- Scheer U, Hock R (1999) Structure and function of the nucleolus. *Curr Opin Cell Biol* 11:385–390
- Sporbert A, Domaing P, Leonhardt H, Cardoso MC (2005) PCNA acts as a stationary loading platform for transiently interacting Okazaki fragment maturation proteins. *Nucleic Acids Res* 33:3521–3528

- Thoren PE, Persson D, Isakson P, Goksor M, Onfelt A, Norden B (2003) Uptake of analogs of penetratin, Tat(48–60) and oligoarginine in live cells. *Biochem Biophys Res Commun* 307:100–107
- Tunnemann G, Martin RM, Haupt S, Patsch C, Edenhofer F, Cardoso MC (2006) Cargo-dependent mode of uptake and bioavailability of TAT-containing proteins and peptides in living cells. *Faseb J* 20:1775–1784
- Tyagi M, Rusnati M, Presta M, Giacca M (2001) Internalization of HIV-1 tat requires cell surface heparan sulfate proteoglycans. *J Biol Chem* 276:3254–3261
- Vives E, Brodin P, Lebleu B (1997) A truncated HIV-1 Tat protein basic domain rapidly translocates through the plasma membrane and accumulates in the cell nucleus. *J Biol Chem* 272:16010–16017
- Wender PA, Mitchell DJ, Pattabiraman K, Pelkey ET, Steinman L, Rothbard JB (2000) The design, synthesis, and evaluation of molecules that enable or enhance cellular uptake: peptoid molecular transporters. *Proc Natl Acad Sci USA* 97:13003–13008

supplementary Fig. 1

Supplementary Figure 1. The nucleolar marker is not removed by fixation. A) HeLa cells were treated with 10 μ M FITC-R10 for 60 min then washed and incubated for 1h in growth medium. Finally the cells were fixed with 3.7% formaldehyde in PBS and the sample was mounted on a coverslip for microscopy analysis. The nucleolar label was comparable to the label in living cells and stable during the washing, fixation and mounting treatments. In B) the cell was fixed in 3.7% formaldehyde before the application of FITC-R10 and the fluorescent peptides did not label the nucleoli. Scalebar 5 μ m (PDF 52 kb)

Kinetics of FITC-R10 uptake into living C2C12 cells. For description see Fig. 3b

2.5 Modulation of muscle contraction by a cell permeable peptide

Modulation of muscle contraction by a cell-permeable peptide

Gisela Tünnemann · Peter Karczewski ·
Hannelore Haase · M. Cristina Cardoso · Ingo Morano

Received: 31 March 2007 / Revised: 18 May 2007 / Accepted: 13 June 2007 / Published online: 24 August 2007
© Springer-Verlag 2007

Abstract In contrast to immortal cell lines, primary cells are hardly susceptible to intracellular delivery methods such as transfection. In this study, we evaluated the direct delivery of several cell-permeable peptides under noninvasive conditions into living primary adult rat cardiomyocytes. We specifically monitored the functional effects of a cell-permeable peptide containing the 15 amino acid N-terminal peptide from human ventricular light chain-1 (VLC-1) on contraction and intracellular Ca^{2+} signals after electrical stimulation in primary adult cardiomyocytes. The transducible VLC-1 variant was taken up by cardiomyocytes within 5 min with more than 95% efficiency and localized to sarcomeric structures. Analysis of the functional effects of the cell-permeable VLC-1 revealed an enhancement of the intrinsic contractility of cardiomyocytes without affecting the intracellular Ca^{2+} . Therefore, peptide transduction mediated by cell-penetrating peptides represents not only a unique strategy to enhance heart muscle function with no secondary effect on intracellular Ca^{2+} but also an invaluable tool for the modulation and manipulation of protein interactions in general and in primary cells.

Keywords Ventricular light chain-1 (VLC-1) · Cell penetrating peptide (CPP) · Peptide transduction · Cardiomyocytes · Drug delivery



GISELA TÜNNEMANN studied chemistry at the Carl von Ossietzky-University in Oldenburg, Germany. She is presently working in the research group “Molecular and Cell Biology of the (Epi) genome” at the Max-Delbrück-Center for Molecular Medicine in Berlin, Germany. Her research interests include peptide delivery into living cells, mechanical aspects of the translocation event of cell-penetrating peptides, and cell cycle regulation.

INGO MORANO received his Ph.D. in human sciences and postdoctoral Habilitation in Human Physiology from the Medical Faculty of the University of Heidelberg. He is presently Professor for Molecular Clinical Physiology at the Medical Faculty of the Humboldt University (Charité), Berlin, and leader of the “Molecular Muscle Physiology Group” at the Max-Delbrück-Center, Berlin. His research interests include expression, regulation, and function of contractile handling proteins in smooth and cardiac muscle.

M. Cristina Cardoso and Ingo Morano contributed equally.

G. Tünnemann · P. Karczewski · H. Haase · M. C. Cardoso (✉) ·
I. Morano (✉)

Max Delbrück Center for Molecular Medicine,
Robert Rössle Str. 10,
13125 Berlin, Germany
e-mail: cardoso@mdc-berlin.de
e-mail: imorano@mdc-berlin.de

I. Morano
Charité Medical School, Johannes Müller Institute for Physiology,
Tucholskystr. 2,
10117 Berlin, Germany

Introduction

Therapeutical delivery of protein or peptides into living primary cells is hampered by the lack of a suitable and efficient method for the introduction of macromolecules. Most commonly used transfections methods work in immortalized cells but mostly fail in primary cells or require specialized and time-consuming protocols, i.e., production

of viral vectors. Moreover, the limited life span of primary cells often does not provide sufficient time for expression of gene products and subsequent analysis of their effects. Physical methods such as microinjection and bead loading are highly invasive procedures and are not tolerated by several cell types. It has been known for quite some time that basic proteins like histones or poly-ornithine as well as stretches of basic amino acids within proteins aid the uptake of proteins into mammalian cells [14, 17, 20, 30]. In the 1990s, transducible peptides like penetratin-1 from the homeodomain of Antennapedia [11] and amino acids 48–57 from the transactivator of transcription of human immunodeficiency virus (HIV)-1 [14] were identified and exploited to introduce drugs or biological macromolecules into mammalian cells. Together with other native and synthetic transducing peptides, they are referred to as cell-penetrating peptides (CPPs) [12]. However, it became evident that the invasive methods used to analyze the transduction mediated by CPPs or effects of interconnected cargoes had led to overestimated transduction results and overrated effects of cargoes fused to CPPs [27]. Nevertheless, CPPs mediate the introduction of fused cargoes into living cells, with cargo-dependent mechanical differences. One uptake mechanism can be described as a slow adsorptive endocytosis and is preferentially used by globular proteins, whereas small compounds like peptides linked to CPPs favor a rapid membrane potential-dependent uptake with overall intracellular availability of the transduced species [33]. CPP-mediated peptide transduction has recently been used to deliver cardioprotective peptides derived from protein kinase C [4, 7–9, 24], the antiapoptotic BH4 peptide derived from the apoptosis regulator protein Bcl-xL [26, 28] and a Nox2-derived peptide [34] into isolated cardiomyocytes or whole hearts. We have tested the feasibility of this approach to study muscle function in living adult primary cardiomyocytes. Therefore, we targeted the interaction between actin and the essential myosin light chain (MLC-1) of cardiac type II myosin by a peptide competition approach. Transgenic overexpression of the N terminus of the human ventricular MLC-1 (residues 1–15; hereafter termed VLC-1), which binds to actin and targets actin/MLC-1 interaction, significantly increased the magnitude and kinetics of the contraction of isolated perfused hearts [21]. We fused the same human VLC-1 peptide to the TAT CPP (VLC-1-TAT) and investigated its uptake, intracellular distribution, and functional consequences in primary living adult rat cardiomyocytes.

Materials and methods

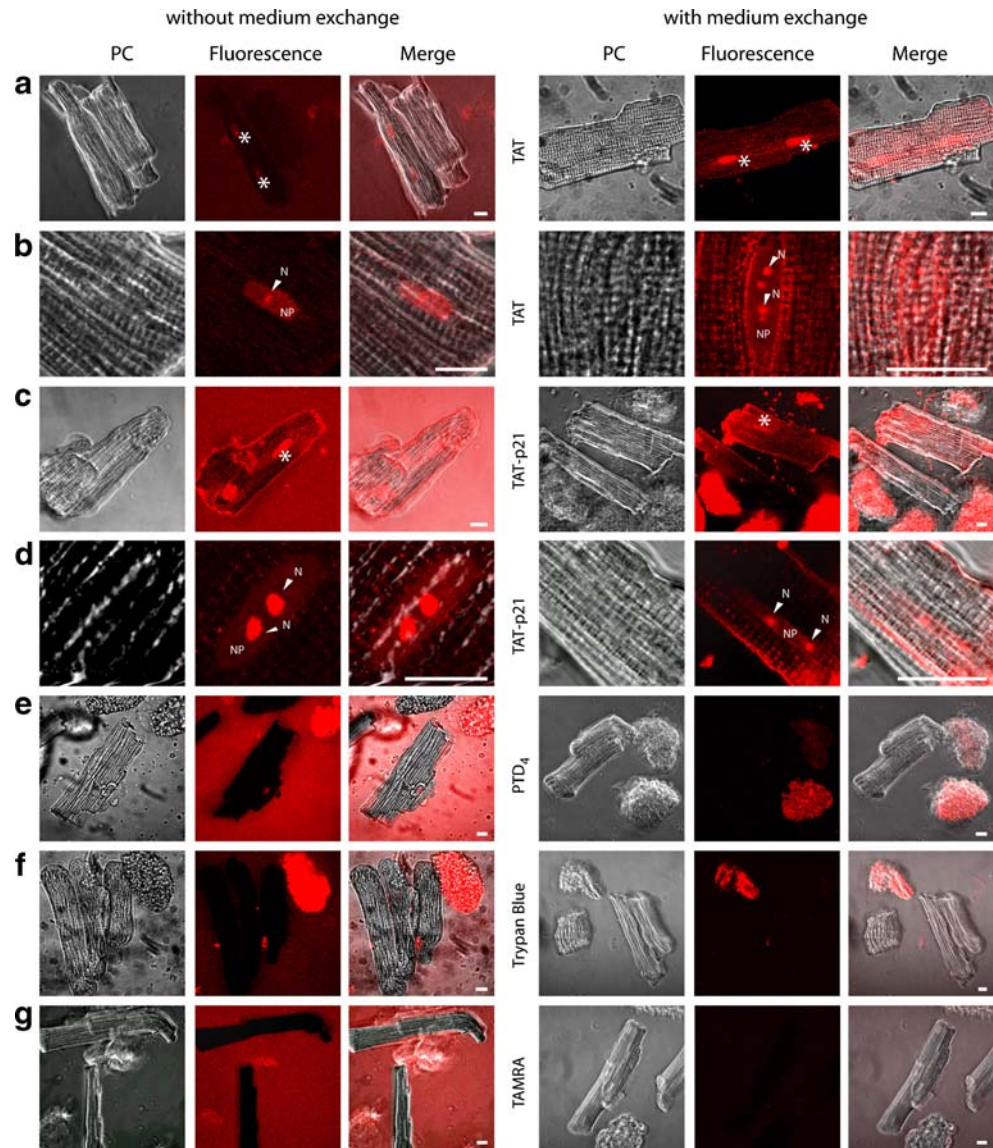
Isolation of adult rat cardiomyocytes Primary cultures of cardiomyocytes from male WKY rats aged 3 months were performed as described previously [1].

Peptides The peptides consisted of either L-amino acids (capital letters) or of D-amino acids (lower case letters). In case of D-amino acid peptides, functional motifs were synthesized as retro-all D-variants (underlined) to maintain their functionality. Peptides were either labeled with the fluorophore 5,6-carboxy-tetramethylrhodamine (TAMRA) or fluorescein isothiocyanate (FITC). TAT (TAMRA- or FITC-rrrqrrkkrg), PTD₄ [23, 33] (TAMRA-araqraaaray), and TAT-p21 (TAMRA-rrrqrrkkrgaaAGRKRRQTSMTDFYHSKRRLIFSa-amide) [33] were labeled directly at their N termini with the indicated fluorophores (Peptide Speciality Laboratories, Heidelberg). In the case of VLC-1 (MAPKKPEPKKSSAKA-C-TAMRA-ME-amide) and VLC-1-TAT (MAPKKPEPKDDAKAPAGRKRRQRRR-C-TAMRA-ME-amide; Biosyntan, Berlin) the TAMRA fluorophore was coupled via an additional cysteine at the C terminus leaving the N terminus free for the interaction with actin.

Uptake of transducible peptides and controls To analyze the transduction ability of different compounds into living adult ventricular cardiomyocytes, the primary cells were plated into a laminin-coated μ -slide eight-well ibiTreat (ibidi, Martinsried) or four-well labtek (Nunc, Wiesbaden) microscopy observation chamber. The respective peptides and controls were added directly to Hank's balanced salts solution buffered with 10 mM 4-(2-hydroxyethyl)-1-piperazineethanesulfonic acid at pH 7.4 (HBSS) or medium and gently shaken to yield a final concentration of 10 μ M in case of the peptides and 5,6-TAMRA-fluorophore. Trypan blue (Sigma-Aldrich) was added to a final concentration of 0.5% (v/v) to the HBSS buffer. For the experiments summarized in Fig. 1 confocal images were acquired 1 h after addition of the respective compounds to living cardiomyocytes. To study the intracellular localization of transducible peptides in Fig. 3, after 15 min of peptide incubation, the medium was removed, and the cells were washed twice with the HBSS buffer. For subsequent confocal image collection, the cells were kept in medium or buffer. To study the effect of the peptide on muscle contraction and intracellular Ca^{2+} (Fig. 4), cardiomyocytes were electrically stimulated (see below) to permit the access of the peptides to all actin molecules with potential binding sites. During confocal image collection, the electric stimulation was temporarily switched off.

Microscopy, image acquisition, and analysis Confocal images were acquired with a Zeiss laser scanning microscope LSM510 Meta mounted on an Axiovert 200M inverted microscope using a 63 \times phase-contrast oil immersion plan-apochromat objective NA1.4 or a 100 \times phase-contrast oil immersion plan-neofluar objective NA1.3. For

Fig. 1 Peptide uptake and intracellular distribution in living adult cardiomyocytes. To study the uptake capacity of different compounds into primary rat cardiomyocytes, different fluorescent compounds were directly added for 1 h to the medium or buffer of freshly isolated cardiomyocytes. After the incubation period, confocal images of the cells were taken without exchange of the medium and after removal of the fluorescent solution and exchange against the fresh medium. Internalization into healthy adult cardiomyocytes occurred after application of 10 μ M of the transducible peptides FITC-TAT shown at low (a) and high magnification (b) and TAMRA-TAT-p21 shown at low (c) and high magnification (d) but not with application of 10 μ M of a basic control peptide PTD₄ (e). Moreover, 0.5% of the vital dye trypan blue (f) or 10 μ M of the TAMRA-fluorophore (g) itself were not able to enter healthy cardiomyocytes (rod-shaped cells in culture). *Scale bar*, 10 μ m. *Stars* indicate the nuclei and *arrowheads* the nucleoli (N) in the higher magnification images. *PC* Phase contrast, *NP* nucleoplasm



all settings, the main beam splitter was HFT UV/488/543/633, and the specific parameters for the single fluorophores were: FITC, excited at 488 nm light, detected with a 500–530-nm bandpass filter; TAMRA or rhodamine excited at 543 nm, detected with 565–615 bandpass filter; and trypan blue, excited with 633 nm, detected with 650 longpass filter. Phase-contrast images were recorded with excitation at 488 nm and detection in the transmission channel. Laser power for observation was typically 1–5% (488 nm, 25 mW) and 50–60% (543 nm, 1 mW) unless otherwise indicated. Settings were adjusted in a way that image pixels were not over- or underexposed with the range indicator function in the Zeiss LSM image acquisition and examiner software version 3.2.

Measurement of cardiomyocyte shortening and Ca²⁺ transients Attached cardiomyocytes were washed with

HBSS. Cells were loaded with Fura-2-AM for 30 min at room temperature in the dark. The dye solution was removed, and cells were left on HBSS for another 15 min. Only cardiomyocytes of optically intact rod-shaped morphology with clear cross-striation were analyzed. Cardiomyocytes were electrically stimulated until a stable steady-state contraction and Fura-2 signal could be monitored.

Cell shortening and Fura-2 signals were simultaneously measured at 30°C on an Ionoptix Contractility and Fluorescence System (Ionoptix). Cardiomyocytes were electrically stimulated with bipolar pulses of 5 ms duration at 1 Hz. Cell shortening, expressed as percentage of resting cell length, was measured using the video-edge technique at a sampling rate of 240 per second. Ca²⁺ transients were monitored as ratio of fluorescence emission at 510 nm was obtained by alternate excitation at 340 and 380 nm (340/

380 ratio). Data files from 15 consecutive beats recorded at intervals were averaged for analysis. Subsequently, the cardiomyocytes were incubated with the peptides for 15 min without electrical stimulation. The peptide was then removed by replacing the peptide-containing HBSS buffer with normal HBSS buffer without the peptide. The cardiomyocytes were subsequently electrically stimulated, and both the shortening and Fura-2 signals were simultaneously recorded. The effect of the peptide on shortening amplitude and the Fura-2 signal was expressed in percent change compared to the steady-state signals obtained in the preincubation period.

Results and discussion

We recently demonstrated by live-cell confocal microscopy that the TAT CPP was able to shuttle fused peptides into primary blood cells and subsequently modulated their functional properties [10]. In this study, we tested whether TAT CPP could penetrate and if a peptide derived from the N terminus of VLC-1 fused to TAT is able to modulate the contractile function of primary adult cardiomyocytes.

Different basic peptides were incubated with freshly prepared cultures of cardiomyocytes, and peptide internalization was analyzed live by laser-scanning confocal microscopy. The fluorescently labeled minimal transduction domain TAT CPP of the transactivator of transcription from HIV-1 was readily taken up into cardiomyocytes and displayed a strong affinity to the nuclear compartment (Fig. 1a). It could also be visualized in a punctate pattern throughout the entire cardiomyocyte (Fig. 1a). To determine whether the TAT CPP is able to shuttle an attached peptide into cardiomyocytes, we used the TAMRA-labeled TAT-p21^{WAF/CIP} (TAT-p21) fusion peptide [33], which in addition to the transducing moiety contains 26 amino acids derived from the C terminus of human p21^{WAF/CIP} protein. The uptake of this cargo peptide (assessed by appearance in nucleoli) occurred on a timescale of 5 to 10 min after peptide application. Its pattern of localization inside the cardiomyocytes was similar to that seen for TAT alone (Fig. 1c). Basic amino acid residues are a prerequisite for the transduction ability of CPPs [13, 25, 35], and peptides containing a minimum of six basic amino acids have been shown to traverse biological membranes [5, 18]. As a nontransducing control peptide, we chose the TAMRA-labeled peptide PTD₄, which contains three arginines in total [23, 33]. More than 1 h after application of this peptide to the cardiomyocyte culture, none of the healthy intact cardiomyocytes took up the fluorescent peptide (Fig. 1e). Similar results were obtained for the vital dye trypan blue (Fig. 1f) and the TAMRA fluorophore (Fig. 1g). Approximately 5% of cardiomyocytes in the cultures were dead or

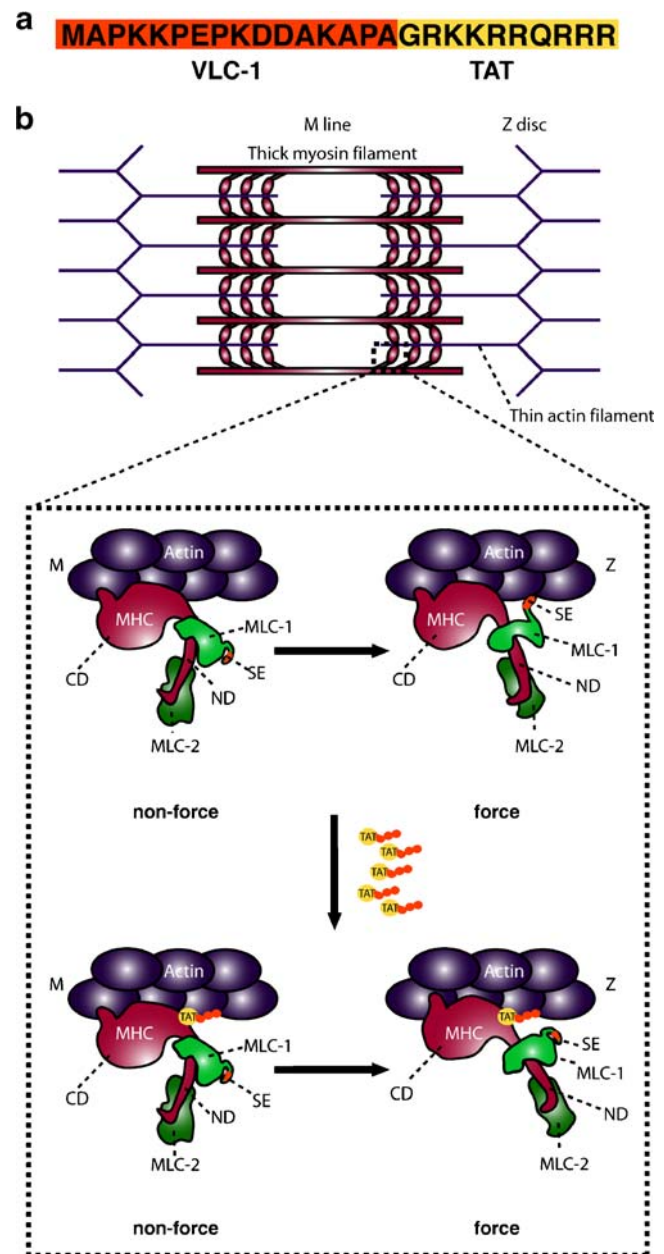


Fig. 2 Molecular hypothesis for the enhancement of cardiomyocyte contractility by the cell-permeable VLC-1 peptide. **a** Primary sequence of VLC-1-TAT peptide color-coded orange for the VLC-1- and yellow for the TAT-moiety. **b** Schematic sliding filament model displaying actin in violet and the MHC in red. The higher magnification shows the catalytic domain (CD) and the neck domain (ND) of one molecule of the MHC. MLC proteins are colored green with the N-terminal SE inside the essential MLC-1 protein highlighted in red. Upon intramolecular conformational changes in the CD of MHC, the ND swings out, exposing the SE of MLC-1 to an actin molecule in direction to the Z-line. Treatment of cardiomyocytes with the transducible TAT peptide (yellow ball) fused to the SE-peptide (orange) blocks potential binding sites of the native MLC-1 N terminus. After the MHC rearrangement, the MLC-1 protein can no longer interact with actin and downregulate the myosin motor activity. The scheme is based on the pre- and postpower stroke model [19] developed with respect to crystallographic data on the Dicyostelium myosin motor domain [15, 32]

harmful (visible in the phase-contrast images as not rod shaped and with no striations). These cells were flooded with both the CPPs as well as any other control dyes (Fig. 1c,e–g). The cell-permeable TAT-derived peptides displayed a similar enrichment in the nuclear compartment with strong accumulation inside nucleoli (arrowheads) as can be seen in the higher magnification images (Fig. 1b,d). This intranuclear distribution is basically determined by the TAT moiety, which includes a nuclear localization sequence [22, 29, 33].

Having shown that CPP TAT was able to shuttle fused peptides into living cardiomyocytes, we designed a transducible peptide comprising the actin-binding element of the ventricular isoform of human MLC-1 (VLC-1), i.e., the N-terminal residues 1–15 (VLC-1 peptide) connected to TAT, termed VLC-1-TAT (Fig. 2). The hearts of transgenic animals harboring minigenes encoding for the VLC-1 peptide revealed enhanced myosin motor activity and positive inotropic effects [21]. A possible molecular mechanism for the increase in myosin motor activity and

contractility is illustrated in the scheme in Fig. 2. MLC-1 isoforms of vertebrate striated muscle play a regulatory role in myosin motor function: The N-terminal part of MLC-1 contains a sticky element (SE), which consists of several positively charged amino acids that bind to the C terminus of actin [3, 6, 16, 31]. The 46 N-terminal amino acids of MLC-1 have previously been modeled on the basis of contemporary crystallographic data [2]. Interactions between the sticky MLC-1 element and actin serve as a negative modulator and decrease the activity of the myosin motor domain. Intracellular delivery of a synthetic sticky MLC-1 element by TAT-mediated transduction therefore would antagonize MLC-1/actin interaction. We predict this would increase myosin motor activity and enhance the shortening amplitude without change of the systolic free Ca^{2+} activation level of intact cardiomyocytes.

To first test whether the VLC-1 peptide itself might be taken up by isolated cardiomyocytes because of its basic charge, VLC-1 and VLC-1-TAT were applied for 15 min to freshly isolated cardiomyocytes under resting conditions or,

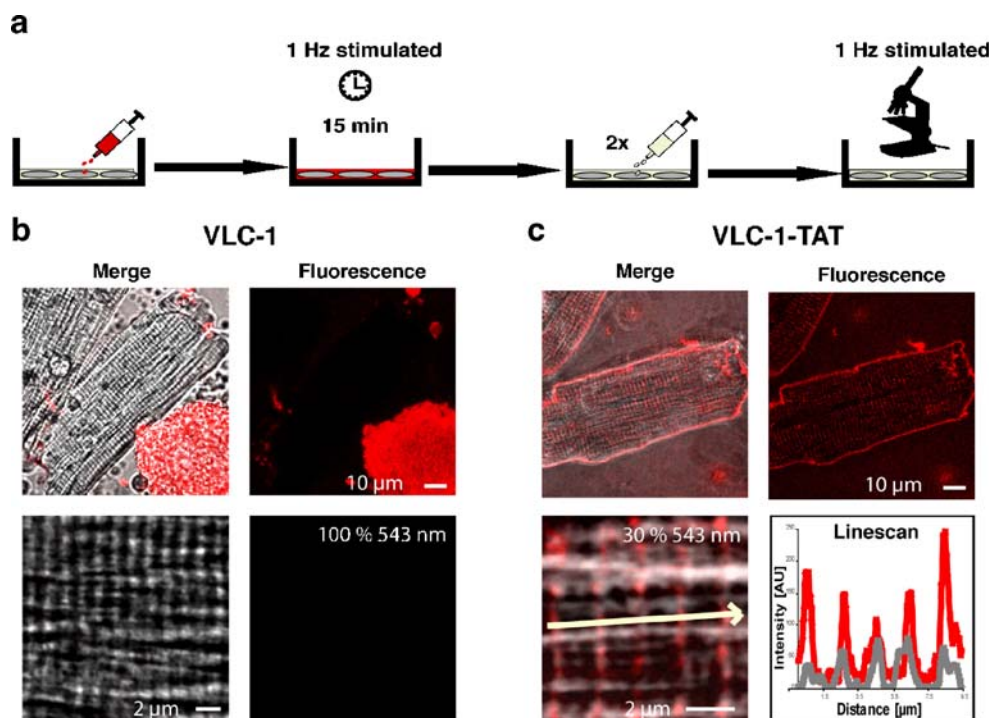
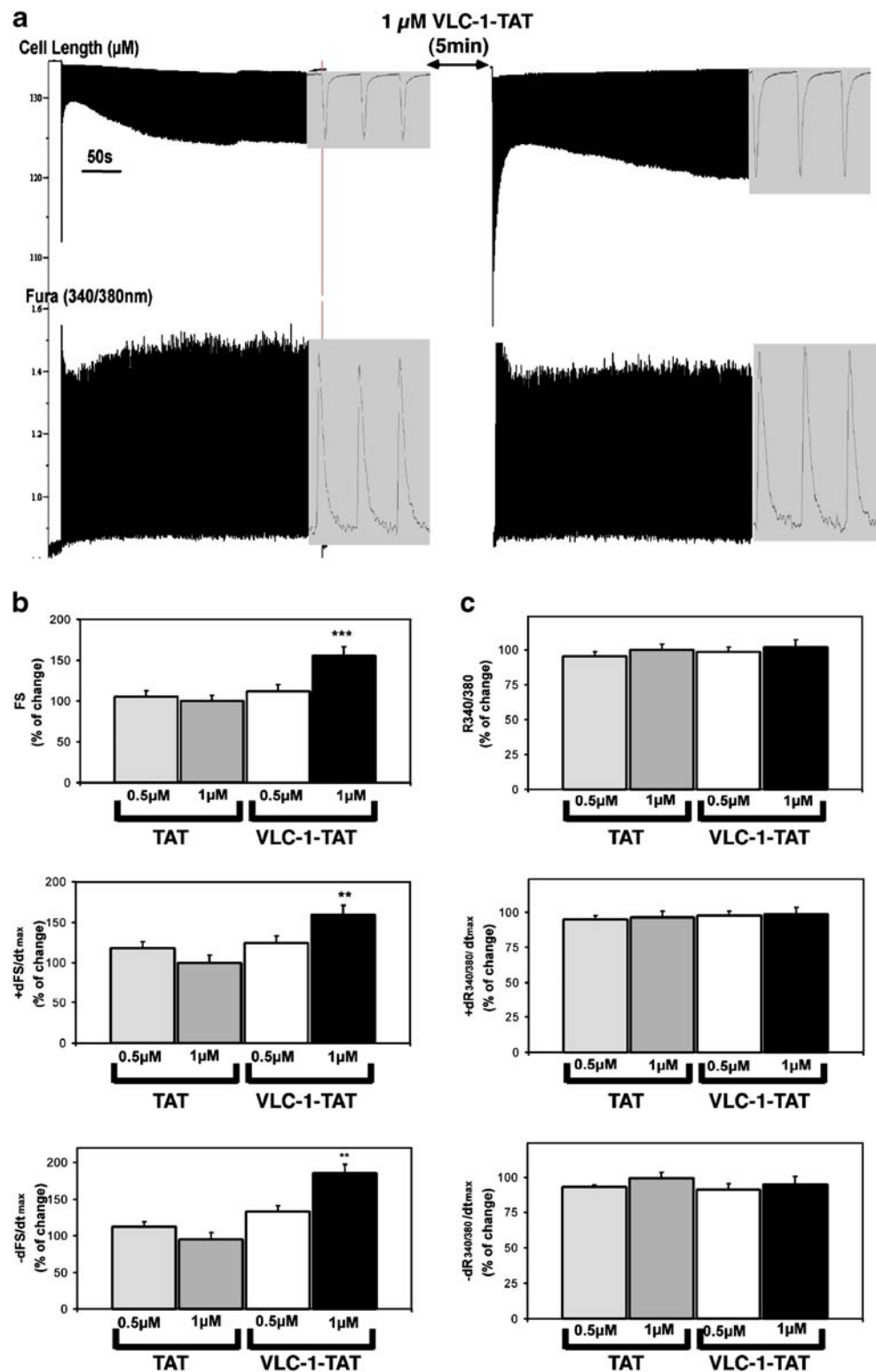


Fig. 3 Transduction and intracellular localization of VLC-1-TAT in isolated adult cardiomyocytes. **a** Scheme for the application of the VLC-1-derived peptides and confocal imaging. Peptides were applied at a concentration of 1 μM , incubated for 15 min to freshly isolated cardiomyocytes. After removal of the peptide solution, the cells were washed twice and kept in buffer or medium for direct live-cell confocal imaging microscopy. Subsequently, the transduced cardiomyocytes were electrically stimulated with 1 Hz for maximally 1 h. **b** The negative control peptide TAMRA-labeled VLC-1 stained only dead cardiomyocytes (low magnification, *upper panel*) but failed to

get internalized into healthy cardiomyocytes even when 100% laser power was used to detect potentially weak signals (*lower panel*). **c** Application of TAT-VLC-1 to living cardiomyocytes led to rapid internalization of the peptide (*upper panel*). The *lower panel* shows transduced VLC-1-TAT at higher magnification in an overlay of the phase contrast and the TAMRA-fluorescence. The *arrow* indicates the direction of the intensity profile of *gray* and *red* intensities in the line scan for the localization analysis of VLC-1-TAT, which was present at sarcomeric structures with enrichment at the actin-containing I-bands (*light bands* in phase-contrast image)

Fig. 4 Functional effects of cell permeable VLC-1-TAT in living adult cardiomyocytes. **a** Original registration of cell length (*top*) and cytosolic Ca^{2+} signals (Fura-2 signal, expressed as ratio R between 340 and 380 excitation; *bottom*) of electrically paced adult rat cardiomyocytes before (basal) and after incubation with $1 \mu\text{M}$ VLC-1-TAT or $1 \mu\text{M}$ TAT as control. **b** Statistical evaluation of the effects of different concentrations of transducible peptides ($0.5, 1 \mu\text{M}$) on fractional shortening (FS ; given in percent of basal contraction obtained before incubation with the peptide), maximal rate of FS ($+dFS/dt_{\text{max}}$), and maximal relaxation rate ($-dFS/dt_{\text{max}}$; both given in percent of basal values obtained before peptide incubation) of control peptide (TAT) and VLC-1-TAT. **c** Statistical evaluation of the effects of different concentrations of transducible peptides ($0.5, 1 \mu\text{M}$) on peak Fura-2 fluorescence signal (expressed as ratio R between 340 and 380 excitation, given in percent of basal $R_{340/380}$ obtained before incubation with the peptide), maximal rate of $R_{340/380}$ ($+dR_{340/380}/dt_{\text{max}}$), and maximal rate of fluorescence decline ($-dR_{340/380}/dt_{\text{max}}$; both given in percent of basal values obtained before peptide incubation) of control peptide (TAT) and VLC-1-TAT. Values are means \pm SEM, $n=6-9$ different cardiomyocytes at each peptide concentration used. *Double asterisk*, $p<0.01$; *triple asterisk*, $p<0.001$ (t test for paired values)



in another set of experiments, constant electric stimulation (1 Hz, 20 V). After the fluorescent peptides were washed away, the cells were analyzed live by confocal laser-scanning microscopy (Fig. 3a). VLC-1 alone was not internalized into healthy cardiomyocytes and stained only

compromised cells (upper panel, Fig. 3b). To ensure that low concentrations of intracellular VLC-1 were not missed, the laser intensity was increased to its maximum, and still no fluorescent signals were measured (lower panel, Fig. 3b). In contrast, VLC-1-TAT reached the intracellular

compartments of more than 95% of adult cardiomyocytes (Fig. 3c).

Unlike the localization of the TAT and TAT-p21 peptides (Fig. 1), the VLC-1-TAT was not detected in the cell nucleus. Detailed analysis of the intracellular distribution of transduced VLC-1-TAT and correlation of the fluorescent signals with the phase contrast images (merge image, lower panel, Fig. 3c) demonstrated that the peptide associates with sarcomeric structures. It showed strong enrichment at the I-bands representing the nonoverlapping zones of the thin actin filaments with the thick myosin filaments (linescan, lower panel, Fig. 3c). After transduction, the VLC-1-TAT peptide remained inside the sarcomeric compartments of the cardiomyocytes for at least 1 h after transferring the loaded cardiomyocytes into the peptide-free buffer solution.

Using the same incubation protocol, we studied the effects of the cell-permeable VLC-1 peptide on muscle function by simultaneously monitoring the shortening amplitude and the systolic and diastolic cytoplasmic Ca^{2+} fluctuations (measured by Fura-2 fluorescence) of paced adult rat cardiomyocytes (Fig. 4a). As shown in Figs. 4b and c, 1 μ M, but not 0.5 μ M, of VLC-1-TAT significantly increased the shortening amplitude of adult cardiomyocyte, while the cytosolic Ca^{2+} signal remained unchanged. The same concentrations of control TAT peptide alone did not change the contractile state or the Fura-2 signals if compared to the basal state during the preincubation period. Higher concentrations of both control and test peptides induced deleterious effects on the cardiomyocyte contraction. It is interesting to note that not only the maximal amplitude of shortening rose but also the maximal rate of shortening and the maximal relaxation velocity increased significantly. Because the Fura-2 signal remained unchanged, the selective effect of the VLC-1-TAT peptide on the contraction parameters suggests a selective and direct effect on the function of the myosin cross-bridges. The Ca^{2+} -sensitizing effect of the VLC-1-TAT peptide could be predicted from the mechanism of action, as the inhibition of the MLC-1/actin interaction may rise selectively myosin motor activity and therefore muscle contraction at a given activating free Ca^{2+} concentration, i.e., an inotropic effect without additional recruitment of Ca^{2+} . It should be noted that the VLC-1-TAT peptide left the intracellular Ca^{2+} -handling system unchanged, as seen by the fact that the kinetic parameters of the Fura-2 fluorescence signals remained normal (Fig. 4c).

In summary, we demonstrate by live-cell microscopy that CPPs and CPPs fused to peptides were taken up by adult cardiomyocytes with high efficiency and localize to their targets inside the cytoplasm and/or nucleus. The cell-permeable peptide VLC-1-TAT accumulated in the actin-containing I-band of the sarcomeres and was able to

enhance the contractility of isolated adult cardiomyocytes without changing the myoplasmic Ca^{2+} levels. Importantly, the fact that VLC-1-TAT did not affect intracellular Ca^{2+} concentration and that it only has targets in striated muscle cells makes this peptide uniquely suited as a novel potential therapeutic tool to modulate heart function. VLC-1-TAT is a powerful new drug candidate to improve the contractile state of the failing heart.

Acknowledgments We thank W.-P. Schlegel and P. Pierschalek for technical assistance, R.M. Martin for invaluable help with confocal microscopy, and Jeff Stear for comments. G.T. was supported by the European Union (ESF Program). This work was funded in part by grants of the Deutsche Forschungsgemeinschaft and the Volkswagen Foundation to M.C.C and Deutsche Forschungsgemeinschaft to I.M.

References

- Alvarez J, Hamplova J, Hohaus A, Morano I, Haase H, Vassort G (2004) Calcium current in rat cardiomyocytes is modulated by the carboxyl-terminal ahnak domain. *J Biol Chem* 279:12456–12461
- Aydt EM, Wolff G, Morano I (2007) Molecular modeling of the myosin-S1(A1) isoform. *J Struct Biol* 159:158–163
- Bottinelli R, Betto R, Schiaffino S, Reggiani C (1994) Unloaded shortening velocity and myosin heavy chain and alkali light chain isoform composition in rat skeletal muscle fibres. *J Physiol* 478(Pt 2):341–349
- Brandman R, Disatnik MH, Churchill E, Mochly-Rosen D (2007) Peptides derived from the C2 domain of protein kinase C epsilon (epsilon PKC) modulate epsilon PKC activity and identify potential protein-protein interaction surfaces. *J Biol Chem* 282:4113–4123
- Cardoso MC, Leonhardt H (2002) Protein transduction: a novel tool for tissue regeneration. *Biol Chem* 383:1593–1599
- Chalovich JM, Stein LA, Greene LE, Eisenberg E (1984) Interaction of isozymes of myosin subfragment 1 with actin: effect of ionic strength and nucleotide. *Biochemistry* 23:4885–4889
- Chen L, Hahn H, Wu G, Chen CH, Liron T, Schechtman D, Cavallaro G, Banci L, Guo Y, Bolli R, Dorn GW 2nd, Mochly-Rosen D (2001) Opposing cardioprotective actions and parallel hypertrophic effects of delta PKC and epsilon PKC. *Proc Natl Acad Sci USA* 98:11114–11119
- Chen L, Wright LR, Chen CH, Oliver SF, Wender PA, Mochly-Rosen D (2001) Molecular transporters for peptides: delivery of a cardioprotective epsilonPKC agonist peptide into cells and intact ischemic heart using a transport system, R(7). *Chem Biol* 8:1123–1129
- Chen M, Won DJ, Krajewski S, Gottlieb RA (2002) Calpain and mitochondria in ischemia/reperfusion injury. *J Biol Chem* 277:29181–29186
- Choi M, Rolle S, Wellner M, Cardoso MC, Scheiderei C, Luft FC, Ketritz R (2003) Inhibition of NF-kappaB by a TAT-NEMO-binding domain peptide accelerates constitutive apoptosis and abrogates LPS-delayed neutrophil apoptosis. *Blood* 102:2259–2267
- Derossi D, Chassaing G, Prochiantz A (1998) Trojan peptides: the penetrating system for intracellular delivery. *Trends Cell Biol* 8:84–87
- Dietz GP, Bahr M (2004) Delivery of bioactive molecules into the cell: the Trojan horse approach. *Mol Cell Neurosci* 27:85–131

13. Dom G, Shaw-Jackson C, Matis C, Bouffieux O, Picard JJ, Prochiantz A, Mingeot-Leclercq MP, Brasseur R, Rezsöházy R (2003) Cellular uptake of Antennapedia Penetratin peptides is a two-step process in which phase transfer precedes a tryptophan-dependent translocation. *Nucleic Acids Res* 31:556–561
14. Fawell S, Seery J, Daikh Y, Moore C, Chen LL, Pepinsky B, Barsoum J (1994) Tat-mediated delivery of heterologous proteins into cells. *Proc Natl Acad Sci USA* 91:664–668
15. Fisher AJ, Smith CA, Thoden JB, Smith R, Sutoh K, Holden HM, Rayment I (1995) X-ray structures of the myosin motor domain of *Dictyostelium discoideum* complexed with MgADP.BeFx and MgADP.AIF₄. *Biochemistry* 34:8960–8972
16. Fodor WL, Darras B, Seharaseyon J, Falkenthal S, Francke U, Vanin EF (1989) Human ventricular/slow twitch myosin alkali light chain gene characterization, sequence, and chromosomal location. *J Biol Chem* 264:2143–2149
17. Frankel AD, Pabo CO (1988) Cellular uptake of the tat protein from human immunodeficiency virus. *Cell* 55:1189–1193
18. Futaki S, Suzuki T, Ohashi W, Yagami T, Tanaka S, Ueda K, Sugiura Y (2001) Arginine-rich peptides. An abundant source of membrane-permeable peptides having potential as carriers for intracellular protein delivery. *J Biol Chem* 276:5836–5840
19. Geeves MA, Holmes KC (1999) Structural mechanism of muscle contraction. *Annu Rev Biochem* 68:687–728
20. Green M, Loewenstein PM (1988) Autonomous functional domains of chemically synthesized human immunodeficiency virus tat trans-activator protein. *Cell* 55:1179–1188
21. Haase H, Dobbernack G, Tunnemann G, Karczewski P, Cardoso C, Petzhold D, Schlegel WP, Lutter S, Pierschalek P, Behlke J, Morano I (2006) Minigenes encoding N-terminal domains of human cardiac myosin light chain-1 improve heart function of transgenic rats. *FASEB J* 20:865–873
22. Hauber J, Malim MH, Cullen BR (1989) Mutational analysis of the conserved basic domain of human immunodeficiency virus tat protein. *J Virol* 63:1181–1187
23. Ho A, Schwarze SR, Mermelstein SJ, Waksman G, Dowdy SF (2001) Synthetic protein transduction domains: enhanced transduction potential in vitro and in vivo. *Cancer Res* 61:474–477
24. Inagaki K, Hahn HS, Dorn GW 2nd, Mochly-Rosen D (2003) Additive protection of the ischemic heart ex vivo by combined treatment with delta-protein kinase C inhibitor and epsilon-protein kinase C activator. *Circulation* 108:869–875
25. Mai JC, Shen H, Watkins SC, Cheng T, Robbins PD (2002) Efficiency of protein transduction is cell type-dependent and is enhanced by dextran sulfate. *J Biol Chem* 277:30208–30218
26. Ono M, Sawa Y, Ryugo M, Alechine AN, Shimizu S, Sugioka R, Tsujimoto Y, Matsuda H (2005) BH4 peptide derivative from Bcl-xL attenuates ischemia/reperfusion injury through anti-apoptotic mechanism in rat hearts. *Eur J Cardiothorac Surg* 27:117–121
27. Richard JP, Melikov K, Vives E, Ramos C, Verbeure B, Gait MJ, Chernomordik LV, Lebleu B (2003) Cell-penetrating peptides. A reevaluation of the mechanism of cellular uptake. *J Biol Chem* 278:585–590
28. Rohrbach S, Muller-Werdan U, Werdan K, Koch S, Gellerich NF, Holtz J (2005) Apoptosis-modulating interaction of the neuregulin/erbB pathway with anthracyclines in regulating Bcl-xS and Bcl-xL in cardiomyocytes. *J Mol Cell Cardiol* 38:485–493
29. Ruben S, Perkins A, Purcell R, Joung K, Sia R, Burghoff R, Haseltine WA, Rosen CA (1989) Structural and functional characterization of human immunodeficiency virus tat protein. *J Virol* 63:1–8
30. Ryser HJ, Hancock R (1965) Histones and basic polyamino acids stimulate the uptake of albumin by tumor cells in culture. *Science* 150:501–503
31. Seharaseyon J, Bober E, Hsieh CL, Fodor WL, Francke U, Arnold HH, Vanin EF (1990) Human embryonic/atrial myosin alkali light chain gene: characterization, sequence, and chromosomal location. *Genomics* 7:289–293
32. Smith CA, Rayment I (1996) X-ray structure of the magnesium (II).ADP.vanadate complex of the *Dictyostelium discoideum* myosin motor domain to 1.9 Å resolution. *Biochemistry* 35:5404–5417
33. Tunnemann G, Martin RM, Haupt S, Patsch C, Edenhofer F, Cardoso MC (2006) Cargo-dependent mode of uptake and bioavailability of TAT-containing proteins and peptides in living cells. *FASEB J* 20:1775–1784
34. Zhang M, Kho AL, Anilkumar N, Chibber R, Pagano PJ, Shah AM, Cave AC (2006) Glycated proteins stimulate reactive oxygen species production in cardiac myocytes: involvement of Nox2 (gp91phox)-containing NADPH oxidase. *Circulation* 113:1235–1243
35. Ziegler A, Blatter XL, Seelig A, Seelig J (2003) Protein transduction domains of HIV-1 and SIV TAT interact with charged lipid vesicles. Binding mechanism and thermodynamic analysis. *Biochemistry* 42:9185–9194

2.6 Cargo-dependent mode of uptake and bioavailability of TAT-containing proteins and peptides in living cells.

Cargo-dependent mode of uptake and bioavailability of TAT-containing proteins and peptides in living cells

Gisela Tünnemann,* Robert M. Martin,* Simone Haupt,[†] Christoph Patsch,[†] Frank Edenhofer,[†] and M. Cristina Cardoso*^{•1}

*Max Delbrück Center for Molecular Medicine, Berlin, Germany; and [†]Institute of Reconstructive Neurobiology, Stem Cell Engineering Group, University of Bonn-Life and Brain Center and Hertie Foundation, Bonn, Germany

ABSTRACT Cell-penetrating peptides (CPPs) are capable of introducing a wide range of cargoes into living cells. Descriptions of the internalization process vary from energy-independent cell penetration of membranes to endocytic uptake. To elucidate whether the mechanism of entry of CPP constructs might be influenced by the properties of the cargo, we used time lapse confocal microscopy analysis of living mammalian cells to directly compare the uptake of the well-studied CPP TAT fused to a protein (>50 amino acids) or peptide (<50 amino acids) cargo. We also analyzed various constructs for their subcellular distribution and mobility after the internalization event. TAT fusion proteins were taken up largely into cytoplasmic vesicles whereas peptides fused to TAT entered the cell in a rapid manner that was dependent on membrane potential. Despite their accumulation in the nucleolus, photobleaching of TAT fusion peptides revealed their mobility. The bioavailability of internalized TAT peptides was tested and confirmed by the strong inhibitory effect on cell cycle progression of two TAT fusion peptides derived from the tumor suppressor p21^{WAF/Cip} and DNA Ligase I measured in living cells.—Tünnemann, G., Martin, R. M., Haupt, S., Patsch, C., Edenhofer, F., Cardoso, M. C. Cargo-dependent mode of uptake and bioavailability of TAT-containing proteins and peptides in living cells. *FASEB J.* 20, 1775–1784 (2006)

Key Words: cell-penetrating peptide • protein transduction • PCNA • PBD • Cre recombinase

THE PHENOMENON OF transduction denotes the size-independent *in vivo* delivery of a wide variety of cargoes into cells and is mediated by cell-penetrating peptides (CPPs). Although the internalization of fluorophores, nucleotides, peptides, globular proteins, nanoparticles, lipids, and drugs interconnected to CPPs into living cells has been described in the literature and resulted in measurable biological effects (1), the reported transduction experiments need to be critically evaluated in terms of the invasiveness of the detection methods utilized (2). Most known CPPs are parts of viral proteins or artificial derivatives thereof, and include several

arginines and/or lysines (reviewed in ref. 3). One of the best-studied CPP is a basic amino acid peptide from the transactivator of transcription (TAT) protein of the HIV-1 with the minimal transduction domain comprising amino acids 48–57 (4). The initializing step in the mechanism of cellular entry of CPPs is thought to be the strong ionic interaction between the positively charged amino acid residues and negatively charged plasma membrane constituents (5–7). Among the cationic groups mediating cellular uptake, the guanidinium group of arginine has been shown to be the most effective (8–10). Subsequent events needed for the internalization, however, differ between reports and are often conflicting. The first mechanistic studies led to the proposal that CPP internalization occurs rapidly in a receptor- and energy-independent manner (6, 9, 11–13) perhaps by destabilizing the lipid bilayer or by the formation of inverted micelles with subsequent release of their contents within the intracellular space (reviewed in ref. 14). More recently, an active mechanism based on vesicular uptake has been proposed as the general mode of internalization of CPP constructs into cells (15–19).

To understand whether the mechanism of entry is dependent on the cargo connected to the CPP, we directly compared TAT fused to globular proteins and TAT-containing peptides with respect to their uptake kinetics and their intracellular distribution after internalization in living cells. Transduced constructs were also analyzed for their ability to reach their targets inside the cell and to exert their biological activity.

MATERIALS AND METHODS

Peptides and proteins

Peptides (complete description in **Table 1**) were synthesized by Biosyntan GmbH (Berlin, Germany), Peptide Specialty Laboratories (Heidelberg, Germany), and Bachem (Weil am

¹Correspondence: Max Delbrück Center for Molecular Medicine, Robert-Rössle-Str. 10, Berlin 13125, Germany. E-mail: cardoso@mdc-berlin.de
doi: 10.1096/fj.05-5523com

TABLE 1. List of peptides and their uptake efficiencies^a

Peptide and label	aa sequence	kDa	pI	Peptide concentration	Transduction efficiency	Transduction threshold
R-PTD ₄	YARAARQARA	1.13	11.71	10 μM	0%	400 μM
F(Ahx)-TAT	YGRKKRRQRRR	1.93	12.31	1 μM	90%	1 μM
R-TAT (ri)	rrrqrkkrg	1.81	13.3	1 μM	90%	1 μM
bt-NLS	SGYGPKKKRKVG	1.93	10.68	10 μM	0%	n.a.
Lig1-PBD-F	MQRDIMSFFQPTKEFKAKK	2.80	10.00	10 μM	0%	n.a.
R-TAT-HA2(ri)	rrrqrkkrg-gdimgewgneifgaiaqflg	3.24	11.71	10 μM	80%	0.1 μM
F(Ahx)-TAT-Control	YGRKKRRQRRR-TALDASALQTE	3.05	11.72	20 μM	70%	n.d.
R-TAT(ri)-p21-PBD	rrrqrkkrg-aaA-GRKRRQTSMTDFYHSKRRLIFSa	4.96	12.43	20 μM	90%	7.5 μM
TAT-Lig1-PBD-R	YGRKKRRQRRR-GGG-MQRSIMSFFQPTKEGKAKK	4.38	12.14	10 μM	80%	5 μM

^aR, TAMRA/rhodamine; F, FITC; Ahx, aminohexanoic acid; capital letters, L-amino acids; small letters, D-amino acids; ri, retro inverso; n.a., not applicable; n.d., not determined.

Rhein, Germany). The PCNA binding domain (PBD) peptide TAT-p21-PBD is derived from human p21^{WAF/Cip} (20) and the Lig1-PBD as well as TAT-Lig1-PBD from mouse DNA Ligase I (21, 22). The peptides were analyzed by HPLC a second time at the end of the experiments to assure their stability under the storage conditions. The pI of the peptides was calculated using the program ProtParam (<http://au.expasy.org/cgi-bin/protparam>). His-NLS-TAT-Cre-recombinase (TAT-Cre) protein was produced, purified (23), and labeled with Alexa Fluor 633 or rhodamine as described (24). BL21 (DE3) cells (Novagen, Madison, WI, USA) were used for production of His-PTD₄-PCNA. Bacterial cultures were grown at 37°C until early-mid log phase and expression was induced by addition of 1 mM IPTG. Cells were harvested 3 h after induction, lysed by lysozyme treatment and ultrasonification, and His-tagged protein purified to >95% purity from cell lysates by affinity chromatography using Talon resin material (BD Bioscience, Franklin Lakes, NJ, USA) according to the manufacturer's instructions. The purified protein was labeled with Atto 633 NHS ester (Fluka, St. Louis, MO, USA) in 0.1 M bicarbonate buffer pH 8.5, then further purified and rebuffered into PBS pH 7.4 over a G25-Sephadex column (Pharmacia, Cambridge, MA, USA). BL21 (DE3) CodonPlus-RIL cells (Novagen) were used to produce His-TAT-MK2 (MAPKAP kinase 2). Bacterial cultures were grown and induced as above, and harvested cells were disrupted by 2-fold homogenization at a 1000 bar with a SLM AMINCO FrenchPress (Spectronic Instruments, Leeds, UK). More than 98% pure protein was obtained from the lysates upon Talon affinity chromatography, as before (BD Bioscience). The purified protein was labeled with Cy5 NHS ester (Amersham Bioscience, Arlington Heights, IL, USA) in 0.1 M bicarbonate buffer pH 8.5, then further purified and rebuffered into PBS pH 7.4 over a G25-Sephadex column (Pharmacia). The Cy5-labeled streptavidin (Amersham) was incubated for 30 min prior to the experiments with NLS-biotin peptides at molar ratios of 1:1 for biotin and biotin binding sites at homotetrameric streptavidin. The streptavidin-coated Quantum dots 525 were obtained from Quantum dot Corp. (Hayward, CA, USA).

Cell culture

The C2C12 mouse myoblast cells and C2C12 mouse myoblasts stably transfected with GFP-PCNA as a fluorescent cell cycle marker were cultured as described (25, 26). Flp 3T3 mouse fibroblasts were from Invitrogen (Carlsbad, CA, USA). 3T3-FDR1.2 Cre reporter cells (27) were cultured in Dulbecco's modified Eagle medium (DMEM) containing 10% fetal calf serum (Life Technologies, Inc., Grand Island, NY, USA). For

live cell microscopy, cells were plated onto 4- or 8-well LabTek coverglass chambers (NalgeNunc, Rochester, NY, USA).

Transduction assays and inhibitor treatments

All peptide and protein transduction experiments, except for the Cre recombinase assay (see below), were performed exclusively with living cells plated on 4- or 8-well LabTek coverglass chambers using an objective heated to 37°C. For transduction experiments, the medium was removed and PBS with the different peptides or proteins was applied directly to the cells. After 10 min incubation, PBS was replaced with the growth medium. Usually uptake was studied continuously starting with the peptide application over a period of at least 2 h, followed by incubation of the cells at 37°C under humidified atmosphere until additional image collection. Transduction efficiencies of peptides were determined by counting the numbers of cells with or without nucleolar signals and internalization efficiencies of proteins by counting cells with or without intracellular vesicles directly on the fluorescence microscope in three fields of view, each containing ~50 cells, or by a similar analysis performed on low magnification overview images. Cell viability after peptide or protein application was monitored by their ability to undergo complete mitotic cell cycles and grow to confluency over a period of 24 to 48 h. Membrane integrity was ascertained by the Trypan blue exclusion assay. Cytochalasin D (Sigma, St. Louis, MO, USA) was dissolved to 10 mg/ml in DMSO and sodium azide (Sigma) to 10% (w/v) in ddH₂O. Both stock solutions were adjusted to 1×PBS at the indicated final concentrations (Fig. 2) before being applied to living cells. The potassium buffer (Fig. 2) corresponds to PBS with all sodium-containing compounds substituted for the equivalent potassium-containing analogues. C2C12 mouse myoblasts were preincubated for the indicated times (t in Fig. 2) with different inhibitors in PBS or the potassium buffer. The TAT-containing peptide and protein were applied directly to the cells and mixed gently. For the potassium phosphate buffer experiment, the protein was dialyzed against the potassium buffer prior to application. After 10 min the cells were washed twice and incubated for another 20–60 min (as annotated in the phase contrast images for each treatment) in DMEM medium, except for the potassium buffer treatment where the medium was replaced by potassium buffer. Transduction thresholds were determined by incubating C2C12 mouse myoblasts with CPP-containing peptides in medium at different concentrations ranging from 0.1 to 500 μM for 1 h. The lowest peptide concentration leading to accumulation

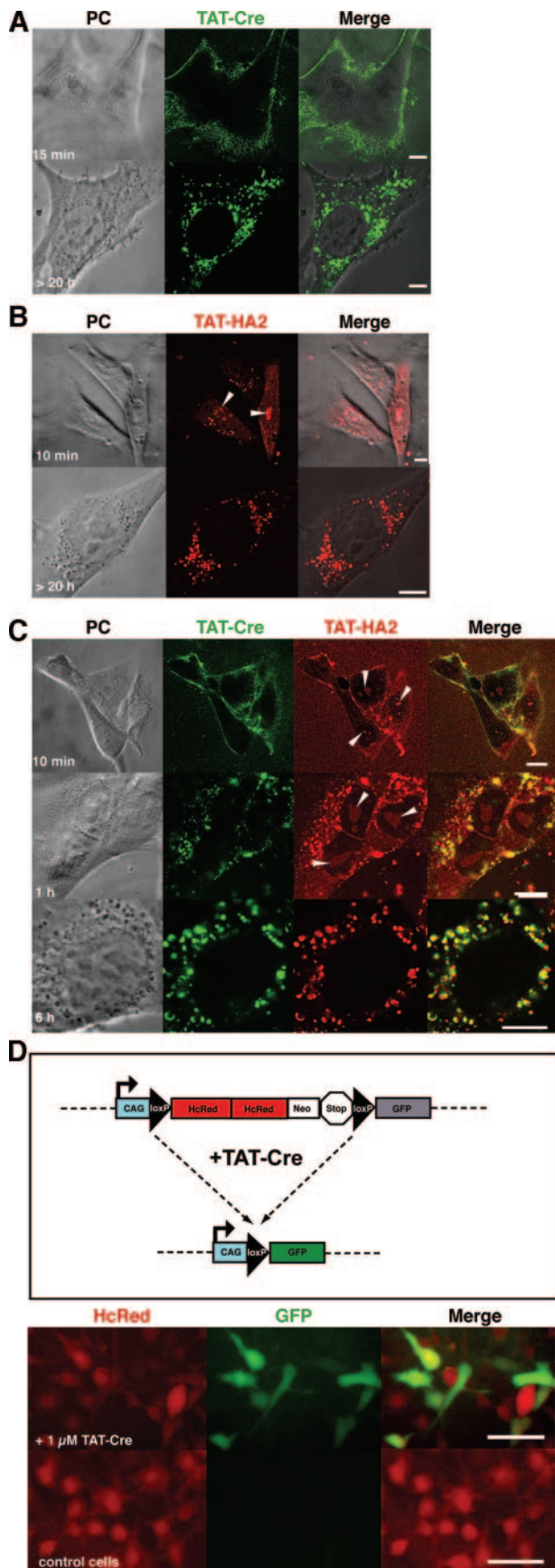


Figure 1. Differences in subcellular distribution of proteins and peptides fused to TAT after internalization in living cells. TAT-Cre and TAT-HA2 were applied to the cells for 10 min,

inside nucleoli was considered to be the transduction threshold from which transduction occurs.

Microinjection and bead loading

Intracellular delivery of the Lig1-PBD-F peptide was accomplished by bead loading using 100 μm silica beads. The beads were washed first in ethanol, then in growth medium, and finally pipetted onto the medium of cells grown in a self-made culture dish with a coverglass bottom. The Lig1-PBD-F solution was added subsequently and the chamber was shaken a few times. The beads were removed for microscopic observation of the labeled cells. Microinjection of the NLS-biotin peptide complexed with streptavidin-Cy5 was performed using an Eppendorf microinjection and micromanipulation system mounted on a Zeiss LSM510Meta inverted microscope setup. The parameters for cytoplasmic microinjection were set to 0.7 s injection time with 15 fPa injection pressure.

Cre recombinase double reporter assay

3T3-FDR1.2 cells (27) were cultured to 50% confluency in 6-well plates. The pFDR reporter gene construct allows detection of bioactive Cre recombinase by switching from constitutive HcRed to GFP expression (Fig. 1 D). For transduction, the cells were incubated with 2 μM TAT-Cre protein diluted into a 50:50 mixture of PBS and DMEM for 3 h, washed once with PBS, then cultivated in normal medium. Fluorescence microscopy was performed 24 h after transduction.

Live cell assay for cell cycle inhibition

C2C12 mouse myoblasts stably expressing GFP-PCNA (26) were synchronized by mitotic shake-off and plated onto 8-well LabTek coverglass chambers. After becoming adherent, the number of cells that entered S-phase was counted and cells

followed by a washing step and change to growth medium without the protein/peptide. Confocal microscopy of live cells was started immediately and cells were returned to the incubator between time points, which are indicated. Representative images and time points are shown. A) Uptake of 2.5 μM TAT fusion protein TAT-Cre (rhodamine-labeled) in living mouse myoblasts. After application of TAT-Cre, internalization started throughout the plasma membrane in the form of vesicles. The next day vesicles containing fluorescent TAT-Cre accumulated in the cytoplasm. B) Diffused and vesicular distribution of the TAT-HA2 peptide (rhodamine-labeled, 5 μM final concentration) soon and a long time after application. C) Simultaneous application of 2.5 μM TAT-Cre protein (Alexa Fluor 633-labeled; 1.7 label to protein ratio) and 5 μM TAT-HA2 peptide (rhodamine-labeled) on living cells resulted in prominent vesicular uptake of the protein into the cytoplasm, whereas the TAT-HA2 peptide also displays a diffuse distribution in cytoplasm and nucleoplasm, and accumulation in nucleoli. The fluorescent fusions colocalize in the majority of vesicles. Nucleoli are indicated by arrowheads. Scale bar = 10 μm . D) Analysis of Cre recombinase activity in TAT-Cre-treated reporter cells. 3T3-FDR1.2 reporter cells contain a loxP-flanked HcRed gene, followed by a nonexpressed GFP gene. TAT-Cre treatment induces recombination of the reporter gene, resulting in a shift from red to green fluorescence (scheme). Untreated control cells do not exhibit green fluorescence. Cells were incubated with 2 μM TAT-Cre for 3 h and analyzed by fluorescence microscopy 24 h later. Scale bar = 50 μm .

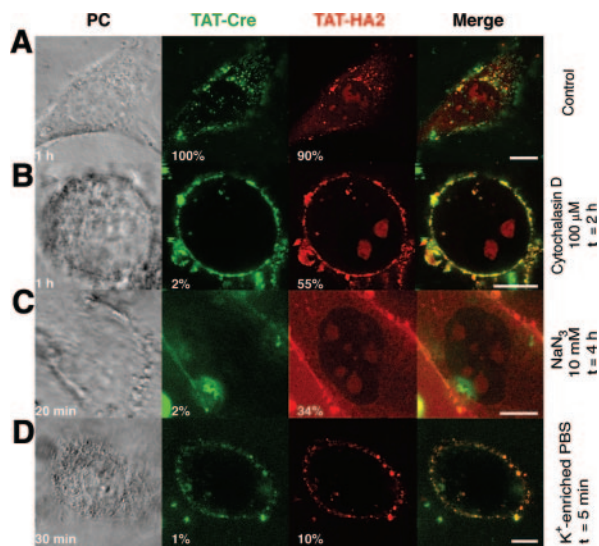


Figure 2. Different mode of uptake of proteins and peptides fused to TAT in living cells. Simultaneous incubation of living mouse myoblasts with 2.5 μM TAT-Cre and 5 μM TAT-HA2 was as shown in Fig. 2C. Confocal images show representative snapshots at the indicated time points in the phase contrast image. The numbers in the images reflect the overall percentage of cells showing intracellular vesicles for the TAT fusion protein and the nucleolar signal for the TAT-HA2 peptide. Substances at the concentrations indicated were preincubated with the cells before addition of the TAT fusions for the indicated time (t) and kept in the culture medium or buffer throughout the experiment. A) Control C2C12 mouse myoblasts treated with the TAT-containing protein and peptide mixture showed internalization in 100% and 90% of the cells, respectively. B) Preincubation of the cells with 100 μM of the F-actin elongation inhibitor cytochalasin D blocked protein uptake completely, but the peptide still transduced into the cells. C) ATP depletion with 10 mM sodium azide reduced entry of both species, albeit a third of the cells still took up the peptide. D) 5 min incubation of the cells in sodium-deficient, iso-osmolar PBS strongly reduced peptide transduction and blocked protein uptake. t = preincubation time, scale bar = 10 μm .

were transduced with fluorescently labeled TAT-p21-PBD, TAT-Lig1-PBD, and the unspecific TAT control peptide at 20 μM concentration in PBS. 10 min later the solutions were aspirated, and the cells were washed twice with medium and kept in growth medium thereafter. The percentage of cells in S-phase was determined directly from the subnuclear focal pattern of GFP-PCNA by counting 10 fields of view at the indicated time points for each peptide. Data of three independent experiments were evaluated.

Microscopy, image acquisition, and analysis

Live cell microscopy was performed with a Zeiss LSM 510 Meta confocal setup mounted on an Axiovert 200 M inverted microscope using a 63 \times phase contrast plan apochromat oil objective NA1.4. For all acquisition settings, the main beam splitter was HFT UV/488/543/633. The parameters specific for each fluorochrome were: FITC, excited at 488 nm light, detected with a 500-530 nm bandpass (BP) filter; TAMRA or rhodamine excited with 543 nm, detected with 565-615 BP and Cy5 or Alexa633 excited at 633 nm and detected with a 650 nm longpass filter.

Image acquisition was done sequentially to minimize cross-talk between the fluorophores. Phase contrast images were

recorded simultaneously with FITC/GFP fluorescence in the transmission channel. Fluorescence recovery after bleaching (FRAP) experiments (Fig. 3) was performed on a Zeiss LSM 5 Live confocal microscope with 100% power of a 75 mW DPSS 532 nm laser. The bleaching was performed in a stripe for 0.44 s, followed by a time series with 400 images recorded at 20 frames per second. Using the Zeiss LSM 510 software version 3.2, the mean fluorescence intensity in the bleached nucleoli and cytoplasm was determined over the time course and averaged for 10 cells. Fluorescence intensity was normalized to zero at the start of recovery and to one at equilibrium to directly compare the curves for both subcellular regions. The FRAP curves were generated with Origin 7 software.

RESULTS

Direct comparison of TAT-mediated peptide and protein uptake in living cells

To study the characteristics of TAT-mediated introduction of globular proteins into living cells, the rhodamine-labeled fusion protein R-TAT-Cre consisting of the CPP TAT moiety and the site-specific Cre recombinase of bacteriophage P1 (23) was applied onto C2C12 mouse myoblasts. As soon as the fluorescent solution was washed off (after 10 min of incubation), fluorescent vesicles emerging from the intracellular side of the plasma membrane were detectable by confocal microscopy (Fig. 2A, upper panel). After additional overnight cultivation, all cells showed a substantial amount of internalized protein stored in vesicles, but release of the protein from the vesicles could not be detected by this method (Fig. 2A, lower panel). Other recombinant proteins showed identical trapping in cytoplasmic vesicles (data not shown) independent of 1) which short basic CPP they were fused to, 2) the fluorophore they were conjugated to, and 3) their known subcellular localization. For instance the nuclear protein His-PTD₄-PCNA (Atto 633-labeled) as well as the nuclear and cytoplasmic protein His-TAT-MK2 (Cy5-labeled) could only be detected inside cytoplasmic vesicles after internalization, and refused to localize at their targets during an observation period of up to 48 h. Proteins lacking a transduction domain could also be internalized in the same manner but the efficiency of internalization was shown to be much lower (23). TAT-Cre was also tested at concentrations between 0.1 and 10 μM with no difference in the uptake behavior (data not shown).

A recent report proposed that the uptake of proteins fused to TAT belongs to the class of rapid lipid raft-mediated macropinocytosis and that the protein could be released from macropinosomes by cotransduction of the fusogenic peptide TAT-HA2 (17). We therefore used TAT-HA2 (Table 1) to 1) work out the characteristics of TAT-mediated peptide (<50 amino acids; ref. 28) transduction and 2) try and liberate the TAT fusion protein trapped into vesicles. Compared to the internalization of proteins, uptake of the TAT-HA2 peptide occurred on a quite different time scale and also showed dissimilarities in its subcellular localization. During the first 3–5 min of incubation with the peptide

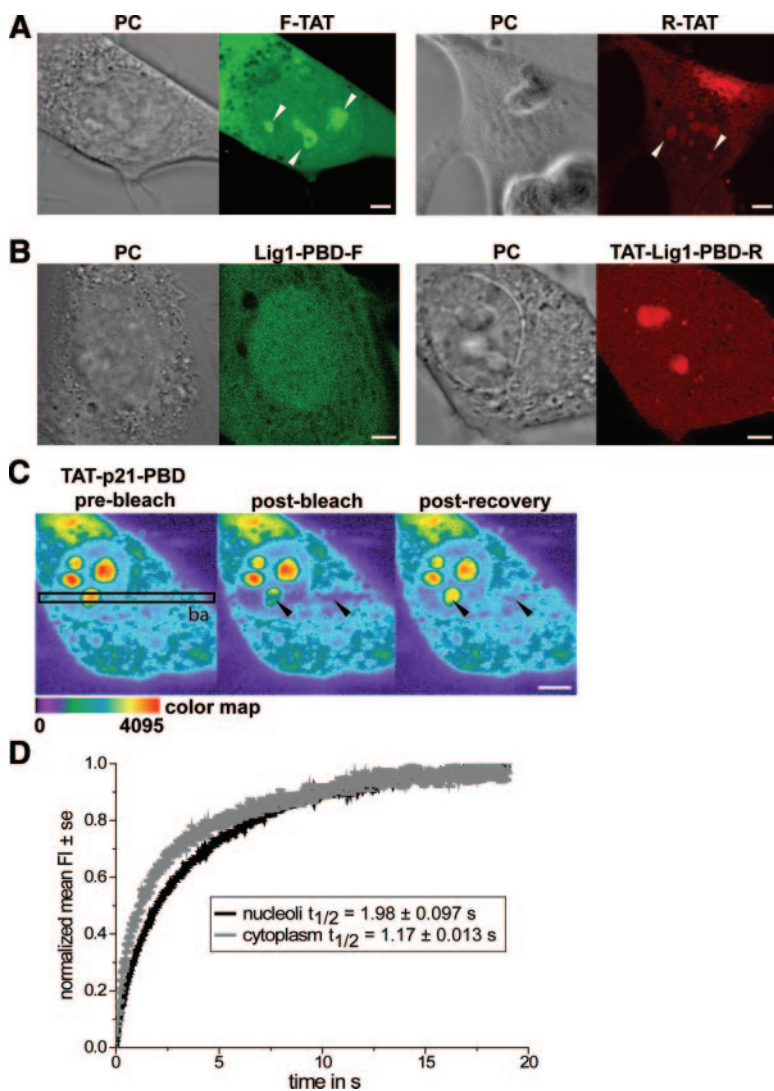


Figure 3. Subcellular localization and intracellular mobility of TAT peptides. *A*) FITC- and rhodamine-labeled TAT peptides (F-TAT 1 μ M, R-TAT 1 μ M) applied to mouse myoblasts were rapidly internalized and accumulated in the nucleoli (white arrowheads). The fluorescent label has no influence on peptide distribution. *B*) In contrast, the non-TAT-containing peptide Lig1-PBD (FITC-labeled) delivered by bead loading showed a homogeneous distribution in nucleus and cytoplasm whereas the addition of the TAT sequence in TAT-Lig1-PBD (rhodamine-labeled) again led to nucleolar accumulation. *C*) Mouse myoblasts were transduced with 20 μ M of TAMRA-labeled TAT-p21-PBD for 10 min, washed, then incubated in growth medium. The FRAP experiment was performed by bleaching a stripe (ba) encompassing one nucleolus and a part of the cytoplasm as seen in the prebleach image. After bleaching, a time series was recorded at a time resolution of 20 frames/second over 20 s. False color images depicting the fluorescence intensity distribution as color map (red denotes highest intensity) of one photobleached cell are shown. The black arrowheads point to the bleached nucleolus and cytoplasmic regions in the first image after the bleaching process (postbleach) and after full fluorescence recovery (postrecovery). *D*) Curves represent the normalized mean fluorescence intensity of the fluorescence recovery in the nucleoli and cytoplasm averaged for 10 measurements. Albeit accumulated in the nucleoli, the TAT-p21-PBD peptide was highly mobile with a half-time of recovery of 1.98 ± 0.097 s. In the cytoplasm, the half-time of recovery is faster (1.17 ± 0.013 s). Scale bar = 5 μ m.

solution, fluorescence signals had already become visible in the nucleoli; after exchange of the fluorescent solution against medium, a diffuse distribution throughout the cell, with accumulation in the nucleoli, could be detected (Fig. 2B, upper panel, arrowheads; see also supplemental movie) in addition to a few developing vesicles adjacent to the membranes. Over longer periods of observation, the diffuse population of the peptide in the cytoplasm, nucleoplasm, and nucleoli became markedly weaker, and in most of the cells vanished overnight. In stark contrast, the peptide-containing cytoplasmic vesicles seemed to be unaffected and their number increased overnight, resulting in a vesicular ring concentrated around the nucleus (Fig. 2B, lower panel). The diffusely distributed fraction of the transduced peptide was detected in $\sim 90\%$ of the cells (Table 1) whereas after overnight incubation all cells showed peptide uptake into vesicles. The loss of diffusely distributed fluorescent peptide in the cytoplasm and nuclei overnight cannot be just a consequence of instability of the fluorophore/peptide in the cell since 1) a rhodamine-labeled antibody (Ab) persisted inside cells for > 24 h (data not shown) and 2)

the fluorescently labeled peptide TAT-HA2 is composed of protease-resistant D-amino acids.

To directly compare the mode and kinetics of uptake of TAT peptides and globular proteins fused to TAT into cells and determine whether TAT-HA2 could drive release of the protein stored in macropinosomes, the Alexa Fluor 633-labeled TAT-Cre protein and the rhodamine-labeled TAT-HA2 peptide were applied simultaneously to living cells. The short- and long-term uptake characteristics for both species remained mostly unchanged (Fig. 2C). Detectable TAT fusion protein was restricted to cytoplasmic vesicles whereas the TAT-HA2 peptide, besides being trapped into vesicles, was rapidly distributed throughout the entire cell. TAT-HA2 and TAT-Cre colocalized in the majority of cytoplasmic vesicles (Fig. 2C, yellow color in merged images). Although both species intermingled substantially, a release of the TAT fusion protein from macropinosomes and entry into the nucleus could not be detected by this method. To test the presence of a low level of TAT-Cre within the nucleus, we used a far more sensitive reporter assay based on Cre-mediated recombination. Since site-specific recombination provides a stable and unambigu-

ous read-out for protein transduction (23, 29–31), we used a NIH-3T3 Cre reporter cell line containing a stably integrated gene cassette consisting of a constitutively expressed HcRed gene, followed by a nonexpressed GFP gene. Upon Cre recombinase-mediated site-specific recombination, excision of the HcRed gene takes place with concomitant expression of the GFP gene (Fig. 2D; L. Nolden and F. Edenhofer, personal communication). Using this more sensitive assay, several cells within the culture exhibited GFP expression upon incubation with TAT-Cre overnight (Fig 2D). These data indicate that a low level of TAT-Cre below the detection range of confocal microscopy was biologically available and could exert its enzymatic activity.

Different mode of entry of proteins and peptides fused to TAT in living cells

To test whether TAT fusion proteins and TAT-containing peptides use different routes of entry and can, as a result, be affected differently in their uptake by treatment with inhibitors, mouse myoblasts were preincubated with inhibitors or buffers, followed by simultaneous application of TAT-Cre and TAT-HA2 (as in Fig. 2C). Subsequently, cells were washed twice and kept in the indicated buffer or medium with constant inhibitor concentration throughout the entire experiment.

Endocytosis requires the formation and migration of vesicles along the cytoskeleton. Therefore, constant concentrations of the F-actin depolymerizing drug cytochalasin D should delay or block internalization of the endocytosed TAT constructs at the membrane level (32, 33). After cytochalasin D treatment, the TAT fusion protein and TAT-HA2 showed strong membrane association, but the diffused fraction of the TAT-HA2 peptide was still detectable inside the cells in nucleoli, albeit the transduction efficiency (as scored by the percentage of cells showing intracellular fluorescence) was reduced to half. All vesicular uptake was abolished (Fig. 1B). Despite the round appearance of the cells indicative of the disruptive effect of the drug on the actin cytoskeleton, the membrane integrity was not decreased as assayed by Trypan blue exclusion (data not shown).

Endocytosis is an energy-consuming process and is therefore blocked by the metabolic inhibitor sodium azide. Accordingly, treatment with 10 mM sodium azide resulted in almost complete inhibition of the internalization of the TAT fusion protein (scored by the absence of intracellular vesicles), whereas the diffused population of the TAT-HA2 was still detected in about one-third of the cells (Fig. 1C).

A recent report proposed that synthetic guanidinium-rich molecules traverse biological membranes by formation of lipophilic ion pairs between the guanidinium groups and abundant phosphate, sulfate, and carboxylate functions on the membrane surface, allowing cell entry by diffusion along the membrane potential and subsequent release of the positively charged CPP into the cytoplasm (5, 10). The directionality of

this process is achieved by the membrane potential and the latter can be efficiently reduced by addition of an isotonic buffer with potassium concentrations equivalent to those found intracellularly (34, 35). We tested this hypothesis by preincubating the cells for 5 min with potassium-enriched, isotonic PBS and adding the peptide/protein solution in the same buffer. This treatment abolished the vesicular internalization of both TAT species. Furthermore, it resulted in strong inhibition of the uptake mode responsible for the intracellularly diffused fraction of TAT-HA2 (Fig. 1D). In summary, in contrast to TAT fused to globular proteins, TAT fusion peptides transduce into cells by a different and very rapid mode that is dependent on the plasma membrane potential. We therefore further investigated the transduction potential and biological applicability of TAT fusion peptides.

Uptake and intracellular availability of TAT-containing peptides

In the first minutes of incubation, the TAT-HA2 peptide flooded into living cells and accumulated in nucleoli; later it was also localized in cytoplasmic vesicles (Fig. 2B, C). To test whether these uptake characteristics were influenced by the HA2 moiety or instead were a general feature of TAT-mediated peptide internalization, several TAT peptide complexes were analyzed for their transduction behavior and intracellular distribution after internalization. Table 1 summarizes the peptides and their respective transduction efficiencies determined, as earlier, by counting the percentage of cells showing intracellular diffused fluorescence upon 10 min incubation with the indicated peptide concentrations and analyzed by confocal microscopy of living cells. The most efficient peptide was the 11 amino acid TAT peptide covalently linked to either a FITC (F) or a rhodamine (R) fluorophore, which was transduced into 90% of all cells at 1 μ M concentration within the first 3 min of observation. The fluorescent signal appeared diffused in the cytoplasm and nucleoplasm and showed strong accumulation of the labeled peptide in nucleoli (Fig. 3A). To test whether the nucleoli accumulation was due to the TAT moiety, we used non-TAT-containing peptides (Lig1-PBD in Fig. 3B and NLS-biotin peptide complexed with streptavidin-Cy5 [data not shown]) and delivered them into the cytoplasm using either bead loading or microinjection. Both peptides were stable intracellularly and able to enter the nucleus, but were not accumulated in the nucleoli (Fig. 3B and data not shown). The same Lig1-PBD peptide fused to TAT (TAT-Lig1-PBD) transduced into cells and again showed nucleolar localization (Fig 3B), indicating that the nucleolar localization is dependent on the TAT characteristics. We investigated other reported CPPs—namely, PTD4 (36)—which showed only detectable uptake (Table 1) at very high concentrations (400 μ M). This suggests that nucleolar association is mediated by the high concentration of positive charges due to arginine and lysine residues.

Since TAT fusion peptides exhibited accumulation in the nucleolar compartment whereas the cargo peptide or protein may perform its function in a different subcellular compartment, we tested the overall bioavailability of cargoes connected to TAT by directly measuring the mobility in living cells using fluorescence photobleaching analysis. Cells transduced with a TAT-containing peptide (TAT-p21-PBD, Table 1) were imaged, and a rectangular region was selected to include one nucleolus and a stripe of cytoplasm. The peptide fluorescence in this stripe was subsequently photobleached with a high intensity laser beam, and redistribution of fluorescence was measured over time until full equilibrium was regained. The peptide intensity distribution before (prebleach), immediately after (postbleach), and at full recovery (postrecovery) is shown in representative false color images in Fig. 3C. The recovery of fluorescence in the bleached region indicates the mobility of peptides from unbleached cellular regions into the bleached area, and therefore is a direct measure of peptide mobility in the living cells. The kinetics of recovery (Fig. 3D) indicated that the peptides, although concentrated in the nucleoli, were mobile with a half-time of recovery of 1.98 and 1.17 s in the nucleoli and cytoplasm respectively. This kinetic difference between nucleoli and cytoplasm suggests binding of the TAT-PBD-p21 within the nucleoli. The high intracellular mobility of the TAT peptides raises the possibility of achieving successful biological effects despite the unfavorable subcellular accumulation.

Cell cycle inhibition by transduced PCNA binding peptides

To directly test whether the transduced TAT peptides in view of their high mobility could be effective in reaching their intracellular targets and exerting a biological effect, we used fusions of TAT with two different peptides comprising the proliferating cell nuclear antigen (PCNA) binding domain (PBD) of p21^{WAF/CIP} and DNA Ligase 1 (Table 1). These two peptides have been shown to bind to PCNA (20, 22). We reasoned that since several PCNA interacting proteins required for S-phase progression utilize the same binding interface on the surface of PCNA, competition for binding should ensue and inhibition of cell cycle progression would be expected. Mouse myoblasts stably expressing the cell cycle progression marker GFP-PCNA (26) were synchronized in the G₁ phase of the cell cycle by mitotic shake off. After becoming adherent, the G₁ synchronized cells were incubated for 10 min with either of these two TAT-PBD peptides as well as a control TAT fusion peptide (37). After washing, peptide uptake efficiency was controlled for by counting the percentage of cells showing intracellular peptide fluorescent signal as before. At different times thereafter, the ability of cells to progress into S-phase was determined by counting the number of S-phase cells scored by the characteristic focal GFP-PCNA subnuclear distribution pattern (see green subnuclear signal in the examples

shown in images in Fig. 4 and ref. 26) directly under the fluorescent microscope. The results of this live cell cycle assay are summarized in Fig. 4. While 70% control cells and cells incubated with TAT control peptide were in S-phase 6 h after peptide incubation, only ~40% TAT-PBD-treated cells entered S-phase within the same time. This inhibition is even more noteworthy if one considers that the peptides were incubated with the cells for only 10 min, after which they were washed away. Toxic effects were not detected by either the Trypan blue exclusion test or by changes in cell morphology. These data demonstrate that both TAT-PBD peptides were bioactive and capable of decelerating cell cycle progression despite the short incubation time and their accumulation in the nucleolus (see also red fluorescence peptide signal in the images in Fig. 4).

DISCUSSION

Although it is generally agreed that the first step in the internalization process of CPP-mediated transduction is the strong ionic interaction between the cationic CPP and negatively charged plasma membrane constituents (6, 15, 38), subsequent steps for CPP-induced cell entry differ in the recent literature and range from endocytic (15, 19) to a rapid and energy-independent process (6, 12). Most studies so far have used fixed cell analysis, which has been shown to result in artificial internaliza-

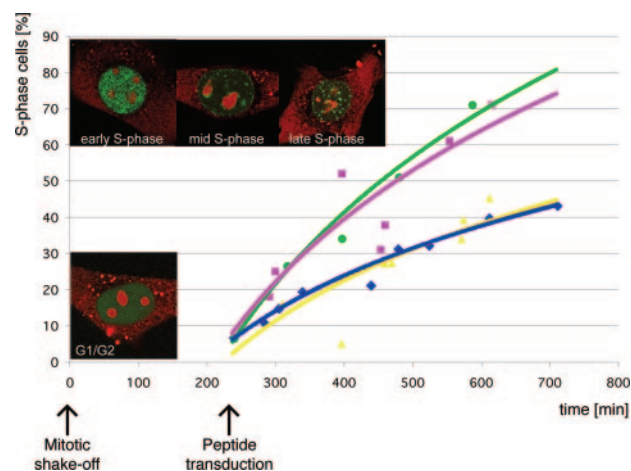


Figure 4. Effect of transduced PBD-containing TAT peptides on cell cycle progression. After mitotic shake-off, GFP-PCNA-expressing mouse myoblasts were allowed to attach and were incubated with different peptides (20 μ M) for 10 min, followed by washing and a change to growth medium. The percentage of S-phase cells was determined at various time points by the subnuclear replication foci pattern of GFP-PCNA. Representative confocal microscopy images of mouse myoblasts transduced with the TAMRA-labeled TAT-p21-PBD peptide (red) show either a diffused distribution of GFP-PCNA (green) in the nucleus, indicating G₁- or G₂-phase or focal GFP-PCNA labeling of replication foci during early, mid and late S-phase. Data points of three independent experiments were fitted logarithmically. Control cells, pink squares; TAT control peptide, green spheres; TAT-Lig1-PBD peptide, yellow triangles; and TAT-p21-PBD peptide, blue diamonds.

tion of CPP-containing constructs. In this work we used exclusively live cell analysis and tested whether the mode of entry is dependent on the cargo connected to the CPP and what the fate and bioavailability of the transduced peptides is.

By directly comparing the uptake of TAT connected to peptides and globular proteins into living cells, we found that the mechanism of entry depends on the size of the cargo fused to TAT. The major fraction of TAT-containing proteins or peptides was taken up into living cells by distinct modes, with the proteins mostly ending up in cytoplasmic vesicles and the peptides distributing throughout the cell and accumulating in the nucleoli (Fig. 2).

The vesicular storage inside the cytoplasm was a general feature of different recombinant proteins fused to a CPP and was independent of protein function, CPP (data not shown), and fluorescent label (Fig. 2A, C). A small population of TAT fusion protein reached the cytosol and nucleus via a different pathway or leaked out from the vesicles, as we detected Cre recombination activity in the nuclei using an extremely sensitive and unambiguous reporter assay for TAT-Cre. This fraction of bioavailable TAT-Cre was not high enough, however, to be detected by direct confocal microscopy of the labeled TAT-Cre protein whereas the population trapped in vesicles was easily detectable. Furthermore, cotransduction of the fusogenic peptide TAT-HA2 (17) did not substantially increase the release of the different TAT fusion proteins from cytoplasmic vesicles as assayed by live cell confocal microscopy (Fig. 2C).

Unlike CPP fusion proteins, TAT fusion peptides could be seen diffusely distributed throughout the cell and concentrated in nucleoli (Fig. 2 and Table 1). Uptake occurred rapidly within 3–5 min after application of the TAT construct on living cells. Upon longer observation times, the diffusely distributed fraction of the TAT peptides disappeared and cytoplasmic vesicles containing the peptides became apparent, suggesting that the peptides were either redistributed or underwent an additional vesicular uptake.

In addition to different uptake kinetics and localization after internalization of proteins and peptides fused to CPPs, inhibitors of endocytosis efficiently blocked the vesicular uptake of both species while having a minor effect on the TAT peptide transduction (Fig. 1), indicating that the latter does not depend on vesicle formation and/or traffic along the cytoskeleton. In fact, the only treatment capable of blocking not only the vesicular uptake of CPP-containing proteins and peptides, but also the rapid translocation of TAT peptides leading to a diffuse intracellular distribution, was incubation of the cells with a sodium-deficient iso-osmolar buffer (Fig. 1), indicating an alternative distinct cellular entry pathway based on membrane potential.

To understand which properties of cargoes fused to TAT allow the rapid membrane transduction, we compared the cellular entry of various TAT-containing constructs (Table 1). Fluorescently labeled TAT had already appeared inside the nucleoli of 90% of living

cells at a concentration of 1 μM . The uptake efficiencies were decreased for TAT fusion peptides. By comparison, differences in the overall pI of TAT due to the addition of a cargo resulted only in minor effects on transduction efficiencies, whereas the amino acid composition of the CPP itself seemed to be more important. For instance, PTD₄ containing three arginines transduced into living cells only at concentrations of >400 μM whereas TAT peptides with eight positive charges (six of them arginines) transduced quite efficiently in a range of 0.1–10 μM (Table 1). Most transduction efficiencies were tested for the CPP TAT at concentrations of 10 μM and resulted in comparable high percentages of transduced cells. However, differences for individual peptides were found to be dependent on the concentration used; for instance, the TAT-HA2 peptide was already diffusely distributed inside cells at a concentration of 0.1 μM , whereas for TAT-p21-PBD uptake was restricted to endocytosis below a concentration of 7.5 μM , and only above 7.5 μM did the peptide enter rapidly and appear in the nucleoli (Table 1). The existence of such a concentration threshold can also explain conflicting reports assigning CPP-mediated membrane translocation to endocytosis (19, 39) or to an unknown mechanism, resulting in a homogeneous distribution in the whole cell (7). Another parameter that should be taken into account is the stability of the transducible peptides themselves since it was shown that CPP peptides could be degraded by extra- and intracellular proteases (40). However, we have not observed dramatic differences in the transduction efficiencies between TAT-HA2 consisting of D-amino acids and other potentially degradable peptides consisting of L-amino acids at comparable concentrations (Table 1).

The TAT-containing peptides exhibited a strong affinity to the nucleolar compartment, with a lower steady-state concentration in the rest of the cell. Alternatively, their enrichment in the nucleoli could be due to a higher viscosity in this subnuclear compartment. However, our fluorescence photobleaching results (Fig. 3) revealed that despite their accumulation in the nucleolus, TAT peptides were mobile and able to reach their targets in the nucleus and cytoplasm. Measurements of protein dynamics in the cell nucleus showed half recovery times of <3 s, and so the peptide dynamics measured for TAT-p21-PBD in nucleoli and cytoplasm (<2 s) can be considered to be similar (41). As a direct test of their bioavailability, we investigated the cell cycle effects of TAT fusion to PBD peptides. PCNA forms a sliding clamp around DNA and plays a central role in DNA replication (reviewed in ref. 42). Multiple factors required for DNA synthesis and cell cycle progression bind PCNA (20) via a consensus PBD Qxx(M/L/I)xxF(Y/F) (43). We fused two different PBD peptides to TAT and tested their effect on cell cycle progression using a novel live cell cycle progression assay. In fact, incubation of the cells with both peptides for as little as 10 min substantially inhibited cell cycle progression (Fig. 4). These data clearly showed that, albeit accumulated in nucleoli, the peptides are fully

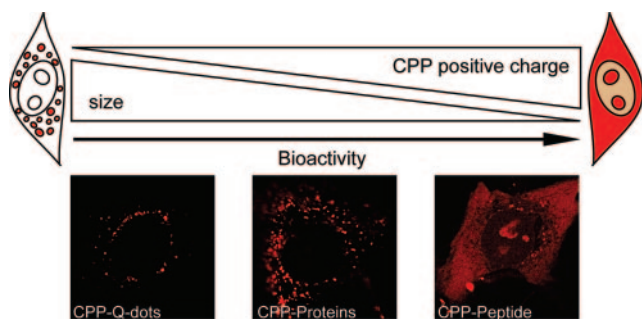


Figure 5. Influence of molecule size and charge on cellular uptake through endocytosis vs. transduction. Cargoes fused to CPPs follow different routes of entry into living mammalian cells. The complexes or fusions of CPPs with large 20 nm diameter Quantum Dots down to globular proteins are mainly endocytosed and remain trapped in cytoplasmic vesicles. Small, nonglobular peptides fused to CPPs are to a certain extent also endocytosed, but in addition are taken up into living cells by membrane transduction; inside the cells they are highly mobile and capable of reaching any subcellular compartment. Thus, transduction of peptides leads to rapid internalization in a bioactive manner whereas globular particles are largely trapped inside vesicles. The mode of uptake is influenced by the charge of the CPP and the size of the cargo connected to it.

able to reach their biological targets elsewhere in the cell and exert a biological effect.

In summary, our data indicate that the translocation of TAT-containing constructs through biomembranes takes place with high efficiency, but at least two functionally distinct mechanisms are involved. Complexes with a globular structure like TAT fused to Q-dots (Fig. 5) or TAT fusion proteins seem to be mostly restricted in their uptake to an endocytic mechanism that is associated with trapping in cytoplasmic vesicles. A minor fraction of internalized TAT fusion proteins, undetectable by confocal microscopy but sufficient to induce enzymatic activity, seems to escape vesicles in the cells. Besides being endocytosed, TAT-containing peptides have the ability to enter living cells by a different pathway. The exact underlying mechanism for this rapid translocation is unknown and could be explained by transient membrane perturbations (14) or lipophilic ion pair diffusion along the membrane potential (5, 10). In general, increasing positive charge of the CPP itself and decreasing size of the cargo fused to the CPP allows rapid internalization to occur in addition to the slow process of adsorptive endocytosis (Fig. 5). The latter implies that CPP-mediated uptake of globular proteins is restricted to cell types capable of endocytosis. CPP-containing peptides can rapidly transduce all cell types tested and, despite their high affinity to the nucleolus, transduced peptides have access to all intracellular compartments, thus making them an ideal tool for therapeutic applications. **[F]**

We thank A. Krella, P. Domaing, and M. Peitz for their participation at earlier stages of this project. We are indebted to R. Kettritz (Franz Volhard Clinic, Berlin) and U. Kubitschek (University of Bonn) for providing some of the pep-

tides used, M. Gaestel (University of Hannover) for the gift of expression plasmids for MK2, and H. Leonhardt (Ludwig Maximilians University, Munich) for advice throughout this work. We thank members of the Stem Cell Engineering Group (University of Bonn) for support and valuable discussions. This work was supported in part by the Max Delbrueck Center and by grants from the Deutsche Forschungsgemeinschaft and the Volkswagen Foundation (M.C.C.) as well as by grants from the Stem Cell Network North Rhine Westphalia, the European Union and the Volkswagen Foundation (F.E.).

REFERENCES

- Dietz, G. P., and Bdeltahr, M. (2004) Delivery of bioactive molecules into the cell: the Trojan horse approach. *Mol. Cell Neurosci.* **27**, 85–131
- Richard, J. P., Melikov, K., Vives, E., Ramos, C., Verbeure, B., Gait, M. J., Chernomordik, L. V., and Lebleu, B. (2003) Cell-penetrating peptides. A reevaluation of the mechanism of cellular uptake. *J. Biol. Chem.* **278**, 585–590
- Cardoso, M. C., and Leonhardt, H. (2002) Protein transduction: a novel tool for tissue regeneration. *J. Biol. Chem.* **383**, 1593–1599
- Vives, E., Brodin, P., and Lebleu, B. (1997) A truncated HIV-1 Tat protein basic domain rapidly translocates through the plasma membrane and accumulates in the cell nucleus. *J. Biol. Chem.* **272**, 16010–16017
- Dom, G., Shaw-Jackson, C., Matis, C., Bouffiuou, O., Picard, J. J., Prochiantz, A., Mingeot-Leclercq, M. P., Brasseur, R., and Rezsosazy, R. (2003) Cellular uptake of Antennapedia Penetratin peptides is a two-step process in which phase transfer precedes a tryptophan-dependent translocation. *Nucleic Acids Res.* **31**, 556–561
- Mai, J. C., Shen, H., Watkins, S. C., Cheng, T., and Robbins, P. D. (2002) Efficiency of protein transduction is cell type-dependent and is enhanced by dextran sulfate. *J. Biol. Chem.* **277**, 30208–30218
- Ziegler, A., Blatter, X. L., Seelig, A., and Seelig, J. (2003) Protein transduction domains of HIV-1 and SIV TAT interact with charged lipid vesicles. Binding mechanism and thermodynamic analysis. *Biochemistry* **42**, 9185–9194
- Mitchell, D. J., Kim, D. T., Steinman, L., Fathman, C. G., and Rothbard, J. B. (2000) Polyarginine enters cells more efficiently than other polycationic homopolymers. *J. Pept. Res.* **56**, 318–325
- Thoren, P. E., Persson, D., Isakson, P., Gokso, M., Onfelt, A., and Norden, B. (2003) Uptake of analogs of penetratin, Tat(48–60) and oligoarginine in live cells. *Biochem. Biophys. Res. Commun.* **307**, 100–107
- Rothbard, J. B., Jessop, T. C., and Wender, P. A. (2005) Adaptive translocation: the role of hydrogen bonding and membrane potential in the uptake of guanidinium-rich transporters into cells. *Adv. Drug Deliv. Rev.* **57**, 495–504
- Scheller, A., Wiesner, B., Melzig, M., Bienert, M., and Oehlke, J. (2000) Evidence for an amphipathicity independent cellular uptake of amphipathic cell-penetrating peptides. *Eur. J. Biochem.* **267**, 6043–6050
- Ziegler, A., Nervi, P., Durrenberger, M., and Seelig, J. (2005) The cationic cell-penetrating peptide CPP(TAT) derived from the HIV-1 protein TAT is rapidly transported into living fibroblasts: optical, biophysical, and metabolic evidence. *Biochemistry* **44**, 138–148
- Futaki, S., Suzuki, T., Ohashi, W., Yagami, T., Tanaka, S., Ueda, K., and Sugiura, Y. (2001) Arginine-rich peptides. An abundant source of membrane-permeable peptides having potential as carriers for intracellular protein delivery. *J. Biol. Chem.* **276**, 5836–5840
- Prochiantz, A. (2000) Messenger proteins: homeoproteins, TAT and others. *Curr. Opin. Cell Biol.* **12**, 400–406
- Vives, E. (2003) Cellular uptake [correction of utake] of the Tat peptide: an endocytosis mechanism following ionic interactions. *J. Mol. Recognit.* **16**, 265–271
- Fittipaldi, A., Ferrari, A., Zoppe, M., Arcangeli, C., Pellegrini, V., Beltram, F., and Giacca, M. (2003) Cell membrane lipid rafts

- mediate caveolar endocytosis of HIV-1 Tat fusion proteins. *J. Biol. Chem.* **278**, 34141–34149
17. Wadia, J. S., Stan, R. V., and Dowdy, S. F. (2004) Transducible TAT-HA fusogenic peptide enhances escape of TAT-fusion proteins after lipid raft macropinocytosis. *Nat. Med.* **10**, 310–315
 18. Caron, N. J., Quenneville, S. P., and Tremblay, J. P. (2004) Endosome disruption enhances the functional nuclear delivery of Tat-fusion proteins. *Biochem. Biophys. Res. Commun.* **319**, 12–20
 19. Kaplan, I. M., Wadia, J. S., and Dowdy, S. F. (2005) Cationic TAT peptide transduction domain enters cells by macropinocytosis. *J. Control Release* **102**, 247–253
 20. Gulbis, J. M., Kelman, Z., Hurwitz, J., O'Donnell, M., and Kuriyan, J. (1996) Structure of the C-terminal region of p21 (WAF1/CIP1) complexed with human PCNA. *Cell* **87**, 297–306
 21. Cardoso, M. C., Joseph, C., Rahn, H. P., Reusch, R., Nadal-Ginard, B., and Leonhardt, H. (1997) Mapping and use of a sequence that targets DNA ligase I to sites of DNA replication in vivo. *J. Cell Biol.* **139**, 579–587
 22. Montecucco, A., Rossi, R., Levin, D. S., Gary, R., Park, M. S., Motycka, T. A., Ciarrocchi, G., Villa, A., Biamonti, G., and Tomkinson, A. E. (1998) DNA ligase I is recruited to sites of DNA replication by an interaction with proliferating cell nuclear antigen: identification of a common targeting mechanism for the assembly of replication factories. *EMBO J.* **17**, 3786–3795
 23. Peitz, M., Pfannkuche, K., Rajewsky, K., and Edenhofer, F. (2002) Ability of the hydrophobic FGF and basic TAT peptides to promote cellular uptake of recombinant Cre recombinase: a tool for efficient genetic engineering of mammalian genomes. *Proc. Natl. Acad. Sci. U. S. A.* **99**, 4489–4494
 24. Caron, N. J., Torrente, Y., Camirand, G., Bujold, M., Chapdelaine, P., Leriche, K., Bresolin, N., and Tremblay, J. P. (2001) Intracellular delivery of a Tat-eGFP fusion protein into muscle cells. *Mol. Ther.* **3**, 310–318
 25. Cardoso, M. C., Leonhardt, H., and Nadal-Ginard, B. (1993) Reversal of terminal differentiation and control of DNA replication: cyclin A and Cdk2 specifically localize at subnuclear sites of DNA replication. *Cell* **74**, 979–992
 26. Leonhardt, H., Rahn, H. P., Weinzierl, P., Sporbert, A., Cremer, T., Zink, D., and Cardoso, M. C. (2000) Dynamics of DNA replication factories in living cells. *J. Cell Biol.* **149**, 271–280
 27. Nolden, L., Edenhofer, F., Haupt, S., Koch, P., Wunderlich, F. T., Siemen, H., and Brustle, O. (2006) Site specific recombination in human ES cells induced by cell permeable Cre recombinase. *Nat. Methods* In press
 28. Seewald, N., and Jakubke, H.-D. (2002) *Peptides: Chemistry and Biology*, Wiley-VCH, Weinheim, Germany
 29. Jo, D., Nashabi, A., Doxsee, C., Lin, Q., Unutmaz, D., Chen, J., and Ruley, H. E. (2001) Epigenetic regulation of gene structure and function with a cell-permeable Cre recombinase. *Nat. Biotechnol.* **19**, 929–933
 30. Joshi, S. K., Hashimoto, K., and Koni, P. A. (2002) Induced DNA recombination by Cre recombinase protein transduction. *Genesis* **33**, 48–54
 31. Will, E., Klump, H., Heffner, N., Schwieger, M., Schiedlmeier, B., Ostertag, W., Baum, C., and Stocking, C. (2002) Unmodified Cre recombinase crosses the membrane. *Nucleic Acids Res.* **30**, e59
 32. Goddette, D. W., and Frieden, C. (1986) The kinetics of cytochalasin D binding to monomeric actin. *J. Biol. Chem.* **261**, 15970–15973
 33. Flanagan, M. D., and Lin, S. (1980) Cytochalasins block actin filament elongation by binding to high affinity sites associated with F-actin. *J. Biol. Chem.* **255**, 835–838
 34. Aidley, D., and Stanfield, P. (1996) *Ion Channels: Molecules in Action*, Cambridge University Press, Cambridge, England
 35. Watanabe, Y., Kameoka, S., Gopalakrishnan, V., Aldape, K. D., Pan, Z. Z., Lang, F. F., and Majumder, S. (2004) Conversion of myoblasts to physiologically active neuronal phenotype. *Genes Dev.* **18**, 889–900
 36. Ho, A. (2001) Synthetic protein transduction domains: enhanced transduction potential in vitro and in vivo. *Cancer Res.* **61**, 474–475
 37. Choi, M., Rolle, S., Wellner, M., Cardoso, M. C., Scheidereit, C., Luft, F. C., and Kettritz, R. (2003) Inhibition of NF-kappaB by a TAT-NEMO binding domain peptide accelerates constitutive apoptosis and abrogates LPS-delayed neutrophil apoptosis. *Blood* **102**, 2259–2267
 38. Tyagi, M., Rusnati, M., Presta, M., and Giacca, M. (2001) Internalization of HIV-1 tat requires cell surface heparan sulfate proteoglycans. *J. Biol. Chem.* **276**, 3254–3261
 39. Vives, E., Richard, J. P., Rispal, C., and Lebleu, B. (2003) TAT peptide internalization: seeking the mechanism of entry. *Curr. Protein Pept. Sci.* **4**, 125–132
 40. Fischer, R., Kohler, K., Fotin-Mleccek, M., and Brock, R. (2004) A stepwise dissection of the intracellular fate of cationic cell-penetrating peptides. *J. Biol. Chem.* **279**, 12625–12635
 41. Phair, R. D., and Misteli, T. (2000) High mobility of proteins in the mammalian cell nucleus. *Nature* **404**, 604–609
 42. Maga, G., and Hubscher, U. (2003) Proliferating cell nuclear antigen (PCNA): a dancer with many partners. *J. Cell Sci.* **116**, 3051–3060
 43. Warbrick, E. (1998) PCNA binding through a conserved motif. *Bioessays* **20**, 195–199

Received for publication December 3, 2005.

Accepted for publication April 10, 2006.

3. Discussion & Outlook

Delivery of hydrophilic compounds over the plasma membrane of living cells provides the fascinating possibility to exploit the macromolecular repertoire of the cell for life sciences and molecular medicine. CPPs promote the uptake of several types of cargoes, like oligonucleotides, proteins, peptides, drugs and nanoparticles^{11,28,30,31,33-35}. We focused in our work on the subclass of arginine-rich peptides (RRPs) and assessed their uptake, toxicity and vector properties.

In the comparative live-cell microscopy study 2.1 oligo-lysines were only taken up via endocytic pathways, whereas oligo-arginines exhibited an additional uptake mode, associated with immediate presence inside cyto- and nucleoplasm and referred to as transduction. This observation underscores the huge differences between individual CPPs depending on the arginine content. The analysis of the transduction abilities of consecutive oligo-arginines R5 to R12 revealed increasing transduction with an increasing number of arginine residues and increasing concentration. Toxicity was monitored concomitantly as the percentage of cells that took up propidium iodide (PI) from the outer solution. R9 and R10 exhibited high transduction rates with low toxicity and R9 was subjected to a more detailed toxicity analysis with non-degradable (D-amino acid) peptides. At concentrations higher than 50 μM and short time incubation toxicity was detected by trypan blue inclusion indicating membrane damage and by the MTT assay as a marker for enzymatic activity. However, long-term effects on the cell cycle could be excluded. The formation of pores during transduction was addressed via concomitant incubation of R9 with PI (2.1) or FITC (2.2). In both experimental setups transduction took place without concomitant internalization of the small chemical compounds, which argues against the formation of transient pores that were discussed in two recent publications^{94,140}. Even simultaneous application of the L- and D-R9 with different fluorescent labels resulted in selective earlier uptake of the non-degradable D-isoform (2.1, movie M1). One possible explanation for this behaviour could be

that multimeric peptide complexes on the membranes are required to provoke transduction and these can only be formed by peptides generated from one isoform. Since L-arginines are susceptible to proteolytic degradation, while the non-degradable D-isomers stay intact, the latter transduced in some cells earlier or selectively. Such coordinative effects would also explain the presence of a critical concentration or transduction threshold (2.6).

The portion of bioavailable and freely diffusing RRP can arise from two different pools: (i) Either they are released after endocytic uptake from pinocytic vesicles (endosomes or lysosomes) or (ii) they cross the plasma membrane by a more direct process. In 2.2 we examined if the endocytic pathways clathrin- and caveolin-dependent endocytosis that were published to be responsible for CPP uptake, are involved in the uptake of the RRP TAT. By inhibiting specifically these pathways we found no change in the freely diffusing portion of TAT and by reduction of the temperature to 4°C we could rule out that the mechanism of TAT-translocation is dependent on any kind of endocytosis. Furthermore, the kinetics of RRP uptake was shown to be cell-type specific as displayed by Fig. 5 in 2.2 and movies M2-11, although all used cell types were susceptible to transduction.

To further understand the mechanism of transduction we investigated structural properties of different CPPs and RRP-fusion peptides by sedimentation velocity ultracentrifugation. In general, an extended conformation of all RRP-containing peptides could be demonstrated, but this conformation was not the *conditio sine qua non* for transduction. A calculation of charges per calculated length (obtained by analytical ultracentrifugation) revealed that the clustering of positive charge derived from arginines is decisive for transduction. This was further tested by the generation of a cyclic variant of the RRP TAT (cTAT) that was realized without the introduction of further charges. Analyzing transduction by live-cell confocal fluorescence microscopy revealed that the circular form transduced more effectively as indicated by a lower average initiation time of transduction and resulted in higher amounts of intracellular peptide than the linear form of TAT (movie M12). Thus cTAT represents a novel RRP with enhanced transduction potential. In the light of cooperative effects, that are necessary for transduction, this might reflect different arrangement of both forms on the

membrane surfaces (2.3). Moreover, the planar ring-like structure of cTAT led to the planar and outwards orientation of the arginine sidechains and thus resulted in a larger interface with the membranes.

Cargoes attached to TAT CPP influence its mode of uptake. Proteins, DNA / RNA, peptides and drugs connected to RRP were taken up by a CPP-enhanced pinocytic mechanism, but only low molecular weight cargoes (fluorophores, drugs, peptides) showed - at intermediate concentrations - the option to enter living cells by transduction (2.6). Nevertheless after pinocytosis the transducible TAT-Cre was able to reach the nucleus, as demonstrated by a switch from hc-Red expression to GFP expression that was caused by Cre-recombination activity in cells containing a reporter gene. Although release of TAT-Cre could not be visualized directly by confocal microscopy this observation proves that at least a marginal amount of a TAT-fusion protein could escape from vesicles and exerted functional effects detected by this sensitive and self-amplifying assay (2.6).

Exploiting the transduction mode of uptake for direct delivery in an instantly bioavailable form, we showed that RRP-mediated translocation is a tool for labeling certain intracellular compartments in cell cultures, either by the intrinsic property of RRP to enrich in the nucleolar compartment or in connection to a actin-targeting peptide in cardiomyocytes (2.4 and 2.5).

Transduction led to the bioactive delivery of TAT-fusion peptides and was used to investigate protein interactions in two examples: (i) A peptide derived from ventricular light chain-1 (VLC-1) was introduced into adult cardiomyocytes. This construct enhanced muscle contractility without causing a change in Ca^{2+} -levels. (ii) Peptides derived from two proteins that bind to the PIP-box of PCNA were delivered to cell cultures by TAT CPP (2.6). This constructs were able to inhibit cell cycle progression after a short incubation time of 15 minutes and thus may serve as antiproliferative drugs in the future. Finally, RPP-mediated delivery of peptides is also well suited for functional studies in primary cells, like human polymorphonuclear neutrophils or cardiomyocytes (2.5) ^{131,141} that are both short-lived and resistant to transfection. The latter involves gene expression and consequently biological effects can only be assayed hours to days after transfection.

General considerations for peptide and protein delivery by CPPs

Strikingly, non-vesicular transduction of RRP does not compromise living cells at intermediate concentrations and, at the same time, results in high intracellular bioavailable concentrations.

The use of degradable CPP constructs (composed of L-amino acids) has the additional advantage to allow for the proteolytic degradation of the non-target bound excess peptide, whereas non-degradable D-amino acid containing CPP constructs will forcedly elicit sustained effects. Internalized degradable CPP constructs can be shielded from the intracellular proteolytic machinery when bound to their targets, while the remaining unbound fraction is rapidly degraded providing a natural control over excess CPP constructs. The attractiveness of this system does of course not apply for non-degradable compounds linked to CPPs, e.g., drugs, heavy metals or retro-inverso and other non-natural peptoids.

Although transduction is sometimes described to occur 'seemingly energy-independent', there has to be a driving force for this kind of cellular uptake. Macromolecular concentration gradients in and out of the cell or the membrane potential are possible parameters and experimental data supports both ^{38,70}. This would imply that transduction could only proceed in one direction, which has though not yet been experimentally demonstrated.

Translation of *in vitro* CPP transduction onto *in vivo* applications should be feasible but the verification is difficult since most often fixation protocols are used to check for uptake in the different organs and the latter leads to artificial redistribution of the substances delivered. Nevertheless, irrespective of the mode of cellular uptake (transduction or endocytosis) several *in vivo* studies have demonstrated uptake and/or biological effects of CPP-mediated delivery of cargoes (see introduction and Table 1).

A priori, the fast uptake and hydrophilic nature of most CPPs should make their use more suitable for topical delivery to the target tissue, which would also provide specificity, rather than for systemic delivery, which would require deep tissue penetration to reach certain organs and cell types. However, TAT-proteins applied *in vivo*, were found in all organs and were even able to cross the blood brain barrier ^{33,112}. A summary of several successful CPP-mediated

in vivo delivery experiments in the last years is listed in Table 1. How can these discrepancies between the marginal penetration of CPP-cargoes and the encouraging effects measured in animals in several studies be explained? At least in part, it might be due to the fact that most studies tackled either inflammatory and apoptotic processes or tumor tissues. The former are associated with enhanced tissue and membrane permeability and the latter with high vascularization, increased interstitial space and the absence of a lymphatic network¹⁴². Therefore, compromised tissue may be reached more facile by CPP-entities circulating in the bloodstream and uptake into harmed cells might be enhanced.

The constraints of the animal experiments do not apply to the exciting possibilities of CPP-mediated cargo delivery in *ex vivo* cell applications, including labeling of cells and subcellular structures, cell-based assays, and modulation of cellular functions. Since all cells so far have proven to be susceptible to transduction by low molecular weight cargoes linked to CPPs, this mode of uptake can be utilized directly. Application of large cargoes (e.g., proteins) that become internalized exclusively by pinocytosis though, require the future optimization of non-toxic strategies to release the CPP cargoes from the vesicles. With the recent developments in cell replacement therapies, this non-DNA based approaches will be extremely useful.

Thus CPP-mediated and in particular RRP-mediated transduction enables the usage of the subclass of hydrophilic compounds with intracellular targets for therapeutical applications. Depending on the CPP chosen and the cargo itself, two different uptake modes can be observed that can be exploited differently. While the instantly bioavailable modus will permit delivery to even primary cells and can be used for interference of LMW cargoes with intracellular targets in *ex vivo* cultures, the more general endocytic uptake, applicable for all types of cargoes, can be utilized for systemic delivery *in vivo*.

Hence, CPP-mediated delivery will vastly increase the number of potential drug targets and lead to the development novel therapeutics in the future.

Table 1: CPP-mediated delivery of peptides & proteins *in vivo*.

Effect	Specific effect	Cargo	CPP	Animals	Application	Citation
Anti-apoptotic, Anti-inflammatory	Reduced cerebral infarct size	Bcl-x _L	TAT	C57BL/6 mice	i.p.	143
	Resistant to sepsis-induced apoptosis, increased survival	Bcl-x _L , BH4-peptide	TAT	Bcl-xL overexpressed in T-lymphocytes, transgenic mice	s.c., miniosmotic pumps	123
	Reduced hippocampal damage in excitotoxic seizure model	BH4-domain of Bcl-x _L	TAT	Sprague-Dawley rats	injection into dental gyrus	144
	Blocked inflammation and tumor angiogenesis	Caveolin-1 peptide (amino acids 82-101)	Pen	Swiss mice	pretreated	128
	ROS-reduction	Cu, Zn-superoxide dismutase	PEP-1	gerbil	i.p.	127
	Prevented delayed neuronal cell death after transient global ischemia	FNK (Bcl-x _L)	TAT	gerbil	i.p.	145
	Protection against chemotherapy-induced alopecia	FNK (Bcl-x _L)	TAT	Wistar rats	topical	146
	Amelioration of established colitis	NBD-peptide (Nemo-binding domain)	K ₈	IL-10 ^{-/-} mice	i.p.	147
	Inhibition of caspase-3 activity	D-JNK11 peptide, c-Jun N-terminal kinase inhibitor	TAT	Wistar rats	i.p.	126
	Decreased infarcted myocardium	p27 (Heat shock protein 27)	TAT	Sprague-Dawley rats	i.p.	148
	Inhibition of OVA-induced lung inflammation	STAT-6 inhibitory peptide	PTD ₄	BALB/c mice	i.n.	129
	Reduction of caspase-3 and -9	XIAP (X-linked inhibitor of apoptosis)	Pen	Sprague-Dawley rats	i.p.	149
Anti-diabetic	Elevates insulin levels in diabetic mice	Pdx1 (pancreatic duodenal homeobox-1)	TAT	BALB/c mice	i.p.	150
Anti-neurodegenerative	Suppressed polyglutamine-induced neurodegeneration	QBP1 (Aggregate inhibitor peptide poly Q binding peptide 1)	TAT	UAS-MJDr-Q78 transgenic Drosophila fly line	mixed with food	151
Anti-proliferative	Attenuates cell migration and metastasis	Grb7 (growth factor receptor-bound protein 7) inhibitory peptide	Pen	BALB/c nu/nu mice	i.p.	108
Pro-apoptotic	Apoptotic effects on tumor	Kla-peptide (klaklaklaklak)	R ₇	athymic nude mice	injected into tumor	122
	Apoptotic effects on tumor		PTD-5	C57BL/6 mice	injected into tumor	152
Protection of microvasculature	Reduced infarct size following an acute stroke	dV1-1 (PKC-derived peptide)	TAT	Sprague-Dawley rats	i.p.	153
Rescue of function	Restores PNP-function in ko-mice	PNP Purine nucleoside phosphorylase	TAT	PNP ^{-/-} C57BL/6 mice	i.p.	130
	Restores functional dystrophin	PMO altering pre-mRNA splicing for dystrophin protein	RRP	mdx-mouse model with nonsense mutation in exon 23	i.p.	154
	Delivery over the blood brain barrier restores function	BDNF (brain-derived neurotrophic factor)	TAT	Kung Ming mice	i.v.	155

Abbreviations: i.p. intraperitoneal; i.v. intravenous; K lysine; s.c. subcutaneous; ROS reactive oxygen species; RRP arginine-rich peptide; Pen penetratin; PTD protein transduction domain, R arginine

4. Appendix

4.1 Abbreviations

AGA	a-galactosidase A
AMD	actinomycin D
BALB/c	albino laboratory mouse strain
Bcl-xL	apoptosis regulator protein
BH4	peptide derived from Bcl-xL
BHK	baby hamster kidney
BJ-hTERT	human fibroblast cell line
BP	band pass
Cav	caveolin
C2C12	mouse myoblast cell line
CD34	Cluster differentiation antigen 34
CHC	clathrin heavy chain
CHO	Chinese hamster ovary
Cip	cycline dependent kinase inhibitor protein
CLSM	confocal laser scanning microscopy
CPP	cell penetrating (permeable) peptide
Cre	Cre-recombinase (from P1 bacteriophage)
D	dextrorotatory
DHFR	dihydrofolatereductase
(DIBAC) ₄	bis-(1,3-dibutylbarbituric acid)-trimethine oxonol
DNA	desoxyribonucleic acid
DMPC	di-meristyl-phosphatidylcholine
DMEM	Dulbecco's modified eagle medium
DOPC	dioleoyl-phosphatidylcholine
DOPS	dioleoyl-phosphatidylserine
DRAQ5	Deep red florescing anthraquinone No. 5
DSPC	di-sphingomyelin-phosphatidylcholine
ECL	enhanced luminescence
FACS	fluorescence activated cell sorting
FCS	fetal calf serum
FITC	fluorescein isothiocyanate
Fluos	fluorescein
FM	fluorescent marker
FRAP	fluorescence recovery after photobleaching
FS	fractional shortening
FU	fluorouridine
GFP	green fluorescent protein

Grb 7	growth factor receptor bound protein 7
GUV	giant unilamellar cell
HA2	hemagglutinin 2
HBSS	Hank's balanced salt solution
HeLa	human cervical cancer cell line
HEPES	N-2-hydroxyethylpiperazine-N'-2-ethane-sulfonic
acid	
HFT	main beam splitter
HIV	human immunodeficiency virus
HPLC	high pressure liquid chromatography
HPMA	N-(2-hydroxypropyl)methacrylamide
HRP	horse radish peroxidase
IgG	Immunoglobuline G
IPTG	Isopropyl- β -D-thiogalactopyranosid
c-Jun	gene coding for AP1 transcription factor
JNK	c-Jun N-terminal kinases
K	lysine
KO	knock out
L	levorotatory
LDH	lactate dehydrogenase
Lig	ligase
LMW	low molecular weight
LSCM	laser scanning confocal microscopy
LSM	laser scanning microscope
LUV	large unilamellar cell
MAP	model amphipathic peptide
MAPKAP	mitogen activated protein kinase activated protein
MDCK	madine darby canine kidney
MHC	myosine heavy chain
MK2	MAPKAP kinase 2
MLC	myosine light chain
mRFP	monomeric red fluorescent protein
mRNA	messenger ribonucleic acid
M ₂ S	multi subunit DNA-binding protein
MTP	membrane transduction peptide
MTT	3-(4,5-dimethylthiazol-2-yl)-2,5-diphenyl tetrazolium bromide
NA	numerical apertur
NBD	7-nitro-2-1,3-benzoxadiol-4-yl, Nemo binding domain
ND	neck domain
NLS	nuclear localization sequence
NMR	nuclear magnetic resonance

ON	oligonucleotides
p21	protein 21
PBD	PCNA binding domain
PBS	phosphate buffered saline
PC	phase contrast
PCNA	proliferating cell nuclear antigen
PEI	polyethylenimine
PGLa	peptide starting with a glycine and ending with a leucine amide
pI	isoelectric point
PI	propidium iodide
PIP	PCNA-interacting protein
PMO	phosphorodiamidate morpholino oligomer
PNA	peptide nucleic acid
PTD	protein transduction domain
pre-mRNA	first transcript from a protein coding gene
PreS2	domain from Hepatitis B virus
Q-dot	nanocrystal
R	arginine
Rab	Ras-related in brain, protein family
Ras	'rat sarcoma', protein family
REMD	replica exchange molecular dynamics
RNA	ribonucleic acid
RNAse	Ribonuclease
RPMI	medium (Roswell Park Memorial Institute)
RRP / R-RP	arginine-rich peptide
SE	sticky end
SEM	standard error of the mean
shRNA	small hairpin ribonucleic acid
siRNA	small interfering ribonucleic acid
STAT-6	signal transducer and activation of transcription-6
SynB1	synthetic pegalin derivative, CPP
TAMRA	5,6-carboxy-tetramethyl rhodamine
TAT	transactivator of transcription
Tet	tetracycline
tetR	tetracycline repressor protein
Tf	transferrin
tTA	tetracycline controlled transcription activator
UC	ultracentrifugation
VLC	ventricular light chain
VP16	transcriptional activator from Herpes simplex VP22 viral protein 22

WAF	wild type p53-activated fragment
wt	wild type
WKY	Wistar Kyoto strain of <i>Rattus norvegicus</i>

4.2 Declaration of contributions

Introductory chapter 1 is modified from an invited book chapter with the title 'Cell penetrating peptides – Uptake, toxicity and applications' written by Gisela Tünnemann and M. Cristina Cardoso, that is accepted for publication in 'Membrane-active peptides: methods and results on structure and function' (tentative title); IUL (International University Line, La Jolla, California, USA; www.iul-press.com).

Results 2.1

Live-cell analysis of cell penetration ability and toxicity of oligo-arginines.

The idea to perform a systematical assessment of the transduction ability and toxicity of oligoarginines was developed jointly by me, Robert Martin and M. Cristina Cardoso. Gohar Ter-Avetisiyan performed, evaluated and illustrated all transduction experiments to assess the transduction frequencies of oligoarginines of different chain length in living cells by confocal microscopy (Fig. 1). Martin Stöckl analyzed the transduction frequency of selected NBD-labeled peptides in large unilamellar vesicles (LUVs) by using a spectrofluorometer (supplementary Fig. 1). Robert Martin supervised pilot experiments and contributed to the movie data analysis (supplementary movie). Andreas Herrmann provided expertise and equipment for the LUV-experiments and M. Cristina Cardoso accompanied all stages of the development of this paper with scientific advice and allocated the laboratory and microscopic facilities.

I contributed to the outline of the paper, supervised (Fig. 1) or performed, evaluated and illustrated the experiments displayed in Fig. 2 and Fig. 3, illustrated supplementary Fig. 1 and wrote the manuscript.

Results 2.2

Cell entry of arginine-rich peptides is independent of endocytosis.

M. Cristina Cardoso, Andreas Herrmann and me developed the initial outline for this paper. Matthias Nitschke and Marek Drab provided cell lines. Gohar

Ter-Avetisyan performed and analyzed all experiments and wrote the manuscript on the basis of my day-to-day supervision.

Results 2.3

Circularization and charge clustering promotes cellular uptake of arginine-rich cell penetrating peptides (Manuscript in preparation)

The initial idea to use analytical ultracentrifugation to gain structural information about CPPs came from Ingo Morano. Joachim Behlke performed the ultracentrifugation analysis, Caroline Palm synthesized some of the peptides and investigated their stability. Manuel Prinz and Daniel Hoffmann modeled the peptide structures. M. Cristina Cardoso supported experiments and the manuscript throughout with scientific advice and provided the laboratory and the confocal microscope facility for live cell imaging.

I coordinated the project, performed, evaluated and illustrated the confocal microscope experiments and wrote the manuscript.

Results 2.4

Nucleolar marker for living cells.

Robert Martin and M. Cristina Cardoso had the idea to use oligoarginines as a live cell marker for the nucleolar compartment. Robert Martin performed and analyzed all experiments, except for the transduction into primary cells (Fig. 1A) and wrote the manuscript. I provided images for the transduction into primary cells and did proofreading of the manuscript.

Results 2.5

Modulation of muscle contraction by a cell permeable peptide.

Adult rat cardiomyocytes were isolated by Wolfgang Schlegel and Petra Pierschalek. Peter Karczewski and Hannelore Haase carried out the measurements for the shortening amplitude and for the systolic and diastolic cytoplasmic Ca^{2+} fluctuations in paced cardiomyocytes, evaluated and illustrated the results summarized in fig. 4. M. Cristina Cardoso had the initial idea for project, supported experiments and manuscripts with scientific advice and provided the laboratory and the confocal microscope facility for live cell imaging. I performed the microscopic transduction assay and the analysis of

intracellular localization of transduced VLC-1-TAT peptide in contracting cardiomyocytes, evaluated and illustrated the results (fig. 1 - 3) and wrote the manuscript.

Results 2.6

Cargo-dependent mode of uptake and bioavailability of TAT-containing proteins and peptides in living cells.

Robert M. Martin conducted, evaluated, illustrated and wrote the respective part of the manuscript for the FRAP experiments (fig. 3) and also took part in the accomplishment for the cell cycle progression assay (fig. 4). Moreover he contributed data for table 1. Simone Haupt, Christoph Patsch and Frank Edenhofer provided the TAT-Cre-reporter gene construct (3T3-FDR1.2 cells) and fluorescently labeled recombinant TAT-Cre protein. They also performed, evaluated and illustrated the result that is described in fig. 1 D. M. Cristina Cardoso supported experiments and manuscripts with scientific advice and provided the laboratory and the confocal microscope facility for live cell imaging.

I performed, evaluated and illustrated the experiments summarized in fig 1A-C and 2 and contributed to the cell cycle progression analysis (fig 4). Moreover I wrote the manuscript except the part describing the FRAP experiments.

The **discussion** is modified from an invited book chapter with the title 'Cell penetrating peptides – Uptake, toxicity and applications' written by Gisela Tünnemann and M. C. Cardoso, that is submitted to be published in 'Membrane-active peptides: methods and results on structure and function' (tentative title); IUL (International University Line, La Jolla, California, USA; www.iul-press.com).

Declaration according to the “Promotionsordnung der LMU München für die Fakultät Biologie”

Betreuung: Hiermit erkläre ich, dass die vorgelegte Arbeit am Max-Delbrück-Centrum für Molekulare Medizin von Frau Dr. M. C. Cardoso betreut wurde.

Anfertigung: Hiermit versichere ich ehrenwörtlich, dass die Dissertation selbstständig und ohne unerlaubte Hilfsmittel angefertigt wurde. Über Beiträge, die im Rahmen der kumulativen Dissertation in Form von Manuskripten in der Dissertation enthalten sind, wurde im Kapitel 4.2 Rechenschaft abgelegt und die eigenen Leistungen wurden aufgelistet.

Prüfung: Hiermit erkläre ich, dass die Dissertation weder als ganzes noch in Teilen an einem anderen Ort einer Prüfungskommission vorgelegt wurde. Weiterhin habe ich weder an einem anderen Ort eine Promotion angestrebt oder angemeldet oder versucht eine Doktorprüfung abzulegen.

(Gisela Tünnemann)

4.3 Acknowledgements

This work would not have been accomplished without the help of many people. Within my present lab I want to thank all group members for the readiness to share knowledge and experience and to take over some tasks, which enabled me to work part-time for certain periods of time. Especially, I want to mention Petra Domaing, who started together with me with great enthusiasm on the project of protein transduction and introduced me to the basics of cell culture work and of confocal fluorescence microscopy. The delivery of peptides into living cells was in wide parts a teamwork with Robert Martin, whose profound biological knowledge helped in many cases. I would like to thank Gohar Ter-Avetisyan, who joined recently on the same subject, for the good cooperation throughout.

Science is always fun, but in some laboratories it is more fun than in others. Therefore I want to thank M. Cristina Cardoso for the possibility to work in her very well organized laboratory and for the cultivation of a nice and helpful atmosphere. Especially her constant and altruistic scientific support has been invaluable for the progress of all projects and for the development of my understanding of biological sciences.

Besides all these people I want to gratefully acknowledge our cooperation with Ingo Morano's group at the MDC. Especially I want to thank Wolfgang Schlegel and Petra Sakel for reliable preparation of adult cardiomyocytes and Peter Karzcewski, Hannelore Haase and Ingo Morano for help and advice on the VLC-1-TAT project. Martin Stöckl and Andreas Herrmann from Humboldt University Berlin helped with their expertise on artificial membrane vesicles and kindly performed a number of transduction experiments with arginine-rich CPPs. Last but not least from the scientific part, I want to thank all the members of Heinrich Leonhardt's group in Munich for their support in bureaucratic as well as scientific questions. Special thanks go to Andrea Rottach for the close cooperation within the p21-project, Uli Rothbauer for sharing his experience in biochemical methods and to Heinrich Leonhardt for scientific advice in many of the projects and the support for my thesis.

Personally I am indebted to my family. I want to express my deep thanks to my father, who will be happy that something I started long time ago is about to finish, to my two little daughters, who delight my days, and of course to Stefan for giving me unfailing support and for keeping the sense of humor even in tough times.

4.4 References

1. Frankel, A.D. & Pabo, C.O. *Cell*. **55**, 1189-93 (1988).
2. Green, M. & Loewenstein, P.M. *Cell*. **55**, 1179-88 (1988).
3. Perez, F. et al. *J Cell Sci*. **102 (Pt 4)**, 717-22 (1992).
4. Joliot, A. et al. *Prog Neurobiol*. **42**, 309-11 (1994).
5. Elliott, G. & O'Hare, P. *Cell*. **88**, 223-33 (1997).
6. Murphy, A.L. & Murphy, S.J. *Gene Ther*. **6**, 4-5 (1999).
7. Elliott, G. & O'Hare, P. *J Virol*. **73**, 4110-9 (1999).
8. Machova, Z. et al. *Chembiochem*. **3**, 672-7 (2002).
9. Trehin, R. et al. *Pharm Res*. **21**, 33-42 (2004).
10. Oess, S. & Hildt, E. *Gene Ther*. **7**, 750-8 (2000).
11. Fawell, S. et al. *Proc Natl Acad Sci U S A*. **91**, 664-8 (1994).
12. Vives, E., Brodin, P. & Lebleu, B. *J Biol Chem*. **272**, 16010-7 (1997).
13. Derossi, D. et al. *J Biol Chem*. **269**, 10444-50 (1994).
14. Fischer, P.M. et al. *J Pept Res*. **55**, 163-72 (2000).
15. Dathe, M. et al. *Biochemistry*. **35**, 12612-22 (1996).
16. Oehlke, J. et al. *Biochim Biophys Acta*. **1414**, 127-39 (1998).
17. Scheller, A. et al. *J Pept Sci*. **5**, 185-94 (1999).
18. Futaki, S. et al. *J Biol Chem*. **276**, 5836-40 (2001).
19. Marshall, N.B. et al. *J Immunol Methods*. **325**, 114-26 (2007).
20. Mi, Z. et al. *Mol Ther*. **2**, 339-47 (2000).
21. Wender, P.A. et al. *Proc Natl Acad Sci U S A*. **97**, 13003-8 (2000).
22. Crespo, L. et al. *J Am Chem Soc*. **124**, 8876-83 (2002).
23. Fernandez-Carneado, J. et al. *Angew Chem Int Ed Engl*. **43**, 1811-4 (2004).
24. Fernandez-Carneado, J. et al. *Biopolymers*. **76**, 196-203 (2004).
25. Lin, Y.Z. et al. *J Biol Chem*. **270**, 14255-8 (1995).
26. Langel, U. et al. *Regul Pept*. **62**, 47-52 (1996).
27. Chaloin, L. et al. *Biochemistry*. **36**, 11179-87 (1997).
28. Rothbard, J.B. et al. *J Med Chem*. **45**, 3612-8 (2002).
29. Rothbard, J.B. et al. *Nat Med*. **6**, 1253-7 (2000).
30. Shibagaki, N. & Udey, M.C. *J Immunol*. **168**, 2393-401 (2002).
31. Astriab-Fisher, A. et al. *Pharm Res*. **19**, 744-54 (2002).
32. Nagahara, H. et al. *Nat Med*. **4**, 1449-52 (1998).
33. Schwarze, S.R. et al. *Science*. **285**, 1569-72 (1999).
34. Lewin, M. et al. *Nat Biotechnol*. **18**, 410-4 (2000).
35. Torchilin, V.P. et al. *Proc Natl Acad Sci U S A*. **98**, 8786-91 (2001).
36. Richard, J.P. et al. *J Biol Chem*. **278**, 585-90 (2003).
37. Silhol, M. et al. *Eur J Biochem*. **269**, 494-501 (2002).
38. Tunnemann, G. et al. *FASEB J*. **20**, 1775-84 (2006).
39. Fittipaldi, A. et al. *J Biol Chem*. **278**, 34141-9 (2003).
40. Lundberg, M., Wikstrom, S. & Johansson, M. *Mol Ther*. **8**, 143-50 (2003).
41. Nakase, I. et al. *Biochemistry*. **46**, 492-501 (2007).
42. Ruan, G. et al. *J Am Chem Soc*. (2007).
43. Wadia, J.S., Stan, R.V. & Dowdy, S.F. *Nat Med*. **10**, 310-5 (2004).
44. Richard, J.P. et al. *J Biol Chem*. **280**, 15300-6 (2005).

45. Brooks, H., Lebleu, B. & Vives, E. *Adv Drug Deliv Rev.* **57**, 559-77 (2005).
46. Duchardt, F. et al. *Traffic.* **8**, 848-66 (2007).
47. Mann, D.A. & Frankel, A.D. *Embo J.* **10**, 1733-9 (1991).
48. Tyagi, M. et al. *J Biol Chem.* **276**, 3254-61 (2001).
49. Ziegler, A. & Seelig, J. *Biophys J.* **86**, 254-63 (2004).
50. Goncalves, E., Kitas, E. & Seelig, J. *Biochemistry.* **44**, 2692-702 (2005).
51. Peitz, M. et al. *Proc Natl Acad Sci U S A.* **99**, 4489-94 (2002).
52. Nolden, L. et al. *Nat Methods.* **3**, 461-7 (2006).
53. Dietz, G.P. & Bahr, M. *Mol Cell Neurosci.* **27**, 85-131 (2004).
54. Maiolo, J.R., 3rd, Ottinger, E.A. & Ferrer, M. *J Am Chem Soc.* **126**, 15376-7 (2004).
55. Caron, N.J., Quenneville, S.P. & Tremblay, J.P. *Biochem Biophys Res Commun.* **319**, 12-20 (2004).
56. Shiraishi, T., Pankratova, S. & Nielsen, P.E. *Chem Biol.* **12**, 923-9 (2005).
57. Hogset, A. et al. *Somat Cell Mol Genet.* **27**, 97-113 (2002).
58. Shiraishi, T. & Nielsen, P.E. *FEBS Lett.* **580**, 1451-6 (2006).
59. Vives, E. *J Mol Recognit.* **16**, 265-71 (2003).
60. Kaplan, I.M., Wadia, J.S. & Dowdy, S.F. *J Control Release.* **102**, 247-53 (2005).
61. Magzoub, M. et al. *Biochem Biophys Res Commun.* **348**, 379-85 (2006).
62. Mai, J.C. et al. *J Biol Chem.* **277**, 30208-18 (2002).
63. Ziegler, A. et al. *Biochemistry.* **44**, 138-48 (2005).
64. Fretz, M.M. et al. *Biochem J.* **403**, 335-42 (2007).
65. Brugidou, J. et al. *Biochem Biophys Res Commun.* **214**, 685-93 (1995).
66. Derossi, D. et al. *J Biol Chem.* **271**, 18188-93 (1996).
67. Futaki, S. et al. *Biochemistry.* **41**, 7925-30 (2002).
68. Martin, R.M. et al. *Histochem Cell Biol.* **127**, 243-51 (2007).
69. Bjorklund, J. et al. *Biophys J.* **91**, L29-31 (2006).
70. Rothbard, J.B. et al. *J Am Chem Soc.* **126**, 9506-7 (2004).
71. Rothbard, J.B., Jessop, T.C. & Wender, P.A. *Adv Drug Deliv Rev.* **57**, 495-504 (2005).
72. Afonin, S. et al. *Chemphyschem.* **7**, 2134-42 (2006).
73. Shaw, J.E. et al. *J Struct Biol.* (2007).
74. Glaser, R.W. et al. *Biophys J.* **88**, 3392-7 (2005).
75. Bellet-Amalric, E. et al. *Biochim Biophys Acta.* **1467**, 131-43 (2000).
76. Ziegler, A. et al. *Biochemistry.* **42**, 9185-94 (2003).
77. Sheldon, K. et al. *Proc Natl Acad Sci U S A.* **92**, 2056-60 (1995).
78. Mitchell, D.J. et al. *J Pept Res.* **56**, 318-25 (2000).
79. Hallbrink, M. et al. *Biochim Biophys Acta.* **1667**, 222-8 (2004).
80. Lindberg, M. et al. *Biochemistry.* **40**, 3141-9 (2001).
81. Dathe, M. & Wieprecht, T. *Biochim Biophys Acta.* **1462**, 71-87 (1999).
82. Matsuzaki, K. et al. *Biochemistry.* **35**, 8450-6 (1996).
83. Futaki, S. *Biopolymers.* **47**, 75-81 (1998).
84. Thoren, P.E. et al. *FEBS Lett.* **482**, 265-8 (2000).
85. Tunnemann, G. et al. *J Pept Sci.* **14**, 469-76 (2008).
86. Hallbrink, M. et al. *Biochim Biophys Acta.* **1515**, 101-9 (2001).

87. Berlose, J.P. et al. *Eur J Biochem.* **242**, 372-86 (1996).
88. Derossi, D., Chassaing, G. & Prochiantz, A. *Trends Cell Biol.* **8**, 84-7 (1998).
89. Joliot, A. & Prochiantz, A. *Nat Cell Biol.* **6**, 189-96 (2004).
90. Magzoub, M., Eriksson, L.E. & Graslund, A. *Biophys Chem.* **103**, 271-88 (2003).
91. Binder, H. & Lindblom, G. *Biophys J.* **87**, 332-43 (2004).
92. Luedtke, N.W., Carmichael, P. & Tor, Y. *J Am Chem Soc.* **125**, 12374-5 (2003).
93. Chung, H.H. et al. *Biopolymers.* **76**, 83-96 (2004).
94. Herce, H.D. & Garcia, A.E. *Proc Natl Acad Sci U S A.* **104**, 20805-10 (2007).
95. Eilers, M. et al. *Philos Trans R Soc Lond B Biol Sci.* **319**, 121-6 (1988).
96. Verner, K. & Schatz, G. *Science.* **241**, 1307-13 (1988).
97. Bonifaci, N., Sitia, R. & Rubartelli, A. *Aids.* **9**, 995-1000 (1995).
98. Becker-Hapak, M., McAllister, S.S. & Dowdy, S.F. *Methods.* **24**, 247-56 (2001).
99. Kwon, H.Y. et al. *FEBS Lett.* **485**, 163-7 (2000).
100. Saar, K. et al. *Anal Biochem.* **345**, 55-65 (2005).
101. El-Andaloussi, S. et al. *Biochem J.* **407**, 285-92 (2007).
102. Jones, S.W. et al. *Br J Pharmacol.* **145**, 1093-102 (2005).
103. Cardozo, A.K. et al. *Biochim Biophys Acta.* **1768**, 2222-34 (2007).
104. Moschos, S.A. et al. *Bioconjug Chem.* **18**, 1450-9 (2007).
105. Abes, S. et al. *J Control Release.* **116**, 304-13 (2006).
106. Youngblood, D.S. et al. *Bioconjug Chem.* **18**, 50-60 (2007).
107. Amantana, A. et al. *Bioconjug Chem.* **18**, 1325-31 (2007).
108. Tanaka, S. et al. *J Natl Cancer Inst.* **98**, 491-8 (2006).
109. Josephson, L. et al. *Bioconjug Chem.* **10**, 186-91 (1999).
110. Zhao, M. et al. *Bioconjug Chem.* **13**, 840-4 (2002).
111. Christian, N.A. et al. *Bioconjug Chem.* **18**, 31-40 (2007).
112. Polyakov, V. et al. *Bioconjug Chem.* **11**, 762-71 (2000).
113. Bullok, K.E. et al. *Bioconjug Chem.* **13**, 1226-37 (2002).
114. Bullok, K.E. et al. *Mol Imaging.* **5**, 1-15 (2006).
115. Jiang, T. et al. *Proc Natl Acad Sci U S A.* **101**, 17867-72 (2004).
116. Haase, H. et al. *Faseb J.* **20**, 865-73 (2006).
117. Nori, A. et al. *J Control Release.* **91**, 53-9 (2003).
118. Nori, A. et al. *Bioconjug Chem.* **14**, 44-50 (2003).
119. Rousselle, C. et al. *Mol Pharmacol.* **57**, 679-86 (2000).
120. Rousselle, C. et al. *J Drug Target.* **10**, 309-15 (2002).
121. Okuyama, M. et al. *Nat Methods.* **4**, 153-9 (2007).
122. Law, B. et al. *Mol Cancer Ther.* **5**, 1944-9 (2006).
123. Hotchkiss, R.S. et al. *J Immunol.* **176**, 5471-7 (2006).
124. Sugioka, R. et al. *Oncogene.* **22**, 8432-40 (2003).
125. Ono, M. et al. *Eur J Cardiothorac Surg.* **27**, 117-21 (2005).
126. Repici, M. et al. *Neuroscience.* **150**, 40-9 (2007).
127. Eum, W.S. et al. *Free Radic Biol Med.* **37**, 339-49 (2004).
128. Bernatchez, P.N. et al. *Proc Natl Acad Sci U S A.* **102**, 761-6 (2005).
129. McCusker, C.T. et al. *J Immunol.* **179**, 2556-64 (2007).
130. Toro, A. & Grunebaum, E. *J Clin Invest.* **116**, 2717-26 (2006).
131. Tunnemann, G. et al. *J Mol Med.* **85**, 1405-12 (2007).

132. Turner, J.J. et al. *Nucleic Acids Res.* **33**, 6837-49 (2005).
133. Abes, S. et al. *Nucleic Acids Res.* **35**, 4495-502 (2007).
134. Moulton, H.M. et al. *Biochem Soc Trans.* **35**, 826-8 (2007).
135. Endoh, T., Sisido, M. & Ohtsuki, T. *Nucleic Acids Symp Ser (Oxf)*. 127-8 (2007).
136. Simeoni, F. et al. *Nucleic Acids Res.* **31**, 2717-24 (2003).
137. Unnamalai, N., Kang, B.G. & Lee, W.S. *FEBS Lett.* **566**, 307-10 (2004).
138. Gratton, J.P. et al. *Nat Med.* **9**, 357-62 (2003).
139. Lavigne, M.D. et al. *Faseb J.* (2008).
140. Mishra, A. et al. *Angew Chem Int Ed Engl.* **47**, 2986-9 (2008).
141. Chen, L. et al. *Proc Natl Acad Sci U S A.* **98**, 11114-9 (2001).
142. Takakura, Y., Mahato, R.I. & Hashida, M. *Adv Drug Deliv Rev.* **34**, 93-108 (1998).
143. Cao, G. et al. *J Neurosci.* **22**, 5423-31 (2002).
144. Ju, K.L., Manley, N.C. & Sapolsky, R.M. *Exp Neurol.* (2007).
145. Asoh, S. et al. *Proc Natl Acad Sci U S A.* **99**, 17107-12 (2002).
146. Nakashima-Kamimura, N. et al. *Life Sci.* **82**, 218-25 (2008).
147. Dave, S.H. et al. *J Immunol.* **179**, 7852-9 (2007).
148. Kwon, J.H. et al. *Biochem Biophys Res Commun.* **363**, 399-404 (2007).
149. Li, T. et al. *Exp Neurol.* **197**, 301-8 (2006).
150. Koya, V. et al. *Diabetes.* (2007).
151. Popiel, H.A. et al. *Mol Ther.* **15**, 303-9 (2007).
152. Mai, J.C. et al. *Cancer Res.* **61**, 7709-12 (2001).
153. Bright, R., Steinberg, G.K. & Mochly-Rosen, D. *Brain Res.* **1144**, 146-55 (2007).
154. Fletcher, S. et al. *Mol Ther.* **15**, 1587-92 (2007).
155. Zhou, J.P. et al. *Brain Res.* **1191**, 12-9 (2008).

4.5 Curriculum Vitae

Name: Gisela Tünnemann
Date of birth: 24.07.1970
Place of birth: Fröndenberg

Education

1990 Allgemeine Hochschulreife
Walburgisgymnasium
Menden, Germany

1990-1997 Diploma in chemistry
Carl von Ossietzky University Oldenburg
Oldenburg, Germany

2003- present PhD in biology (LMU, München, Germany)
Max Delbrueck Center for Molecular Medicine
Berlin, Germany

Positions and teaching

1997 student assistant in AG toxicology
Carl von Ossietzky University Oldenburg
Oldenburg, Germany

1998-2003 scientist in AG crystallography
Max Delbrück Center for Molecular Medicine
Berlin, Germany

2003-present graduate student in the group of M. Cristina Cardoso
2007-now co-supervision of the diploma thesis of Gohar Ter-Avetisyan

4.6 Conference contributions

November 2004, **Gisela Tünnemann** & Robert M. Martin. “Minimal invasive methods to deliver macromolecules to living cells. “ Oral presentation at the *Cardiovascular Retreat* of the Max Delbrueck Center for Molecular Medicine in Groß-Dölln, Germany.

November 2006, **Gisela Tünnemann**. “Transducible peptides in cardiovascular research: modulation of contractile mechanism. “ Oral presentation at the *Cardiovascular Retreat* of the Max Delbrueck Center for Molecular Medicine at the communication center Hubertusstock, Germany.

March 2006, **Gisela Tünnemann**. “Delivery of proteins and peptides by cell penetrating peptides into living cells and their application to the modulation of cellular proliferation and differentiation. Invited oral presentation at the *Wollenberger Seminar*, Berlin, Germany.

July 2006, **Gisela Tünnemann**, Robert M. Martin, Hannelore Haase, Wolfgang Schlegel, Petra Pierschalek, Ingo Morano und M. Cristina Cardoso. “Inhibition of cellular proliferation and modulation of muscle contractility by cell permeable TAT-peptide fusions.“ Poster at the *International Symposium on optical analysis of biomolecular machines*, Berlin, Germany.

April 2007, **Gisela Tünnemann**, Robert M. Martin, Hannelore Haase, Peter Karczewski, Prisca Bosguerin, Rudolf Volkmer, Joachim Behlke, Ingo Morano and M. Cristina Cardoso. “Application of cell penetrating peptides in the modulation of cell proliferation and differentiation.“ Poster at the *2nd Workshop on Biophysics of membrane-active peptides*, Lisbon, Portugal.

May 2007, **Gisela Tünnemann**, Robert M. Martin and M. C. Cardoso. “Application of cell penetrating peptides in the modulation of cell proliferation and differentiation. “ Poster at the Biochemical Society meeting “*Cell penetrating peptides*“ at the University of Wolverhampton, Telford, UK.

September 2007, **Gisela Tünnemann**, Robert M. Martin, G. Ter-Avetisyan and M. C. Cardoso. “Toxicity and applications of cell penetrating peptides in the modulation of cell proliferation and differentiation. “ Poster at the *2nd Intracellular delivery of therapeutic molecules*, Grenoble, France.

4.7 List of publications

Haase, H., Dobbernack, G., **Tünnemann, G.**, Karczewski, P., Cardoso, M. C., Petzhold, D., Schlegel, W., Lutter, S., Pierschalek, P., Behlke, J. & Morano, I. (2006). Minigenes encoding N-terminal domains of human cardiac myosin light chain-1 improve heart function of transgenic rats. *FASEB J.* **20**, 865-873.

Tünnemann, G., Martin, R. M., Haupt, S., Patsch, C., Edenhofer, F. & Cardoso, M. C. (2006). Cargo-dependent mode of uptake and bioavailability of TAT-containing proteins and peptides. *FASEB J.* **20**, 1775-1784.

Martin, R.M., **Tünnemann, G.**, Leonhardt, H. & Cardoso, M.C. Nucleolar marker for living cells. *Histochem Cell Biol.* **127**, 243-251.

Von Vietinghoff, S. **Tünnemann, G.**, Eulenberg, C., Wellner, M., Cardoso, M. C., Luft, F. C. & Kettritz, R. (2007). NB1 mediates surface expression of the ANCA antigen proteinase 3 on human neutrophils. *Blood* **109**, 4487-4493.

Tünnemann, G., Karczewski, P., Haase, H., Cardoso, M. C. & Morano, I. (2007). Modulation of muscle contraction by a cell-permeable peptide. *J Mol Med.* **85**, 1405-1412.

Tünnemann, G., Ter-Avetisyan, G., Martin, R. M., Stöckl, M., Herrmann, A. & Cardoso, M. C. (2008). Live-cell analysis of cell penetration ability and toxicity of oligo-arginines. *J Pept Sci.* **14**, 469-476.

Nitschke, M., Korte, T., Tievesch, C., Ter-Avetisyan, G., **Tünnemann, G.**, Cardoso M. C., Veit, M. & Herrmann, A. (2008). Equine arteritis virus is delivered to an acidic compartment of host cells via clathrin-dependent endocytosis. *Virology.* **377**, 248-254.

Tünnemann, G. & Cardoso, M. C. Cell penetrating peptides – Uptake, toxicity and applications. In "Membrane-active peptides: methods and results on structure and function", edited by M. Castanho, IUL (International University Line, La Jolla, California, USA; www.iul-press.com), In Press.

Ter-Avetisyan, G., **Tünnemann, G.**, Nowak, D., Nitschke, M., Herrmann, A., Drab, M. & Cardoso, M. C. Cell entry of arginine-rich peptides is independent of endocytosis. Submitted.

Ciobanasu, C., Harms, E., **Tünnemann, G.**, Cardoso, M. C. and Kubitscheck, U. Cell-penetrating HIV1 TAT peptides float on anionic model lipid bilayers. Submitted.

Tünnemann, G., Behlke, J., Morano, I., Palm, C., Prinz, M., Hoffmann, D & Cardoso, M. C. Circularization and charge clustering promotes cellular uptake of arginine-rich cell penetrating peptides. Manuscript in preparation.

4.8 Movies

M1: Confocal microscopy time lapse of the transduction of the L- and D-isomers of R9 simultaneously applied to C2C12 mouse myoblasts at a concentration of 10 μ M. Derived from Tünnemann et al., *J Pept Sci.* **14**, 469-476.

M2-M8: Confocal microscopy time lapses of the transduction of TAT into BHK21-tTA/anti-clathrin heavy chain) hamster kidney cells at a concentration of 10 μ M. M2=control cells, M3-8 transduction in cells after day 1-6 after knock down of the clathrin heavy chain-protein. Derived from Ter-Avetisyan et al., submitted.

M9-M10: Confocal microscopy time lapses of the transduction of TAT into an endothelioma cell line from wildtype (WT) and caveolin-1 knockout (KO) mice at a concentration of 10 μ M. M9=wt, M10=KO. Derived from Ter-Avetisyan et al., submitted.

M11: Confocal microscopy time lapses of the transduction C2C12 mouse myoblasts at a concentration of 10 μ M at different temperatures. M11=37°C. M12= 4°C. Derived from Ter-Avetisyan et al., submitted.

M12: Confocal microscopy time lapses of the transduction of linear and circular TAT into C2C12 mouse myoblasts at a concentration of 20 μ M at different temperatures. M11=37°C. M12= 4°C. Derived from Tünnemann et al., manuscript in preparation.

M13: Confocal microscopy time lapse of the transduction of the nucleolar marker into C2C12 mouse myoblasts at a concentration of 10 μ . Derived from Martin et al., *Histochem Cell Biol.* **127**, 243-251.